Impact of iron on CHO metabolism and recombinant protein production

TECHNISCHE UNIVERSITÄT DARMSTADT

Vom Fachbereich Chemie
der Technischen Universität Darmstadt

Zur Erlangung des Grades
Doctor rerum naturalium (Dr. rer. nat.)

Dissertation
von

Christine Hilde Weiß, M. Sc.

Erstgutachter: Prof. Dr. Harald Kolmar
Zweitgutachter: Prof. Dr. Karlheinz Preuß

Darmstadt 2022

Weiß, Christine Hilde: Impact of iron on CHO metabolism and recombinant protein production
Darmstadt, Technische Universität Darmstadt
Tag der Einreichung: 14. Dezember 2021
Tag der mündlichen Prüfung: 16. Februar 2022
Jahr der Veröffentlichung der Dissertation auf TUprints: 2022

Die vorliegende Arbeit wurde unter der Leitung von Herrn Prof. Dr. Harald Kolmar am Clemens-Schöpf-Institut für Organische Chemie und Biochemie der Technischen Universität Darmstadt sowie bei Merck KGaA in Darmstadt von Oktober 2018 bis Dezember 2021 angefertigt.

Publications derived from this PhD thesis project

Parts of this work have been published and/or are currently submitted/under review.

Weiss CH, Merkel C, Zimmer A. Impact of iron raw materials and their impurities on CHO metabolism and recombinant protein product quality. *Biotechnology Progress*. 2021; 37(4):e3148. doi:10.1002/btpr.3148

Table of contents

Abstract

Iron is an essential transition metal required in cell culture medium (CCM) due to its vital role in many cellular processes such as energy metabolism, deoxyribonucleic acid (DNA) biosynthesis or antioxidant functions. However, due to its redox capabilities, iron can also catalyze Fenton reactions favoring the formation of reactive oxygen species (ROS) that may cause severe cellular damages. This study sought to investigate the impact of iron in CCM on Chinese hamster ovary (CHO) cell line performance, on critical quality attributes (CQAs) of different recombinant proteins, on messenger ribonucleic acid (mRNA) expression levels of genes involved in iron homeostasis, and on intracellular iron or labile iron pool (LIP) levels, whereby for the last two readouts a method development was performed prior to analyzing the project relevant samples.

Besides the successful establishment of a ferrozine-based assay for detecting total intracellular iron amount and the promising results obtained upon testing the fluorescent probe RhoNox-1 for detecting changes in LIP concentrations, none of the other two (fluorescent) probes tested during method development, namely calcein and TRX-PURO, were able to determine LIP amounts within CHO cells. Since those probes rely on a rather high LIP concentration present within cells, a low LIP present within CHO cells either due to a limited, saturated or low iron uptake, or due to an immediate distribution or usage of iron within the cells once taken up was thus suggested.

Data also revealed that iron raw material impurities are strongly impacting cell performance and CQAs. Whereas manganese was identified as the main impurity improving cell performance and altering protein glycosylation level within Cellvento® 4CHO and 4Feed fed-batch platform with manganese presenting additionally an opposite effect on cell culture compared to iron, copper impurity contributed to an overall increased cell performance of the tested CHOZN® cell line in EX-CELL® Advanced CHO Fed-Batch-Medium platform. Usage of low impurity iron raw materials is therefore crucial to decouple the effects of iron and its trace element impurities by controlling and adjusting each element concentration independently and thereby guarantee the run of consistent and stable cell culture processes.

Among the different iron sources tested within CCM during a fed-batch experiment, non-chelated iron sources caused a faster decrease in measured iron concentration within the supernatant and led to a higher detected iron amount present within the cell pellets taken during the course of the fed-batch process compared to the tested chelated iron sources, whereas no cell growth was obtained upon ferric chloride ($FeCl_3$) usage. At a first glance, data suggest an increased uptake efficiency for CHO cells upon usage of non-chelated iron sources, however, differences might have rather come from a faster iron precipitate formation within CCM upon usage of non-chelated iron sources, additionally, since mRNA expression levels of genes involved in iron uptake did not indicate for a difference between chelated and non-chelated iron sources. The removal of possible iron precipitates prior to intracellular iron

measurement as well as the investigation of the fate of iron in CCM seems thus to be crucial to understand iron-related uptake mechanisms.

Zusammenfassung

Eisen ist ein essentielles Übergangsmetall und wichtiger Bestandteil von Zellkulturmedien, da es in vielen zellulären Prozessen, unter anderem im Energiestoffwechsel, der Biosynthese von Desoxyribonukleinsäure (DNA) oder bei antioxidativen Mechanismen, eine wichtige Rolle spielt. Aufgrund seiner Redoxaktivität kann Eisen jedoch auch Fenton-Reaktionen katalysieren, die die Bildung reaktiver Sauerstoffspezies (ROS) begünstigen, welche mitunter zu schweren Zellschäden führen können. In dieser Arbeit wurde daher der Einfluss von Eisen im Zellkulturmedium auf das Wachstum und die Produktion von Ovarienzellen eines chinesischen Hamsters (CHO) und auf kritische Qualitätsmerkmale verschiedener rekombinanter Proteine untersucht. Zudem wurde die Wirkung von Eisen auf das Expressionslevel von Boten-Ribonukleinsäure (mRNA) von Genen, die an der Eisenhomöostase beteiligt sind, und auf den intrazellulären Eisengehalt beziehungsweise den labilen Eisenpool (LIP) analysiert, wobei für die beiden letzteren Untersuchungen eine Methodenentwicklung vorausging.

Neben der erfolgreichen Etablierung eines Ferrozin-basierten Assays zum Nachweis der gesamten intrazellulären Eisenmenge und den Ergebnissen, die bei der Testung der Fluoreszenzsonde RhoNox-1 zum Nachweis von veränderten LIP Konzentrationen erzielt wurden, konnte keine der beiden anderen während der Methodenentwicklung getesteten (Fluoreszenz-)Sonden (Calcein oder TRX-PURO) LIP Konzentrationen in CHO Zellen nachweisen. Da die Verwendung dieser Sonden eine relativ hohe LIP Konzentration in Zellen voraussetzt, wurde eine geringe LIP-Konzentration in CHO Zellen vermutet. Dies könnte entweder auf eine begrenzte, gesättigte oder geringe zelluläre Eisenaufnahme, oder auf eine sofortige Verteilung beziehungsweise Verwendung des aufgenommenen Eisens innerhalb der Zellen zurückzuführen sein.

Die Daten zeigten zudem, dass sich Verunreinigungen im Eisenrohstoff stark auf das Wachstum, die Produktion und auf die kritischen Qualitätsmerkmale des rekombinanten Proteins auswirken. Erhöhte Manganverunreinigungen trugen zu einem verbesserten Zellwachstum, einer gesteigerten Proteinproduktion und einem veränderten Proteinglykosylierungsprofil in der Cellvento® 4CHO und 4Feed Fed-Batch Medienplattform bei, wobei Mangan zusätzlich einen gegensätzlichen Effekt im Vergleich zu Eisen auf die Zellkultur aufwies. Kupferverunreinigung wurden dahingegen als Hauptursache für eine gesteigerte Zellleistung der getesteten CHOZN®-Zelllinie in der EX-CELL® Advanced CHO Fed-Batch Medienplattform identifiziert. Die Verwendung von Eisenrohstoffen mit geringen Verunreinigungen ist daher von entscheidender Bedeutung, um die Auswirkungen von Eisen und seinen Spurenelementverunreinigungen in der Zellkultur zu entkoppeln. Durch die unabhängige Zugabe der einzelnen Elemente zum Zellkulturmedium können die Konzentrationen besser voneinander kontrolliert und angepasst werden, um so letztendlich konsistente und stabile Zellkulturprozesse zu gewährleisten.

Von den verschiedenen Eisenquellen, die im Zellkulturmedium während eines Fed-Batch Experiments getestet wurden, verursachten nicht-chelatierte Eisenquellen im Vergleich zu chelatierten Eisenquellen eine schnellere Abnahme der gemessenen Eisenkonzentration im Zellkulturüberstand und führten zu einer höheren nachgewiesenen Eisenmenge in den Zellpellets, die während des Fed-Batch Prozesses der Zellkultur entnommen wurden. Die Verwendung von Eisenchlorid ($FeCl_3$) führte dagegen zu gar keinem Zellwachstum. Auf den ersten Blick deuten die Daten auf eine erhöhte Eisenaufnahmeeffizienz der CHO Zellen bei Verwendung von nicht-chelatierten Eisenquellen hin. Jedoch könnten die Unterschiede auch auf eine schnellere Bildung von Eisenpräzipitaten innerhalb des Zellkulturmediums bei Verwendung von nicht-chelatierten Eisenquellen zurückzuführen sein, da auch die untersuchten mRNA-Expressionslevel von Genen, die in die Eisenaufnahme involviert sind, auf keinen Unterschied zwischen chelatierten und nicht-chelatierten Eisenquellen hinwiesen. Die Entfernung möglicher Eisenpräzipitate vor der Bestimmung von intrazellulärem Eisen sowie die Charakterisierung der vorliegenden Eisenformen nach der Eisenzugabe zum Zellkulturmedium scheinen daher essentiell, um ein umfangreicheres und tiefgründigeres Verständnis und Wissen für eisenbezogene Aufnahmemechanismen zu entwickeln.

1 Introduction

1.1 Production process of biopharmaceutical proteins

Biopharmaceutical proteins are high-molecular mass substances produced for therapeutic applications[1], whereby the majority of the approved recombinant proteins belong to the class of monoclonal antibodies (mAbs).[1–3] By now, over 55 mAbs were introduced into the market targeting several diseases for example within the oncological, hematological or rheumatological field.[4] One of the top-selling mAbs is adalimumab for the treatment of rheumatoid arthritis[3,4], however, due to the growing need for therapeutics targeting as well chronic or infectious diseases, an increasing number of mAbs is currently under development indicating the immense potential and efficacy of mAbs.[4–6] Besides the identification of the mAb lead sequence and the respective target antigen, the development of the production process of the biopharmaceutical protein, including cell line and cultivation mode selection as well as cell culture medium (CCM) development, is highly important.[7]

1.1.1 Cell lines as expression systems

The production of biopharmaceutical proteins is based on the overexpression of the recombinant protein within a suitable host cell line that can be either of prokaryotic or eukaryotic nature. However, mammalian cell lines are the preferred expression systems due to their ability to perform post-translational modifications (PTMs) similar to human proteins.[7] Among the mammalian expression systems, there are three major representatives, namely human, mouse and hamster cell lines including for example human embryo kidney (HEK293) cells, murine myeloma cells (NS0 and Sp2/0) and Chinese hamster ovary (CHO) cells, respectively.[8,9] Overall, CHO cells contribute to more than 70% of the total recombinantly produced proteins as they provide several benefits over other cell lines.[8] Besides their robust growth in suspension cultures, CHO cells are showing a high potential for gene amplification leading to high production rates.[8,10,11] However, cell line engineering is still continuously developing, aiming to increase productivity and robustness of the cell line even further, for example by decoupling cell growth from productivity leading to an enhanced specific productivity, or by developing apoptosis-resistant cell lines leading to a prolonged cell culture viability.[2,12] Therefore, different CHO cell lineages such as CHO-K1, CHO-DG44 or CHO-S are available on the market comprising different genetic characteristics and thus are able to cover different needs and preferences such as biomass formation or mAb expression.[13]

To ensure high and stable expression of the recombinant protein within the selected host cell line, different selection approaches exist. Common antibiotic-free selection markers preferred in industry are the dihydrofolate reductase (DHFR) and the glutamine synthetase (GS), which are essential enzymes involved in nucleic acid precursor and glutamine synthesis, respectively. Co-transfection of the selection

marker gene with the target gene into cells lacking the DHFR or GS enzymes only allows the growth of successfully transfected cells when cultured in either hypoxanthine and thymidine (HT)- or glutamine-deficient medium, respectively.[8,9,12,14,15] Addition of the DHFR inhibitor methotrexate (MTX) or the GS inhibitor methionine sulfoximine (MSX) during cell culture expansion can increase the selection pressure even further resulting in higher target gene amplification rates.[8,14,15]

Aside from cell line selection and cell line engineering, the identification of an appropriate production process for the biopharmaceutical protein is a further crucial step during the development phase.

1.1.2 Manufacturing process

The design and decision for a manufacturing process of the biopharmaceutical protein is mainly based on achieving low production costs with a concomitant high product quantity at the desired product quality. Thereby, the cultivation mode mainly impacts the decision as it defines the process duration, complexity and needed cultivation conditions.[16] Among the common cultivation modes used in industry are batch, fed-batch and perfusion cultures.[17] Whereas the cell growth and productivity within a batch cultivation mode is limited by the provided amount of nutrients supplied within the CCM, usage of a fed-batch mode extends the duration of the cell culture significantly by providing a regular supply of key nutrients in form of a concentrated feed. Thus, high cell densities and final titers of more than 10 g/L can be reached.[12,18,19] Product harvest for a batch and fed-batch mode takes place at the end of the process, while a continuous product harvest for over several weeks is obtained during perfusion cultures by retaining the cells within the bioreactor. The volume loss due to the continuous harvest is compensated by a continuous addition of nutrients to the cell culture and thereby maintaining the cell culture state.[18] With perfusion cultures, even higher cell densities and higher yields can be achieved in comparison to fed-batch or batch modes. However, a higher validation effort is needed to ensure genetic stability of the cell line as well as product quality during the complete process.[20]

Besides the cultivation mode, culture operating parameters such as temperature, agitation speed, pH and gas flow rate of dissolved oxygen (DO) and CO_2 need to be optimized and well characterized since they also impact cell culture performance and product quality.[12,19] However, during the last few years, the potential of CCM formulation to support cellular growth and proliferation as well as its capability to actively modulate critical quality attributes (CQAs) of the protein became more important resulting in a continuous growing research area.

1.1.3 Cell culture media

The first in vitro cultivation of animal tissue with a medium-like salt solution dates back to the year of 1882. In the following decades as cell culture technology was discovered for the production of biopharmaceuticals, CCM formulation improved immensely.[21] Whereas in the beginning mainly natural

media were used that consisted of natural biological fluids, such as serum or plasma, or tissue extracts, synthetic media were developed later on.[21,22] Those media were initially composed of a basal medium and were supplemented with serum stimulating cell growth and proliferation. However, usage of serum revealed several disadvantages in cell culture due to its risk of bearing microbial contamination or its undefined composition and lot-to-lot variability, gaining less reproducible culture processes.[21–23] Although serum was then replaced by either hydrolysates, growth factors or hormones, the composition of those additives was still not fully characterized and lot-to-lot variations were still existent.[21,24] Therefore, the development of chemically defined media progressed, providing all essential nutrients at a high specificity.[25] Nowadays, chemically defined media are composed of a defined basal medium supporting cell growth and productivity of multiple cell lines, whereas further highly purified supplements such as growth factors or hormones can be added depending on the cell line requirements.[12,25] The basal medium consists of amino acids, buffering systems, carbohydrates, inorganic salts, lipids, trace elements and vitamins, whereby each of these components perform a specific function for or within the cells as listed in Table 1.[22,25,26] In addition to the overall medium composition, the final compound concentrations are decisive for achieving high cell growth and antibody production demonstrating the huge variety and development potential within the field of CCM.[27]

Table 1: Basic components included in a CCM.

Listed are the components, their functions for/within the cells, and some examples.[21,22,25,26]

General components	Function	Example
Amino acids	Building blocks for protein synthesis Energy delivery through amino acid catabolism	Arginine, cysteine, leucine, tyrosine, valine
Buffering systems	pH regulation	Natural buffering system with CO_2/HCO_3 Chemical buffering system with HEPES
Carbohydrates	Main energy source	Glucose, galactose
Inorganic salts	Maintaining osmotic balance for the cells Regulation of membrane potential	Na^+, K^+, Cl^-
Lipids	Building blocks for cellular membranes Involved in nutrient storage and transport and in signal transduction	Cholesterol, fatty acids
Trace elements	Present in the active centers of enzymes and physiologically active substances as electron transfer activators	Cu, Fe, Mn, Mo, Zn
Vitamins	Essential for cell growth and proliferation due to their precursor function of various cofactors	Vitamin A, B and D

1.2 Antibodies

1.2.1 Structure of biopharmaceutical antibodies

Antibodies, also known as immunoglobulins (Igs), are about 150 kDa large proteins that play a highly important role in the human immune system to defeat pathogens or disease targets.[28,29] Each antibody consists of two fragment antigen binding (Fab) regions, responsible for the antigen binding, and one fragment crystalline (Fc) region, able to bind to the Fc receptor on effector molecules of the immune system and thereby triggering an immune response (Figure 1).[28] Depending on the effector function and length of the Fc region, antibodies are further categorized into five isotypes, namely IgA, IgD, IgE, IgG and IgM. Among those isotypes, IgG is the most abundant showing the longest serum half-life.[30] IgG consists of two identical 50 kDa heavy chains (H) and two identical 25 kDa light chains (L), whereby each heavy chain encompasses three constant domains (C_H1, C_H2 and C_H3) and one variable domain (V_H), and each light chain consist of only one constant domain (C_L) and one variable domain (V_L), respectively.[28] Each light chain is attached to one heavy chain by inter-chain disulfide bonds, whereas the connection of both heavy chains takes place via disulfide bonds in a flexible hinge region and via non-covalent interactions between the two C_H3 domains. Structural and functional differences of the heavy chain, mainly within the C_H1 and C_H3 domains, define four subclasses of IgG (IgG1, IgG2, IgG3 and IgG4), whereby IgG1 is the most common antibody subclass used for therapeutic approaches.[28–31]

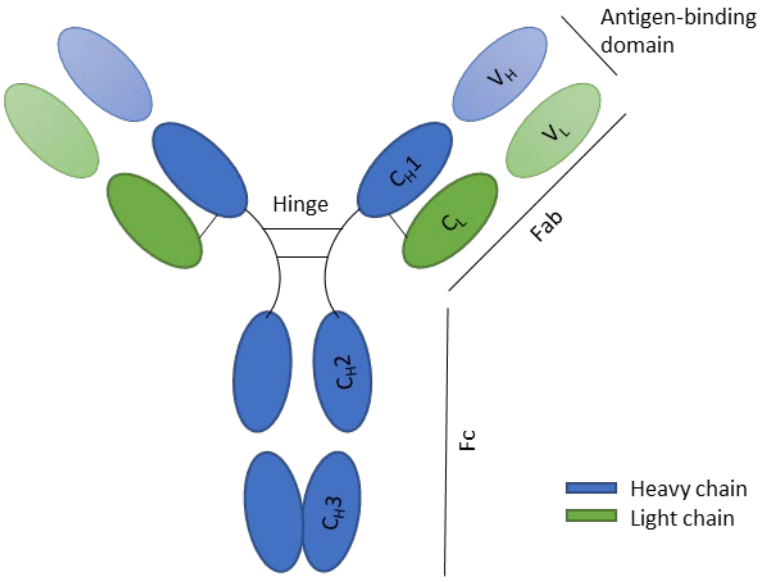

Figure 1: Schematic representation of an IgG1 molecule.

The antibody is built up of two heavy chains (H) and two light chains (L). The variable domains of the heavy and light chains (V_H and V_L) together with the constant domain 1 of the heavy chain (C_H1) and the constant domain of the light chain (C_L) form the Fab region, responsible for the antigen binding. The remaining two constant domains of the heavy chains (C_H2 and C_H3) comprise the Fc region.[29]

The efficacy of an antibody as a therapeutic protein is determined by the independent mode of action of its specific binding to the target antigen and its effector function induction.[31] However, besides the functional properties of the antibody, further characteristics such as quality attributes are highly

important to assess and monitor during the manufacturing process since they not only impact immunogenicity, but also affect drug safety and efficacy.[32]

1.2.2 CQAs of biopharmaceutical antibodies

The production process of biopharmaceutical antibodies mainly defines the quality of the therapeutic protein. Selection of the host cell line, the process conditions as well as the CCM composition may induce product variabilities and thereby altering and impacting the safety and efficacy of the protein.[19,32] To ensure a certain product quality allowing the antibody to perform its intended purpose, CQAs are defined during the biopharmaceutical production process, which need to be within defined ranges.[32] CQAs for a mAb include general properties such as pH and appearance, excipient levels such as surfactants or buffers, contaminants such as viruses, process-related impurities such as host cell proteins, bioactivity attributes such as effector function, and product variants such as aggregates, fragments and PTMs including oxidation and glycosylation or the creation of charge isotypes.[32,33] In the following, a brief overview of three, to this work relevant, product variants will be given.

Aggregation

Aggregates or high molecular weight (HMW) species can be formed during all steps of the mAb production process.[34] Thereby, protein molecules are self-associated to each other leading to a loss of product efficacy and eventually to an immune response in patients, compromising drug safety.[34,35] The unwanted change in protein conformation during cell culture processes is mainly triggered by stress.[36] Stress-associated process conditions that were identified to favor the formation of aggregates in CHO cell cultures are inter alia temperature, agitation speed, antifoam content and osmolality, as well as overall CCM formulation.[37,38] Additionally, oxidative stress to the cells was identified to induce protein aggregation.[39] Furthermore, expression of high protein amounts may lead to aggregation formation due to a disturbed recognition of the polypeptide chains by chaperones that are responsible for the correct protein folding.[40,41]

During downstream applications, including several chromatographic purification steps to obtain a highly pure protein in the end, operating parameters such as buffer nature, salt concentration and pH may induce aggregation.[42] Furthermore, physical stress and mechanical shear forces caused by pumping of the antibody solution onto the unit operations, as well as final formulation and storage conditions may also cause protein aggregation formation.[34]

Oxidation

Oxidation is a chemical PTM impacting the stability and biological activity of the protein by altering the primary structure of the proteins and peptides.[43,44] Among the amino acids that are prone to oxidation

are methionine, cysteine, tryptophan, histidine and tyrosine due to the high reactivity of their containing sulfur atoms or aromatic rings.[43,45] Oxidation may be influenced by several process parameters such as pH, temperature and DO concentration[43,45], or may arise due to formulation or storage conditions.[46] Especially the presence of transition metals such as iron or copper may favor protein oxidation as they can catalyze oxidation reactions.[44,47]

Glycosylation

Glycosylation is a PTM process referring to the attachment of carbohydrate moieties (glycans) to the protein. Depending on whether the glycan is attached at the nitrogen of the side chain of asparagine (Asn) of the consensus amino acid sequence Asn-Xxx-serine (Ser)/threonine (Thr), whereby Xxx can be any amino acid except proline, or at the oxygen of the amino acids Ser or Thr, N-linked or O-linked glycosylation can be distinguished, respectively.[48,49] Within a human IgG, typically the N-glycosylation site at position Asn^{297} located within each C_H2 domain of the Fc part is occupied, whereas further N-glycosylation sites may be present within the Fab region.[48,50]

The metabolic pathway of glycosylation is a complex enzymatic procedure comprising a high possibility of branching and linkage of sugar moieties, namely N-acetylglucosamine (GlcNAc), mannose (Man), galactose (Gal), fucose (Fuc) and sialic acid (SA) in case of N-glycosylation and GlcNAc, Gal, Fuc, SA and N-acetylgalactosamine (GalNAc) for O-glycosylation, leading to an immense amount of structural diversity of the protein.[51] A structural diversity within the protein pool coming from a sub-stoichiometric addition of glycans to a specific site resulting thereby in the presence or absence of glycans at that site is called macroheterogeneity. In contrast, a difference within the glycan structure at one specific site is referred to as microheterogeneity.[52]

The glycosylation profile of an antibody has an enormous impact on its effector function, half-life and safety and is thus one of the most important CQAs.[19,51] Aside from the expression system that decisively determines possible glycan formations[53], several process parameters are known to affect the mAb glycosylation profile. For instance, culture conditions such as temperature and pH were identified as possible factors impacting the protein glycosylation profile.[51,54,55] Furthermore, several CCM compounds were identified to affect protein glycosylation. Limited glucose availability within CCM was demonstrated to affect protein glycosylation by interfering with the glycan or precursor synthesis thereof[19,56], whereas especially metal concentrations within CCM were shown to be critical for glycosylation as metals in general are known cofactors for many enzymes that may also be involved in the glycosylation pathway.[54,57–60]

1.3 Iron - an essential trace element for life

Iron is one of the most abundant metallic elements in the Earth's crust and an essential trace element for nearly all living organisms.[61] It is involved in many physiological processes by taking part in enzymatic reactions or cellular respiration, however, an excess of iron can turn into a toxicity for cells.[62,63] Within humans, abnormalities within the iron homeostasis due to iron overload or iron deficiency are responsible for many diseases. For instance, hereditary hemochromatosis, an iron overload disease that eventually leads to diabetes mellitus, or several anemia due to an insufficient iron amount may arise.[64] Consequently, the presence of iron within the cells needs to be tightly regulated to control the chemical and functional properties of iron.[62]

1.3.1 Iron chemistry

Iron is a transition metal with the atomic number 26 and a relative atomic mass of 55.845 g/mol.[65] At physiological conditions, iron is mainly present in two oxidation states, namely the ferrous (Fe^{2+}) and the ferric (Fe^{3+}) state, although iron can exist in nine different oxidation states (from Fe^{2-} to Fe^{6+}). The electron configuration of Fe^{2+} is $[Ar]3d^6$, whereas it is $[Ar]3d^5$ for Fe^{3+}.[66] Due to its ability to gain and lose electrons, iron participates in many oxidation-reduction reactions in biological systems.[67,68] However, this property may also be hazardous for the cells, especially when reactive oxygen species (ROS) are formed. One of the most well-known reactions leading to the formation of ROS is the Fenton reaction.[69] Thereby, a hydroxyl radical ($OH^{\cdot}$) is formed due to the oxidation of ferrous ion by hydrogen peroxide (H_2O_2) (Equation 1). The regeneration of ferric to ferrous ion can then take place by the reaction of ferric ion with hydroperoxyl radical ($HO_2^{\cdot}$) leading to the production of molecular oxygen (O_2) and a hydrogen ion (H^+) (Equation 2), but also other regeneration mechanisms are possible.[69,70]

Equation 1: Fenton reaction.

Oxidation of ferrous (Fe^{2+}) to ferric (Fe^{3+}) ion by hydrogen peroxide (H_2O_2) leading to the formation of a hydroxide ion (OH^-) and a hydroxyl radical ($OH^{\cdot}$).[69,70]

$$Fe^{2+} + H_2O_2 \rightarrow Fe^{3+} + OH^- + OH^{\cdot}$$

Equation 2: Reduction of ferric to ferrous ion by hydroperoxyl radical.

Reduction of ferric (Fe^{3+}) to ferrous (Fe^{2+}) ion by hydroperoxyl radical ($HO_2^{\cdot}$) leading to the formation of molecular oxygen (O_2) and a hydrogen ion (H^+).[69,70]

$$Fe^{3+} + HO_2^{\cdot} \rightarrow Fe^{2+} + O_2 + H^+$$

Whether the oxidation from ferrous to ferric or the reduction from ferric to ferrous ion in aqueous solutions is thermodynamically favored does not only depend on the electrode potential of the Fe^{3+}/Fe^{2+} couple but is also strongly pH-dependent (Figure 2).[71–73] For instance, the standard electrode potential of the Fe^{3+}/Fe^{2+} couple in aqueous solution at pH 0 is +0.77 V (against standard hydrogen

electrode (SHE)), which is greater than the standard electrode potential of $H^+/½\ H_2$ ($E^\circ = 0$ V) but smaller than the standard electrode potential of O_2/H_2O ($E^\circ = 1.229$ V), whereby the latter two are representing the stability limits of water.[66,71,73] Thus, in the presence of oxygen, soluble ferric ions are the predominant iron species found at pH 0 in aqueous solution since the oxygen acts as the oxidizing agent for iron due to its higher standard electrode potential compared to the iron redox couple ($E^\circ(O_2/H_2O) > E^\circ(Fe^{3+}/Fe^{2+})$). However, this standard electrode potential of Fe^{3+}/Fe^{2+} is only relevant within a pH range from 0 to 2.2.[67,71] As soon as the pH increases, other soluble but also insoluble iron species are formed. At physiological pH, iron initially exists as ferrous ions, however, upon the presence of oxygen, the ferrous ions quickly oxidize to ferric ions that precipitate in form of insoluble ferric hydroxide ($Fe(OH)_3$).[71,73]

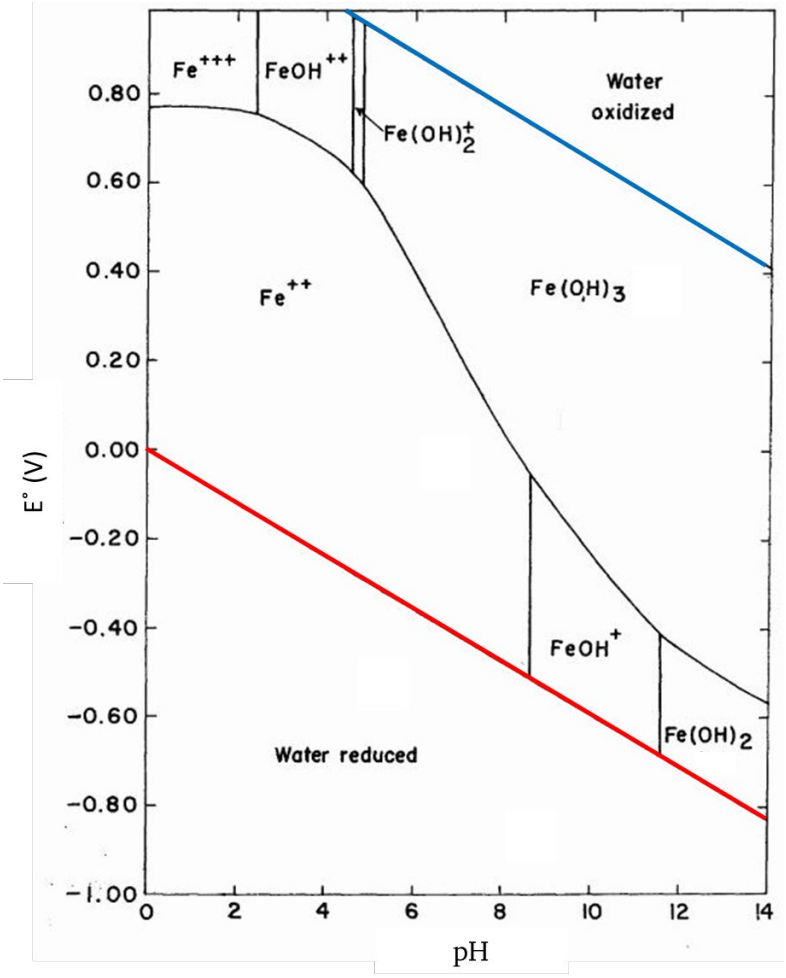

Figure 2: Stability-field diagram of iron species present in aqueous solution from pH 0 to pH 14 as a function of standard electrode potential.

Shown are the iron species present at different pH values in aqueous solution, namely soluble Fe^{3+}, Fe^{2+}, $FeOH^{2+}$, $Fe(OH)_2^+$ and $FeOH^+$, and solid $Fe(OH)_3$ and $Fe(OH)_2$ as a function of the standard electrode potential E° in V, whereas the stability field is restricted to the area at which water is stable and not being reduced to hydrogen (bottom boundary, labeled in red) or oxidized to oxygen (top boundary, labeled in blue). Solid black lines represent the equilibrium state between two neighbored species for an iron concentration of 2×10^{-7} mol/kg, whereas the horizontal lines were determined from the electrochemical equilibria and the vertical lines were derived from the chemical equilibria. The graphical plot was taken and slightly modified from Hem *et al.* 1959.[73]

To overcome the insolubility of ferric ions in neutral aqueous solution and to avoid the formation of ROS due to iron redox cycling, soluble ferrous and ferric ion species can be obtained by strong complex formation that also allows organisms to have iron accessibility.[74,75] The resulting Fe^{3+}/Fe^{2+} electrode potentials of the iron complexes cover a wide range from -0.5 V to +0.6 V, that are present and relevant within biological systems, demonstrating the extreme variability of iron in organisms.[76]

1.3.2 Iron coordination chemistry

Coordination compounds, also known as complexes, are a type of chemical compounds, whereby a charged or uncharged central atom, mostly a transition metal, is coordinatively bound to one or more charged or uncharged non-metallic atoms, the so-called ligands. Contrary to the covalent bond, whereby the electron pair consists of two electrons with one coming from each of the binding partners, the coordination bond is formed by one pair of electrons coming solely from the ligand. Thereby, the lone electron pair of the ligand, which is the electron donor, overlaps with an empty orbital of the electron acceptor, the central atom. Depending on the number of free orbitals within a metal that are used for the binding, the coordination number of the complex is given.[66,77] For Fe^{2+} and Fe^{3+}, the most preferred coordination number is six resulting in an octahedral conformation, whereby the ligand causes the five 3d orbitals to split into two different energy levels, with three orbitals ($3d_{xy}, 3d_{yz}, 3d_{xz}$) having a lower energy than the other two ($3d_{x^2-y^2}, 3d_{z^2}$). The electron occupation within the 3d orbital of the metal upon the ligand binding then determines the type of the complex. In case the electrons are spin paired and thus causing empty 3d orbitals ($3d_{x^2-y^2}, 3d_{z^2}$) that are able to take up electrons of the ligand, low-spin complexes are formed. In case there is no electron spin pairing taking place and the overlap of an outer d-orbital of the metal with the ligand occurs, high-spin complexes are formed that are kinetically more labile than low-spin complexes (Figure 3). This concept is part of the crystal field theory and can also be used to explain the different colors observed for some complexes, as electronic transitions can occur between the split and partially filled d orbitals.[66,76,78] Examples for a high-spin and low-spin iron complex are hexafluoridoferrate(III) and hexacyanoferrate(III), respectively.[66] In addition to six-coordinated iron complexes, four and five-coordinate iron complexes also exist forming tetrahedral and trigonal bipyramid or square pyramid structures, respectively, whereby the ligand causes again the 3d orbitals to split into different energy levels in a specific manner.[76,78]

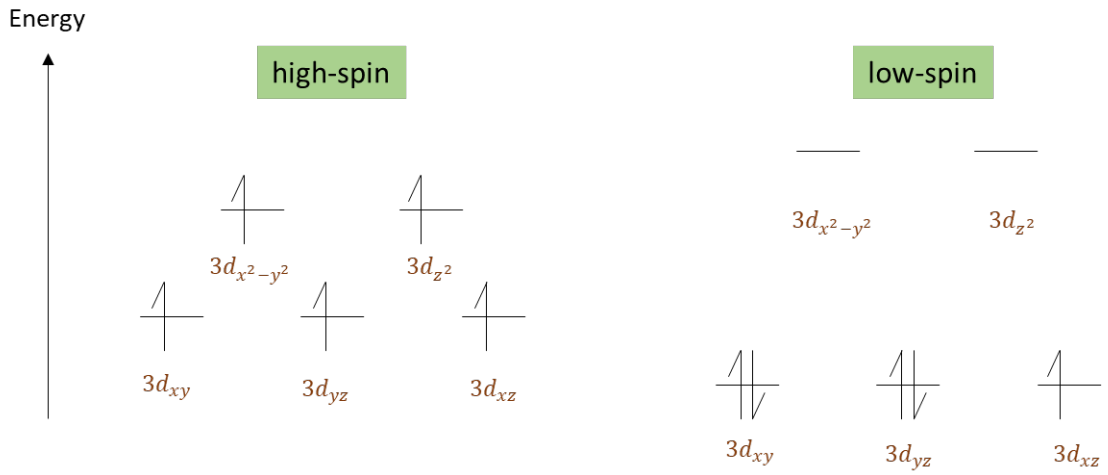

Figure 3: Occupation of the 3d orbitals for d^5 complexes in a high- and low-spin octahedral conformation.

Upon ligand binding to a first-row transition metal, the ligand causes the splitting of the 3d orbitals resulting in three orbitals ($3d_{xy}, 3d_{yz}, 3d_{xz}$) having a lower energy level than the other two orbitals ($3d_{x^2-y^2}, 3d_{z^2}$). Depending on the electron occupation within the 3d orbitals of the metal, two different complexes can be formed. The avoidance of spin pairing and thus a single electron occupation within the orbitals leads to a high-spin complex formation, as a further outer d-orbital needs to be used for overlapping with a filled ligand orbital. Contrary, spin pairing leads to a low-spin complex formation, as the remaining free 3d orbitals can overlap with a filled ligand orbital. The concept is part of the crystal field theory.[66,76,78]

A further characteristic of the complex is described by the denticity of the ligand. Ligands binding with only one free electron pair to the central atom are called monodentate, whereas ligands binding with two, three or six free electron pairs to the atom are called bi-, tri- or hexadentate, respectively, and are also named chelators.[66,77,79] The ligand denticity also contributes to the thermodynamically stability of a complex, which is defined by the complex stability constant K_n for one individual complex formation step (Equation 3), or by the overall stability constant β_n taking all complexation steps into account that lead to the final complex formation (Equation 4).[66,78] Since the size of K_n or β_n is usually large, the use of $\log_{10} K_n$ or $\log_{10} \beta_n$ is more common to use. A higher stability constant defines a more stable complex.[66,77] For instance, the $\log_{10} \beta_n$ constant for an ethylenediaminetetraacetic acid (EDTA) complex with Fe^{2+} is 14.3, whereas the $\log_{10} \beta_n$ value for an EDTA complex with Fe^{3+} is 25.1 indicating the higher stability of the Fe^{3+}-EDTA complex.[80]

Equation 3: Complex stability constant K_n in aqueous solution.

Stability constant K_n defined as the equilibrium constant between the free ligand [L], the free metal or ligand-metal complex $[ML_{(n-1)}{}^m]$ and the ligand-metal complex $[ML_n{}^m]$ concentrations in aqueous solution, with m representing the charge state and n being the number of ligands.[66,77]

$$K_n = \frac{[ML_n{}^m]}{[ML_{(n-1)}{}^m][L]}$$

M: Metal atom
L: Ligand
m: Charge
n: Number of ligands

Equation 4: Overall complex stability constant β_n in aqueous solution.

Overall stability constant β_n defined as the equilibrium constant between the free ligands $[L]^n$, free metal $[M^m]$ and ligand-metal complex $[ML_n^m]$ concentrations in aqueous solution, which is the sum of each individual complex stability constant K_n, leading to the final complex formation, with m representing the charge state and oxidation state of the metal, and n being the number of ligands.[66,77]

$$\beta_n = K_n! = \frac{[ML_n{}^m]}{[M^m][L]^n}$$

M: Metal atom
L: Ligand
m: Charge, which is also the oxidation state of the metal
n: Number of ligands

An additional characteristic that defines the stability of a complex is the ligand affinity to the metal that can be described by using the hard and soft acids and bases (HSAB) concept. By definition, a hard acid, an atom having a high electron density due to a high charge and a small ion radius, and that is rather nonpolarizable, prefers binding to a hard base having similar characteristics. Vice versa, soft acids bind strongly to soft bases since they both have a rather low electron density as they are large in size, having a low charge, and since they are highly polarizable.[77,81] First-row transition metals having a high oxidation state, such as Cr^{3+}, Mn^{2+} and Fe^{3+}, are defined as hard acids. Other metal ions such as Cu^{+}, Ag^{+} and Au^{+} are classed as soft acids.[78,81] However, there also exist borderline cases, whereby the atoms express characteristics lying between the hard and soft acid/base definition. One example is the Fe^{2+} ion, that also prefers forming a complex with borderline bases.[78,81] The HSAB concept also demonstrates that ligands comprise a certain metal selectivity as they have different affinities to different metals. Hence, the stability of a complex varies with different metal or ligand compositions.[80] Furthermore, the ion radius of the metal also impacts the possible denticity a ligand can embrace. A higher ligand denticity is often observed for complexes with smaller metal atoms thus resulting in a higher complex stability. However, also a bulky ligand can impact denticity and the overall coordination number, thus affecting the stability of the complex.[77,82]

Preferred ligands of ferric ion include oxygen-containing groups such as OH^{-}, NO_3^{-} or SO_4^{2-}, whereas ferrous ion favors the coordination with nitrogen and sulfur atoms.[75,83] This preference is also observed within biological systems and defines the function and properties of many iron-containing proteins.

1.3.3 Classes of iron proteins

Within organisms, iron-containing proteins can be categorized in one of three protein types, namely hemeproteins, iron-sulfur cluster-containing proteins, and non-heme and non-iron-sulfur cluster-containing proteins. Each of these protein types share similar characteristics and involve several cellular mechanisms in which the iron mainly switches between the ferrous and the ferric state and thus acts as an important protein cofactor.[62,84]

Hemeproteins consist of a porphyrin molecule with four ring nitrogen atoms the iron ion is coordinated to, whereas one to two further ligands can be bound in axial position to the ion.[62,84] Depending on the protein function, hemeproteins can be further categorized into three sub-classes. Firstly, hemeproteins

involved in oxygen transport and storage belong to the class of oxygen carrier proteins. Prominent examples are hemoglobin and myoglobin, respectively.[84,85] The second sub-class includes proteins that are involved in activating molecular oxygen by converting peroxides into less damaging and less reactive reagents. Representatives of this group are for instance catalases and peroxidases.[62,83] Lastly, proteins that are involved in the electron transport comprise the third sub-class of hemeproteins. This class includes the cytochromes, which are responsible for the electron transfer within the respiratory chain taking place within the mitochondria.[62]

The second type of iron-containing proteins are the iron-sulfur cluster-containing proteins. Within those proteins, iron is coordinated to sulfur that is either part of a cysteine residue of the protein or coming from an inorganic sulfide.[86,87] Depending on the amount of iron and sulfur atoms included in the bonding, different cluster structures can be distinguished. The most simple clusters are the rhombic [2Fe-2S] and the cubane [4Fe-4S] clusters, however, also more complex structures with up to nine Fe-S clusters are known.[87,88] Some iron-sulfur cluster-containing proteins may also additionally contain a heme group.[87] Since the Fe-S-containing proteins comprise a wide range of electrode potentials relevant for biological systems by switching between the ferrous and ferric oxidation state, those proteins are involved in several essential reactions. For instance, Fe-S clusters are present in enzymes involved in enzyme catalysis (e.g. aconitase as part of the citric acid cycle), in enzymes needed for the electron transfer within the respiratory chain (e.g. complex I, II or II), or perform regulatory functions (e.g. iron regulatory protein 1 (IRP1)).[88,89]

Iron-containing proteins that are neither hemeproteins nor belong to iron-sulfur cluster-containing proteins are categorized into the third type of iron-containing proteins. This category also includes several proteins that are involved in iron uptake and export, iron metabolism and iron storage and will be addressed in more detail within the next chapter.[63]

1.3.4 Iron metabolism in mammals

On the one hand, intracellular iron amount within the cell needs to be kept as low as possible to avoid ROS formation but on the other hand, the accessible amount should be as high as needed to ensure and maintain the synthesis of iron-containing proteins needed for essential cellular functions. Therefore, mammalian cells have developed distinct proteins involved in the iron uptake and export, the usage and the storage of iron (Figure 4), as well as evolved tight regulation mechanisms for the expression of those proteins.[90]

Uptake

The main iron uptake route used in most mammalian cell types is the transferrin (Tf)-bound iron uptake pathway. Within the extracellular space, one apo-Tf molecule binds with high affinity two ferric ions

forming the holo-Tf that in turn is recognized by the Tf receptor 1 (TfR1) at the outer cell membrane.[63] Via receptor-mediated endocytosis, the iron-containing TfR1-diferric Tf complex is transported across the cell membrane forming an intracellular vesicle also known as endosome.[91] Due to the acidic milieu within the endosome, ferric ion dissociates from Tf followed by a subsequent reduction to ferrous ion by a ferrireductase enzyme such as the six-transmembrane epithelial antigen of the prostate 3 (STEAP3).[63,92] The final release of ferrous ion into the cytoplasm of the cells takes place by the ferrous ion transporter divalent metal-ion transporter 1 (DMT1), a metal-ion transporter that not exclusively transports iron across cell membranes.[63] Other ions transported by DMT1 include Mn^{2+}, Ni^{2+}, Cu^{2+} or Zn^{2+}.[93] Although DMT1 is the main transporter described, there are also other membrane transporters capable of releasing ferrous ions from the endosome into the cytoplasm such as the Zrt- and Irt-like protein 14 (ZIP14) or the transient receptor potential mucolipin 1 (TRPML1) protein.[94,95] After iron dissociation, the TfR1-Tf complex within the endosome is transported back to the cell surface, where the apo-Tf molecule dissociates from TfR1, is released into the extracellular space and is able to enter another round of Tf-bound iron uptake.[96]

The second major uptake pathway comprises the non-Tf-bound iron (NTBI) uptake route, which is independent of Tf. This uptake mechanism includes the binding of iron to small molecular weight ligands such as citrate or albumin, whereby mainly the ferric ion state dominates.[63,91,97] Although the exact NTBI uptake pathway is not fully characterized, several surface ferrireductases, such as the duodenal cytochrome b (DCYTB), are suggested to be involved in reducing the ferric NTBI into ferrous NTBI that is then transported across the cell membrane through membrane ion transporters.[98] Among those membrane ion transporters are for instance DMT1, ZIP14 or the Zrt- and Irt-like protein 8 (ZIP8).[63,98] Further NTBI uptake routes may involve L-type voltage-dependent calcium channels or the transient receptor potential cation channel subfamily C member 6 (TRPC6) protein.[99,100]

Besides the mentioned active uptake pathways, iron may also enter the cells via passive diffusion, however, charge, size and hydrophobicity of the iron complex immensely impact the efficacy.[80,101]

Utilization

Once iron is taken up into the cells, iron is present in the labile iron pool (LIP) that consists of chelated iron species, predominantly in the ferrous state.[62] The complexes are mainly formed by low-molecular weight compounds such as amino acids, nucleotides or citrate, but also glutathione has been suggested.[90,91,98,102] From the LIP, iron gets delivered to different cellular compartments where the iron is further needed and utilized. The majority of iron is distributed to the mitochondrion for the synthesis of hemeproteins or iron-sulfur cluster-containing proteins that comprise essential biological functions.[103] Iron uptake across the inner mitochondrial membrane is facilitated by the mitochondrial iron transporter mitoferrin (MFRN).[98]

Storage

Aside from the distribution to the different compartments, iron present within the LIP may also be stored as a reserve that the cells can draw on in times of iron limitation.[104] This process is initiated by chaperones such as the poly(rC)-binding proteins (PCBPs), that deliver the iron to the storage proteins, whereby the major one is ferritin.[103] Ferritin consists of 24 subunits of heavy (ferritin H) and light (ferritin L) chains building a cavity that is able to store up to 4000 iron atoms.[104,105] Depending on the proportion of those subunits, cells can adapt to different intracellular situations. A higher ferritin L subunit proportion is suggested to be relevant for iron storage due to iron excess, whereas a higher ferritin H subunit proportion is thought to be relevant in case iron is needed for cellular metabolism.[91] For the incorporation process of iron into ferritin, ferrous ions enter the cavity via a hydrophilic channel, where the oxidation of ferrous to ferric ions takes place due to a ferroxidase activity of ferritin H.[104,106] The oxidized iron is then stored in form of ferric-oxyhydroxide phosphate.[90,91] Re-mobilization of the stored iron is suggested to involve the degradation of ferritin within the lysosomes, however, the exact mechanism is not yet fully understood.[107,108]

Oxidative damage

Under normal conditions, the percentage of iron present within the LIP is rather low.[109] However, an excess of ferrous ions may lead to oxidative damages for the cells due to the formation of uncontrollable amounts of ROS.[62] For instance, ascorbate or nicotinamide adenine dinucleotide phosphate (NADPH) induced lipid peroxide formation caused by iron may result in membrane damage of the mitochondrion, lysosomes or of the endoplasmic reticulum.[110] Furthermore, excessive Fe^{2+} may bind to the negatively charged backbone of the deoxyribonucleic acid (DNA) and may form reactive hydroxyl radicals upon the presence of H_2O_2. Those are able to damage the DNA at the phosphate backbone and the nucleotide bases that eventually may lead to DNA strand breakage.[111]

More recently, ferroptosis, a form of regulated cell death, was reported to be caused by iron-dependent peroxidation of phospholipids with polyunsaturated acyl tails (PL-PUFAs), which is favored upon iron excess.[112–114]

Export

Contrary to the large amount of known proteins involved in iron uptake, up to date, only one mammalian iron exporter is known.[115] Ferroportin (FPN), which is also known as metal transporter protein 1 (MTP1), enables iron to be exported from the cytoplasm and is thus contributing to a well-balanced intracellular iron level.[115,116] Since FPN was observed to require the interplay of an extracellular ferroxidase such as ceruloplasmin (Cp) that oxidizes ferrous to ferric ion, ferrous-containing compounds are likely the main substrates for the exporter.[115] In addition to iron, FPN was reported to also facilitate the export of manganese out of the cells and is thus not exclusively responsible for the iron export.[117]

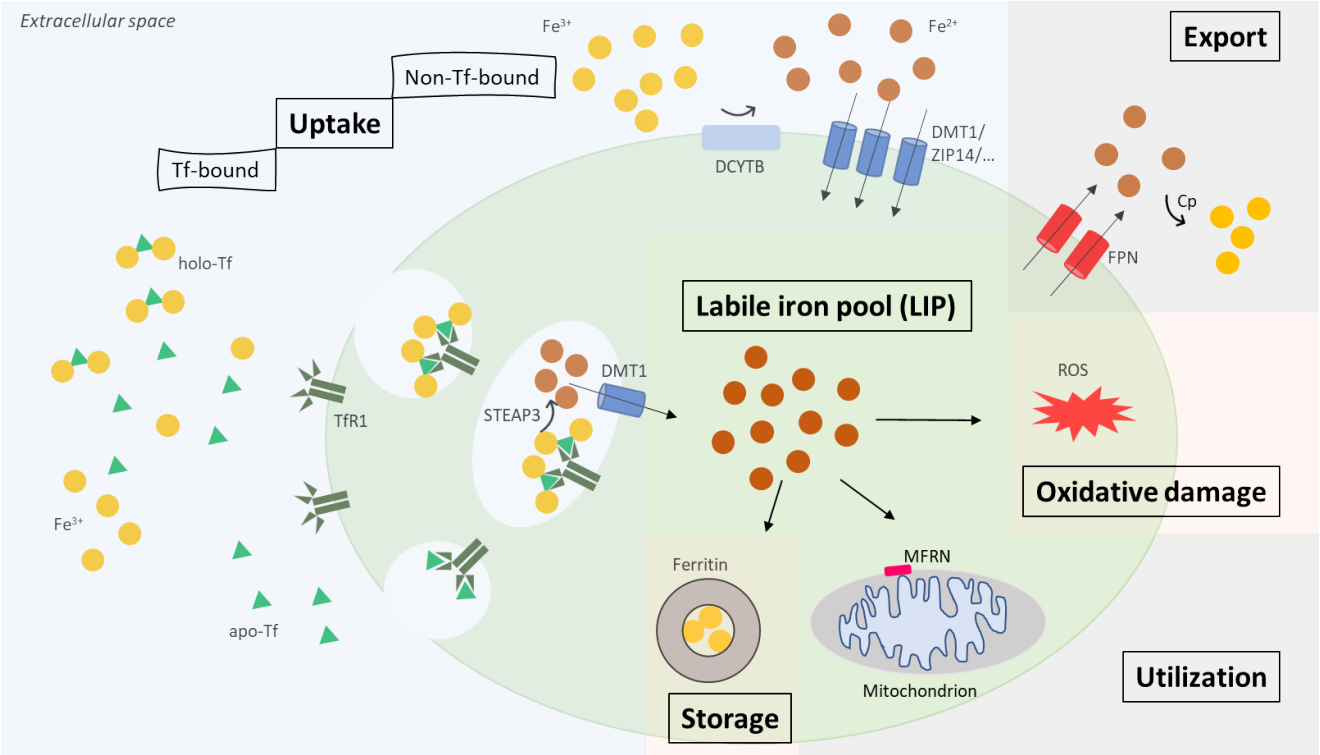

Figure 4: Overview of iron-related mechanisms in mammalian cells.

Iron uptake takes place either via the transferrin (Tf)-bound or the non-Tf-bound iron (NTBI) uptake pathways. For the Tf-bound iron uptake, two ferric ions are bound to Tf that in turn is bound by the Tf receptor 1 (TfR1) located at the outer cell membrane. Via receptor-mediated endocytosis, the iron-containing TfR1-diferric Tf complex is internalized, and the ferric ions are released from the complex due to the acidic milieu present within the endosome. Subsequently, ferric ions are reduced to ferrous ions by the six-transmembrane epithelial antigen of the prostate 3 (STEAP3) enzyme and are released into the cytoplasm via the divalent metal-ion transporter 1 (DMT1). The TfR1-Tf complex is then transported back to the cell surface where it is recycled for further Tf-bound iron uptake cycles. Uptake of NTBI is initiated by the reduction of ferric NTBI to ferrous NTBI by the surface ferrireductase duodenal cytochrome b (DCYTB) prior to the transport into the cytoplasm via either DMT1 or other membrane ion transporter such as Zrt- and Irt-like protein 14 (ZIP14). Once taken up, iron, mainly existent in the ferrous state, is present within the labile iron pool (LIP) from which it can be either stored within ferritin or utilized for the synthesis of iron-containing proteins for which iron mainly enters the mitochondrion via mitochondrial iron transporter mitoferrin (MFRN). Excessive iron present in the LIP may also cause oxidative damage to the cell by forming reactive oxygen species (ROS). Aside from storage and utilization, iron can also be exported via the membrane transporter ferroportin (FPN) that acts in combination with the extracellular ferroxidase ceruloplasmin (Cp).[64,118,119]

Regulation of cellular iron homeostasis

The expression of proteins involved in iron uptake, storage or export can be regulated at different levels.[62] At the transcriptional level, the gene expression of several proteins involved in iron uptake are controlled by the hypoxia-inducible factor (HIF) system. Upon iron deficiency, two alpha subunits of HIF (HIF1α and HIF2α) form a heterodimeric complex together with HIF1β that translocates to the nucleus and binds to the hypoxic response element (HRE) of the target gene regulatory sequence. Due to the binding, the transcription of the respective genes is stimulated. However, at high iron levels, the degradation of HIF2α is initiated by the prolyl hydroxylase (PHD) and thereby prevents the transcription and thus the import of iron.[64,120]

The majority of the cellular iron homeostasis regulation takes place at a post-transcriptional/translational level by IRP1 and iron regulatory protein 2 (IRP2).[62] In case of an iron

deficiency, IRP1 and IRP2 bind to the iron responsive elements (IREs) at either the 5' or 3' untranslated regions (UTRs) of messenger ribonucleic acid (mRNA), targeting the expression of inter alia ferritin and FPN, or TfR1 and DMT1, respectively. The binding results in the formation of a hairpin structure that is decisive whether the translation takes place or not. Hairpin structure formation at the 5' UTR represses the translation of the respective mRNA, whereas binding of IRP1 and IRP2 at the 3' UTR leads to a stabilization of the mRNA and thus permits the translation. An increase in iron uptake is thus induced, while the storage and export of iron is prevented.[64,121,122] Upon iron overload conditions, the IREs stay unoccupied due to the degradation of IRP2 by the F-box/leucine-rich repeat protein 5 (FBXL5) and the functional conversion of IRP1 to cytosolic aconitase upon ligation of an Fe-S cluster. Hence, only mRNAs coding for proteins involved in iron storage and export are translated, while mRNA degradation takes place for unoccupied 3' UTR IREs.[64,122]

Post-translational regulation mechanisms include the previous mentioned control of HIF2α and IRP2 protein levels by PHD and FBXL5, respectively, as well as the control of FPN expression by hepcidin that is able to internalize the exporter upon binding.[62,123]

1.3.5 Iron in cell culture processes

Addition of iron to CCM is crucial for nearly all industrially used cell lines due to the essential cellular functions of iron. Commonly used iron sources in CCM include ferric ammonium citrate (FAC), ferric citrate (FC), ferric nitrate ($Fe(NO_3)_3$) or ferrous sulfate ($FeSO_4$) as disclosed in several patents and publications.[124–128]

Altering the iron concentration within CCM can impact cell performance and final CQAs of the product. An overall improved cell growth and productivity for a CHO cell culture was observed upon increasing iron concentrations[127,129], however, other studies demonstrated an iron-related effect on CQAs. For instance, elevated iron levels in CHO CCM were shown to correlate with increased color formation and an increased acid charge variant level of the recombinantly produced proteins, whereby both effects are likely to be caused by iron-related oxidation effects due to the formation of ROS.[130,131] Iron-mediated ROS production was also shown to be responsible for an increased protein aggregation level, for example in neuronal or lens crystallin proteins.[132,133] Additionally, iron was also identified to impact and influence the recombinant protein glycosylation profile. An increased site-occupancy of the glycoprotein tissue plasminogen activator was reported upon the addition of iron to CCM and thereby affecting the glycosylation macroheterogeneity.[54] Furthermore, iron citrate addition to the medium was reported to stabilize macroheterogeneity of interferon gamma (IFN-γ) glycosylation due to a resulting constant glycosylation pattern, whereas an increased level of non-glycosylated IFN-γ was observed for the non-supplemented version.[134] Moreover, within the US Patent No. 9598667B2, iron was demonstrated to cause a significant increase in glycoprotein galactosylation when added to CCM.[135]

2 Objective

Iron is an essential component needed within CCM to support cellular growth and recombinant protein production. However, iron excess can lead to the formation of ROS that may cause severe cellular damages. The objective of this study was thus to investigate the impact of iron on CHO cell metabolism, on CQAs of the recombinant produced proteins and on intracellular iron levels, as well as to study the impact of iron on certain mRNA expression levels.

In order to determine changes in intracellular iron level, the first part of this study aimed to develop a method for detecting either changes in total intracellular iron amount or changes within the LIP. In particular, a colorimetric assay for evaluating total intracellular iron amounts was adapted from literature and further developed and established, whereas several (fluorescent) probes were studied for their potential to detect differences in LIP concentration upon flow cytometry usage.

The second part of this study focused on the impact of iron in CCM in fed-batch processes, whereby different iron concentrations and iron sources were investigated for different CHO cell lines. Therefore, cell culture parameters, recombinant protein product quality attributes, namely aggregation, glycosylation and oxidation profiles, as well as intracellular iron changes were evaluated and analyzed. Additionally, mRNA expression levels of genes involved in iron uptake and transport, storage and export were evaluated.

In a last section, the impact of iron raw material impurity on cell performance and CQAs in a CHO fed-batch medium platform was studied, which was a continuation of the work that has been already published in *Biotechnology Progress* in 2021[136] as part of this underlying PhD thesis project.

3 Material and Methods

3.1 Materials

3.1.1 General chemicals and reagents

Dimethyl sulfoxide (DMSO)	Sigma Aldrich
Ethanol 96%	Merck KGaA
Hydrochloric acid (HCl) solution 1 M	Merck KGaA
Hydrochloric acid (HCl) solution 25%	Merck KGaA
Phosphate-buffered saline (PBS) 10X	ThermoFisher Scientific
Sodium hydroxide (NaOH) solution 2 M	Merck KGaA
Sodium hydroxide (NaOH) solution 50%	Merck KGaA
Spectroquant® Iron Test	Merck KGaA

3.1.2 Iron sources with chemical structures drawn with Marvin Sketch

Ferric ammonium citrate (FAC) — Merck KGaA

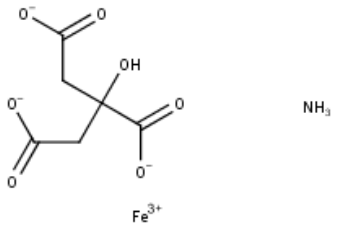

Ferric chloride ($FeCl_3$) hexahydrate — Merck KGaA

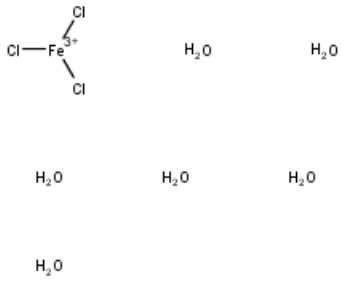

Ferric citrate (FC) — Merck KGaA

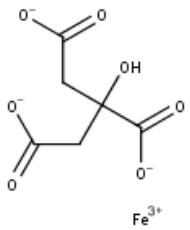

Ferric sodium citrate (F(III)SC)	Dr. Paul Lohmann

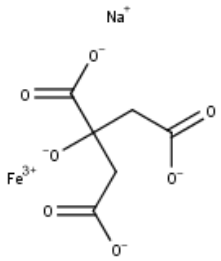

Ferrous chloride ($FeCl_2$) tetrahydrate	Alfa Aesar

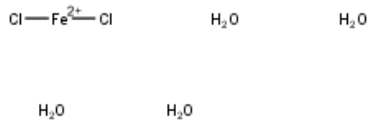

Ferrous sodium citrate (F(II)SC)	Dr. Paul Lohmann

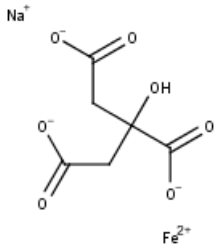

Ferrous sulfate ($FeSO_4$) heptahydrate	Merck KGaA

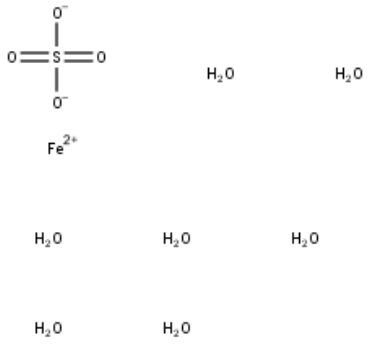

3.1.3 Cell lines

CHO K1 cell lines	Merck KGaA
CHOZN® cell line	Merck KGaA

3.1.4 CCM platforms

Cellvento® 4CHO	Merck KGaA
Cellvento® 4Feed	Merck KGaA

EX-CELL® Advanced CHO Fed-Batch-Medium	Sigma Aldrich
EX-CELL® Advanced CHO Feed 1	Sigma Aldrich

3.1.5 Chemicals for cell culture and fed-batch experiments

Copper (II) sulfate pentahydrate	Sigma Aldrich
D-(+)-Glucose	Merck KGaA
Glutamine	Merck KGaA
HT-supplements (100X or 50X)	ThermoFisher Scientific
Manganese (II) chloride	Merck KGaA
MSX	Sigma Aldrich
Puromycin	Merck KGaA
Sodium bicarbonate	Merck KGaA
Sodium molybdate (VI) dihydrate	Merck KGaA
Tin (II) chloride dihydrate	Merck KGaA

3.1.6 Chemicals, reagents and kits for antibody purification and CQA analyses

Acetonitrile (ACN)	Merck KGaA
AdvanceBio 8-aminopyrene-1,3,6-trisulfonic acid (APTS) trisodium Bracketing standard, DP2 and DP15	Agilent Technologies
AdvanceBio APTS Maltodextrin ladder	Agilent Technologies
Ammonium bicarbonate	Sigma Aldrich
Citric acid monohydrate	Merck KGaA
Di-sodium hydrogen phosphate, anhydrous	Merck KGaA
Dithiothreitol (DTT)	ThermoFisher Scientific
Formic acid	ThermoFisher Scientific
GlykoPrep®-plus N-glycan with APTS	Agilent Technologies
N-linked carbohydrate separation buffer	AB Sciex
PBS tablets	Merck KGaA
ProteaseMAX™ surfactant solution	Promega
Sodium chloride	Merck KGaA
Sodium dihydrogen phosphate, monohydrate	Merck KGaA
Sodium perchlorate, monohydrate	Merck KGaA

Trifluoracetic acid (TFA)	ThermoFisher Scientific
Tris(hydroxymethyl)aminomethane	Merck KGaA
Trypsin Gold, Mass Spectrometry Grade	Promega

3.1.7 Chemicals for ferrozine-based assay

Ammonium acetate	Sigma Aldrich
CytoBuster™ Protein Extraction Reagent	Merck KGaA
Ferrospectral (=ferrozine)	Merck KGaA
L-ascorbic acid	Sigma Aldrich
Neocuproine	Sigma Aldrich
Potassium permanganate ($KMnO_4$)	Merck KGaA

3.1.8 Chemicals, antibodies and kits for flow cytometry

2,2'-Bipyridyl (BPY)	Sigma Aldrich
Anti-Puromycin, clone 12D10, Alexa Fluor® 488 Conjugate Antibody	Sigma Aldrich
BD Cytofix/Cytoperm Kit	BD Biosciences
BioTracker 575 Red Fe2+ Dye (=RhoNox-1)	Sigma Aldrich
Calcein-acetoxymethyl (Calcein-AM)	Signa Aldrich
Deferiprone (DFP)	Ark Pharma
Mouse IgG2a kappa Isotype Control (eBM2a), Alexa Fluor® 488, eBioscience™	ThermoFisher Scientific
Puromycin, Dihydrochloride	Sigma Aldrich
Salicylaldehyde isonicotinoylhydrazone (SIH)	Finetech Industry Limited
TRX-PURO	Adam R. Renslo lab, UCSF

3.1.9 Primers, reagents and kits for mRNA analysis

Diethyl pyrocarbonate (DEPC)-Treated Water	ThermoFisher Scientific
RNAlater™ ribonucleic acid (RNA) Stabilization Reagent	Qiagen
RNase-Free DNase Set	Qiagen
RNeasy® Mini Kit	Qiagen
TaqMan™ Fast Universal PCR Master Mix (2X), No AmpErase™ UNG	ThermoFisher Scientific

TaqMan™ Gene Expression Assay Mix (20X)	ThermoFisher Scientific
Cybrd1 (Mm01335929_m1)	
Fth1 (Cg04450260_g1)	
Ftl (Cg04641275_g1)	
Gapdh (glyceraldehyde 3-phosphate dehydrogenase) (Cg04424038_gH)	
Pcbp1 (Cg04619637_s1)	
Slc11a2 (Cg04548732_m1)	
Slc39a14 (Cg04456222_m1)	
Slc40a1 (Cg04543215_m1)	
Tfrc (Cg04423853_m1)	
TaqMan™ Reverse Transcription Reagents	ThermoFisher Scientific

3.1.10 Consumables

96-deepwell block	Mettler Toledo
Acclaim™ PepMap™ trap column, 100 μm x 2 cm, NanoViper	ThermoFisher Scientific
Centrifuge tubes, Falcon® (15 ml, 50 ml)	Corning Life Science
Combitips® advanced (several sizes)	Eppendorf
Corning® 96-well ultraviolet (UV)-transparent microplates	Corning Life Science
Eppendorf serological pipettes	Eppendorf
Eppendorf tubes® (1.5 ml and 2 ml)	Eppendorf
LCGC Certified Clear Glass 12 x 32 mm Screw Neck Vial	Waters
MicroAmp™ Fast Optical 96-Well Reaction Plate	ThermoFisher Scientific
MicroAmp™ Optical Adhesive Film	ThermoFisher Scientific
Microcentrifuge tubes with flat screw caps	Avantor®
nanoEase™ M/Z Peptide CSH C18 column	Waters
N-CHO (Polyvinyl alcohol (PVA) coated) capillary	AB Sciex
Non-Stick RNase-Free 1.5 ml Microfuge Tubes	ThermoFisher Scientific
Nunc™ 96-Well microplates	ThermoFisher Scientific
PCR 8-tube strips	VWR
PCR Microvials	AB Sciex
Pipette tips (several sizes)	Eppendorf
Protein A PhyTips® columns (20 μl, 40 μl, 80 μl, 160 μl)	PhyNexus

Rectangular cells 10 mm	Merck KGaA
Stericup® Quick Release-GP sterile vacuum filtration systems	Merck KGaA
Steriflip® filter units	Merck KGaA
Syringe filters (0.2 μm pore size, polyethersulfone (PES) membrane)	Avantor®
TruView™ LCMS Certified Vials	Waters
TSK gel SuperSW series column	Tosoh Bioscience
TubeSpin® Bioreactor 50	TPP
Universal Vial Cups	AB Sciex
Universal Vials	AB Sciex

3.1.11 Equipment

Acquity ultra-performance liquid chromatography (UPLC)	Waters
Applied Biosystems 7500 Fast Real-Time PCR System	ThermoFisher Scientific
Bravo Automated Liquid Handling Platform	Agilent Technologies
Cedex Bio HT	Roche
Centrifuge 5430 R	Eppendorf
Centrifuge Allegra TM X-22R	Beckman Coulter
CESI 8000 Plus	AB Sciex
Cryoscopic osmometer, Osmomat®	Gonotec
Electronic balance Q-Stat	Sartorius
EnVision 2104 Multilabel Reader	PerkinElmer
EZ-Stream™ Pump, Vacuum pump	Merck KGaA
Incubator, Climo-Shaker ISF4-XC	Kuhner
IntelliCyt® iQue3 Screener PLUS - VBR	Sartorius
Laboratory Fume Hood	Waldner
Liquid nitrogen tank, 1500 Series-190	German Cryo
Magnetic stirrer	Thermo Electron Corporation
Manual multichannel pipette (several sizes)	Eppendorf
Manual single channel pipette (several sizes)	Eppendorf
Milli-Q® Advantage A10 water purification system	Merck KGaA
MiniAmp Plus Thermal Cycler	ThermoFisher Scientific

Multipette® E3/Multipette® E3x	Eppendorf
NanoDrop™ One Microvolume UV/VIS Spectrophotometer	ThermoFisher Scientific
pH-Meter Seven Excellence Multiparameter	Mettler Toledo
Pipetboy	Avantor®
Plate shaker	BMG Labtech
PTR-60, Multi-Rotator	Grant Instruments
Q-ToF Impact II™ equipped with CaptiveSpray™ source	Bruker
Rainin E4 XLS electronic multichannel pipette	Mettler Toledo
Shaking water bath SW23	JULABO
Spectroquant® Prove 600, UV/VIS Spectrophotometer	Merck KGaA
SpeedVac SPD1030	ThermoFisher Scientific
Sterile bench: HerasafeTM KS EN12469: 2000, class II safety cabinet	ThermoFisher Scientific
Thermo Scientific™ Forma™ High-Performance Chromatography Refrigerator	ThermoFisher Scientific
ThermoMixer® C	Eppendorf
UltiMate™ 3000 RSLCnano System	ThermoFisher Scientific
Ultrasonic Cleaner USC-THD/HF	VWR
Vi-Cell™ XR 2.06.3	Beckman Coulter
Vortex Shaker	VWR

3.1.12 Software

7500 Software 2.3	ThermoFisher Scientific
Byonic™ 3.1	Protein Metrics
Cedex Bio HT Application Software 5.1.1	Roche
CESI 8000 Plus Main 10.3.20 with 32 Karat Software 10.3	AB Sciex
Empower™ 3 Software 7.30	Waters
EnVision 1.14	PerkinElmer
GraphPad Prism 9.1.2	GraphPad
iQue Forecyt® Enterprise Client Edition 8.1 (R3)	Sartorius
MarvinSketch 18.22.2	ChemAxon
Mendeley Desktop 1.19.8	Elsevier
Microsoft Office 365	Microsoft Corporation

Progenesis® QI for proteomics 4.2	Waters
Protein Sample Prep Workbench 2.0.0 with VWorks Automation Control software 11.4.	Agilent Technologies
Vi-CELL™ XR 2.06.3	Beckman Coulter

3.2 Methods

3.2.1 Iron stock preparation

Iron solutions were prepared by dissolving the iron sources in Milli-Q® water for at least 30 minutes targeting final iron stock solution concentrations of 5 mg Fe/L. In case of poor solubility, the Milli-Q® water was additionally heated up to 75°C during the dissolution step. The dissolved stocks were then filtered by using 0.2 μm pore size PES membrane syringe filters. The actual iron concentrations were determined using the Spectroquant® Iron Test in combination with the Spectroquant® UV/VIS spectrophotometer, which is able to detect iron concentrations between 0.05 and 5.00 mg Fe/L. Therefore, the dissolved and filtered iron stocks were diluted 1:2000 and 5 ml of each of those solutions were then mixed with 3 drops of Fe-1 reagent consisting of ascorbic acid and a triazine derivative. Upon mixing, ferric ions were reduced to ferrous ions forming a red-violet complex that was then determined spectrophotometrically at 565 nm after 20 minutes of incubation at room temperature (RT).

3.2.2 Cell culture and fed-batch experiments

3.2.2.1 Cell lines

Cell culture experiments were performed with two different CHO K1 cell lines and one CHOZN® clone producing either two different recombinant IgGs or a fusion protein, respectively. The underlying selection principles of the used CHO K1 cell lines were either based on a puromycin resistance (cell line 1) or on a GS overexpression (cell line 2) allowing the growth of successfully transfected cells in either puromycin- or GS inhibitor MSX-containing medium, respectively. For the CHOZN® clone, GS knockout cells were used as a host so that only recombinant cells co-transfected with GS gene were able to survive in glutamine-free medium upon selection process.

3.2.2.2 Medium and feed preparation

CHO K1 cell lines and the CHOZN® clone were cultivated in the chemically defined Cellvento® 4CHO and 4Feed fed-batch platform. Therefore, iron-deficient Cellvento® 4CHO medium was dissolved in 80% of the final volume Milli-Q® water for 30 minutes, whereas 4 - 8 mM glutamine, 1X HT supplements and optionally 5 mg/L puromycin (cell line 1) or 25 μM MSX and 1X HT supplements (cell line 2) were added additionally. After fully dissolved, 2 g/L sodium bicarbonate were added and the CCM was further stirred for 10 minutes. Then, pH was adjusted to 7.0 ± 0.3 and the iron stock solution was added at its desired concentration to the CCM. Finally, volume was filled up to final volume with Milli-Q® water and osmolality was determined to confirm a value of 310 ± 30 mOsmol/kg. Feed was prepared by adding Cellvento® 4Feed to Milli-Q® water while stirring for 30 minutes until fully dissolved. Then, final volume was adjusted, and the pH was set to 7.0 ± 0.3. Osmolality was measured to confirm a value of 1220 ± 50 mOsmol/kg.

CHOZN® clone was also cultivated in the EX-CELL® Advanced CHO Fed-Batch-Medium platform. Medium was prepared by dissolving the iron-deficient powder in 80% final volume Milli-Q® water for 15 minutes. Subsequently, pH was adjusted to 5.0 and stirred for further 5 minutes before 1.9 g/L sodium bicarbonate were added. After stirring for further 30 minutes, pH was adjusted to 7.2 ± 0.1, iron stock solution was supplemented at its desired concentration and Milli-Q® water was added to reach the final volume. Osmolality was determined to confirm a value of 300 ± 20 mOsmol/kg. For the feed preparation, the powder was added to 80% final volume Milli-Q® water for 30 minutes. Then, pH was adjusted to 9.5 ± 0.1 while stirring for further 10 minutes. Subsequently, a final pH of 8.5 was adjusted and Milli-Q® water was added to reach the final volume.
All media and feed solutions were filtered after preparation by using a 0.22 μm filter unit and were stored at 4°C light-protected until further usage.

3.2.2.3 Cultivation

Cultivation of the used cell lines was started by thawing the respective cryovial containing 1 x10^7 cells at 37°C in the water bath after removing it from a liquid nitrogen tank used for long-term storage. Subsequently, the cells were transferred into a 50 ml spin tube with vented cap containing 10 ml of the respective medium. Cells were then centrifuged at 1200 rpm (277 g) for 5 minutes, the supernatant was discarded, and the cell pellet was resuspended in 30 ml of the respective CCM. The cells were then cultivated at 37°C, 5% CO_2, 80% humidity and at a rotation speed of either 320 rpm (CHO K1 cell lines and CHOZN® clone in Cellvento® 4CHO platform) or 230 rpm (CHOZN® clone in EX-CELL® Advanced CHO Fed-Batch-Medium platform). Subcultivation took place three times a week with a seeding density of either 2 x10^5 cells/ml in case the next subculture step was 3 days later, or 3 x10^5 cells/ml in case the next subculture step was performed already after 2 days. Therefore, cell concentration was determined with the Vi-Cell™ XR 2.04 cell counter and the required volume of the pre-culture was added to fresh CCM reaching again a final volume of 30 ml.

3.2.2.4 Fed-batch experiments

Fed-batch experiment conditions were similar to the cultivation conditions, whereby the fed-batch process was initiated by seeding a starting cell amount of 2 x10^5 cells/ml in a total starting volume of 30 ml independently of the used cell line. Feed (v/v) was then added on day 3, 5, 7, 10, 12, 14 as presented in Table 2. Glucose (400 g/L) was added on demand to maintain a glucose level of up to 6 g/L during the week and up to 11 g/L over the weekend. During the course of the fed-batch processes, viable cell density (VCD) and viability were measured with the Vi-Cell™ XR 2.04 cell counter, whereas other small molecules and proteins present within the supernatant such as glucose, titer, iron and ammonium were analyzed by using the Cedex Bio HT after centrifugation of the samples at 4500 rpm (2287 g) for

5 minutes. For determining CQAs of the recombinantly produced proteins, further supernatant samples were taken on day 7, 10 and 12 of the fed-batch processes and stored at -20°C until further usage. In case the intracellular iron amount was studied, cell pellet samples were taken on day 0, (3), (5), 7, 10 and 12. Therefore, 1 x10^7 cells were taken, centrifuged at 1200 rpm (277 g) for 5 minutes and washed two times in 1 ml PBS. Subsequently, cell pellets were flash frozen in liquid nitrogen for around 15 seconds and transferred to -80°C for long-term storage until further used for analysis. For studying the mRNA expression levels of certain genes involved in iron homeostasis, cell samples were additionally taken on day 0, (3), (5), 7, 10 and 12. Therefore, 1 x10^7 cells were taken, centrifuged at 1200 rpm (277 g) for 5 minutes, resuspended in 1.5 ml RNAlater™ RNA Stabilization Reagent solution and stored at -20°C until further analysis.

Table 2: Feeding strategy applied for the CHO K1 cell line 1 and the CHOZN® clone in fed-batch experiments.

Feed was added on day 3, 5, 7, 10, 12 and 14 of the fed-batch processes, whereby different feeding schemes were applied for the different medium platforms, namely Cellvento® 4CHO and EX-CELL® Advanced CHO Fed-Batch-Medium.

% v/v	Day 3	Day 5	Day 7	Day 10	Day 12	Day 14
CHO K1 cell line 1 and CHOZN® clone in Cellvento® 4CHO platform	1.5	3	3	3	3	3
CHOZN® clone in EX-CELL® Advanced CHO Fed-Batch-Medium platform	5	5	5	5	5	5

3.2.3 Antibody purification and CQA analyses

3.2.3.1 Antibody purification

Antibodies and fusion proteins were purified with protein A PhyTips® according to the manufacturer's protocol. Briefly, in a first step, the protein A-containing gel within the spire of the PhyTips® was equilibrated by applying PBS. Subsequently, the sample load took place for which varying amounts of aliquots were loaded depending on the available sample volume and concentration, which both determined the used tip size. After sample loading, two wash steps were performed with a low (PBS) and a high salt-containing (140 mM NaCl) wash buffer for removing all unbound residual matrix from the gel. Finally, the target protein was eluted by applying an acidic elution buffer consisting of 30 mM citric acid adjusted to pH 3. In order to avoid protein denaturation due to the acidic elution buffer, neutralization buffer consisting of 0.375 M Tris adjusted to pH 9.0 was added additionally. Concentration of the purified samples was then determined spectrophotometrically using the NanoDrop™ before stored at -20°C until further usage.

3.2.3.2 Aggregation analysis

Aggregation profile determination of the recombinantly produced antibody and fusion protein was performed by size-exclusion chromatography coupled to an UV detector (SEC-UV) using an Acquity UPLC and a TSK gel SuperSW series column at RT. Therefore, previously purified samples were adjusted to a final concentration of 1 mg/ml with storage buffer consisting of 85% (v/v) elution buffer and 15% (v/v) neutralization buffer. Then, 10 μl of the sample, that were loaded to a LCGC Certified Clear Glass 12 x 32 mm Screw Neck Vial, were applied to the system at a flow rate of 0.35 ml/min, whereas 0.05 M sodium phosphate, 0.4 M sodium perchlorate solution adjusted to pH 6.3 was used as the mobile phase. After separation, proteins were detected by a photodiode array optical detector detecting the UV signal at 214 nm at which the protein peptide bond is absorbing. Data analysis was performed with Empower 3 software by applying a horizontal baseline integration allowing to determine the relative peak area in % of the aggregates.

3.2.3.3 Glycosylation analysis

Glycosylation profile analysis of the mAb was performed by capillary gel electrophoresis with laser induced fluorescence (CGE-LIF). Therefore, samples were first prepared by using the GlykoPrep®-plus N-glycan with APTS kit in combination with the Bravo Automated Liquid Handling Platform, which was used according to the manufacturer's protocol. Briefly, the purified antibody was denatured and immobilized on a resin, followed by the glycan release from the antibody due to N-Glycanase® (PNGase F) digestion. After a drying step using a vacuum centrifuge (SpeedVac SPD1030), glycans were fluorescently labelled with APTS for 60 minutes at 50°C, followed by a cleaning step removing excessive dye. Glycan analysis was then performed using the CESI 8000 Plus with a laser-induced fluorescence detector (λ_{ex}: 488 nm and λ_{em}:520 nm). Therefore, 100 μl sample were mixed with 5 μl APTS Bracketing standard, DP2 and DP15, and the mixture was then transferred to a 200 μl PCR Microvial that was then placed into an Universal Vial to which an Universal Cap was placed on top. Separation of the samples was performed in a N-CHO (PVA coated) capillary filled with N-linked carbohydrate separation buffer (total length: 50.2 cm, inner diameter: 50 μm). The used protocol comprised the following steps. First, the capillary surface was rinsed with separation buffer at 30 psi for 3 minutes followed by pressure injection of the sample at 0.5 psi for 12 seconds. Subsequently, the capillary tip was cleaned by applying a dipping step for 0.2 minutes. Then, the actual separation took place at 23 kV for 20 minutes with a 0.17 minutes ramp applying reverse polarity. Inlet and outlet buffer vials were changed every 20 cycles. Peaks were then identified by using the CESI 8000 Plus and 32 Karat software. Therefore, a valley-to-valley peak integration was performed with the following parameters allowing to determine the relative peak area in % of each glycan species: peak width: 0.1, threshold: 500, minimum area: 1000, shoulder sensitivity: 10000.

In contrast, fusion protein glycosylation profile was determined by UPLC coupled to a mass spectrometer (UPLC-MS) using GlycoWorks™ RapiFluor-MS™ N-Glycan Kit as described elsewhere[137], which was done in-house by the Biomolecule Analytics laboratory.

3.2.3.4 Oxidation analysis

Oxidation analysis of the fusion protein was performed by nanoscale liquid chromatography coupled to a tandem mass spectrometry (nanoLC-MS/MS) using an UltiMate™ 3000 RSLCnano System with an Acclaim™ PepMap™ trap column and a nanoEase™ M/Z Peptide CSH C18 column coupled to Q-ToF Impact II™ equipped with a CaptiveSpray™ source after enzymatic digestion of the samples. Therefore, 7 μl of the sample adjusted to 0.285 ng/μl in 25 mM citric acid, 56 mM Tris HCl and adjusted to pH 5.6 were mixed with 1 μl of 500 mM ammonium bicarbonate solution. Then, proteins were denatured and reduced by adding successively 1 μl of 1% ProteaseMAX™ surfactant solution and 1 μl of 250 mM DTT, respectively. Samples were then incubated at 37°C for 30 minutes. Subsequently, excessive alkylating reagent was quenched by adding 1 μl of 250 mM DTT and 86 μl of 50 mM ammonium bicarbonate solution. For the enzymatic digestion, 1 μl of 0.2 μg/μl trypsin solution were added to the sample and incubated at 37°C for 3 hours. The reaction was stopped by adding 1 μl formic acid. After a centrifugation step, 50 μl of the sample supernatant were then transferred into TruView™ LCMS Certified Vials containing 50 μl of 4% ACN and 0.2% TFA. 10 ng of the sample were then injected and analyzed by nanoLC-MS/MS. The respective parameters for LC and MS performance are listed in Table 3.

Table 3: NanoLC-MS/MS parameters for determining the peptide oxidation level of fusion protein.

Listed are the main parameters for LC, MS and MS/MS performance.

LC parameters			
Loading pump flowrate	5 μl/minutes		
Nano pump flowrate	300 nl/minutes		
Column temperature	40°C		
Gradient	**Retention (minutes)**	**% of 0.1% formic acid**	**% of 80% ACN and 0.1% formic acid**
	0.0	95.0	5.0
	5.0	95.0	5.0
	42.0	60.0	40.0
	45.0	40.0	60.0
	46.0	5.0	95.0
	50.0	5.0	95.0
	50.1	95.0	5.0
	60.0	95.0	5.0
MS parameters			
MS mode	positive		
Capillary voltage	1100 V		
Dry gas	3 L/minutes (180°C)		
MS scan level	2 Hz		
Mass range	50-2200		
Calibration	Lockmass (m/z 1221.9906)		
MS/MS parameters			
MS-MS/MS cycle time	2 seconds		
MS/MS scan level	2 Hz (2500 cts); 5 Hz (15000 cts)		
Active exclusion	ON (exclude after 2 spectra for 0.10 minutes)		
Reconsider precursor	ON (>3)		

Peptide identification was performed by using Byonic software, whereby the oxidized and non-oxidized peptides abundances were extracted by using Progenesis QI software. The oxidation level was then determined by using Equation 5.

Equation 5: Determination of peptide oxidation level of fusion protein.

The peptide oxidation level in % was obtained by dividing the oxidized peptide abundance by the sum of the oxidized and non-oxidized peptide abundances.

$$Oxidized\ peptide\ (\%) = \frac{Oxidized\ peptide\ abundance}{Oxidized\ peptide\ abundance + non\text{-}oxidized\ peptide\ abundance}$$

3.2.4 Method development for detecting intracellular iron

Since the method development for detecting intracellular iron is one major part of the results section, only the basic preparation steps of the different reagents will be described in the following.

3.2.4.1 Colorimetric ferrozine-based assay

For the development of the colorimetric ferrozine-based assay, CHO K1 cell pellets were prepared from a subculture, whereby the desired cell amount was taken and transferred into a new tube. Then, cells were centrifuged at 1200 rpm (277 g) for 5 minutes and washed two times with 1 ml PBS before the cell pellets were flash frozen in liquid nitrogen for around 15 seconds. Subsequently, flash frozen cells were transferred to -80°C and stored until further usage.

$FeCl_3$ stock solution for the iron standards was prepared as already described in chapter 3.2.1. The iron standard working solutions were then prepared in 10 mM HCl. The iron releasing reagent was prepared freshly by mixing equal volumes of 1.4 M HCl with 4.5% (w/v) $KMnO_4$ prepared in Milli-Q® water. For neocuproine, L-ascorbic acid and ammonium acetate, stock solutions with final concentrations of 0.4, 1.5 and 10 M, respectively, were prepared in Milli-Q® water, whereas for neocuproine, additionally 25% HCl solution was added to the stock until fully dissolved (ratio Milli-Q® water/HCl around 4.88). Ferrozine (Figure 5) was dissolved in Milli-Q® water to obtain a stock solution concentration of 0.05 M. The iron detection reagent was then prepared by mixing neocuproine, L-ascorbic acid, ammonium acetate and ferrozine reaching final concentrations of 6.5 mM, 0.9 M, 2.5 M and 6.5 mM, respectively. The iron-ferrozine complex was detected at its absorption wavelength of 550 nm.

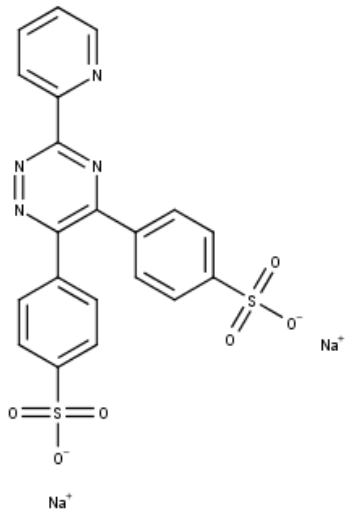

Figure 5: Chemical structure of ferrozine drawn with Marvin Sketch.

3.2.4.2 Flow cytometry for detecting LIP

For the development of a flow cytometry method for detecting LIP present within CHO K1 cells coming from a subculture, several different (fluorescent) probes were tested.

First, the fluorescent probe calcein-AM (Figure 6A) was applied, for which 1 mg calcein-AM was dissolved in DMSO to obtain a final stock concentration of 0.5 mM. Working solutions were prepared by diluting the stock further with PBS. Excitation and emission maxima of the probe were at 494 and 517 nm, respectively. For the used chelators that were used in combination with calcein-AM, namely DFP, BPY and SIH (Figure 6B-D, respectively), the different stock solutions were prepared by dissolving the chelators in PBS, whereby the stock concentrations varied depending on the concentrations tested and applied during the experiment.

As a second fluorescent probe, RhoNox-1 (Figure 6E) was tested. Therefore, 50 μg of the probe were dissolved in DMSO to obtain a final stock concentration of 1 mM. Working solutions were prepared by diluting the stock further with PBS. The excitation and emission maxima of the probe were at 540 and 575 nm, respectively. For determining the fluorescence response of the probe in dependency of increasing iron concentrations, a 5 mM $FeSO_4$ stock solution in Milli-Q® water was prepared from which the working solutions were prepared by diluting the stock further with Milli-Q® water.

Lastly, TRX-PURO (Figure 6F) was tested as an immunofluorescence-based approach for detecting LIP. Therefore, the BD Cytofix/Cytoperm™ Fixation/Permeabilization Kit was used, for which the provided 10X BD Perm/Wash buffer solution was diluted with Milli-Q® water to a 1X solution. The provided BD Cytofix/Cytoperm™ solution was ready to use. TRX-PURO as well as the positive control puromycin were diluted in DMSO to obtain a stock concentration of 1 mM, whereby the working solutions were obtained by diluting the stock further with PBS. The used antibody solutions of either Alexa Fluor® 488

conjugated mouse IgG2a kappa (isotype control) or Alexa Fluor® 488 conjugated mouse anti-puromycin were prepared in 1X BD Perm/Wash buffer.

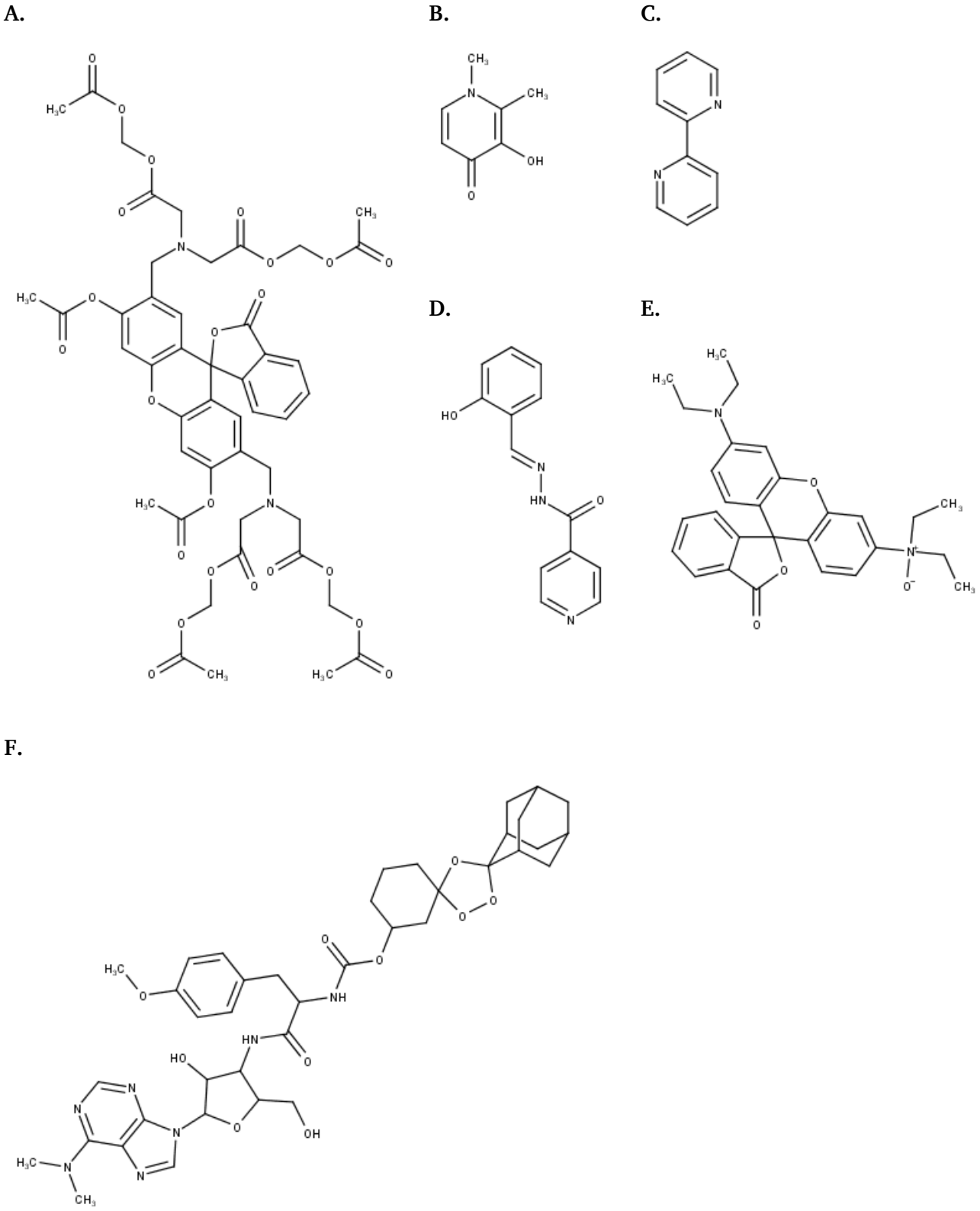

Figure 6: Chemical structures of the fluorescent probes and chelators used for developing a flow cytometry method to determine LIP drawn with Marvin Sketch.

A. Calcein-AM. B. DFP. C. BPY. D. SIH. E. RhoNox-1. F. TRX-PURO.

3.2.5 Intracellular iron determination with HR-ICP-MS

Determination of total intracellular iron amount with high resolution inductively coupled plasma mass spectrometry (HR-ICP-MS) was done in-house by the Element Analytics laboratory. Briefly, a microwave-assisted sample digestion involving nitric acid was performed prior to the iron quantification by standard addition calibration using an ELMENT 2™ HR-ICP-MS (ThermoFisher Scientific). Therefore, appropriate amounts of iron standard solution were spiked to the calibration standards to achieve addition levels similar or close to the amount of iron present in the samples, whereas indium was used as an internal standard.

3.2.6 Iron source characterization

Inductively coupled plasma mass spectrometry (ICP-MS) analysis was done in-house by the Element Analytics laboratory to determine and quantify trace elements within iron sources. Briefly, a microwave-assisted sample digestion involving nitric acid was performed. Elements were then either semi-quantitatively determined involving the adaption of the system response curve as intensity per ng/ml of analyte by a single-point calibration using an ELAN 6000 (PerkinElmer) or a quantification by external calibration using an ELMENT 2™ HR-ICP-MS (ThermoFisher Scientific) was performed. In both cases, a known amount of analyte was spiked to the samples to be able to determine the recovery rate, whereas indium was used as an internal standard for all analyses.[138,139]

3.2.7 mRNA analysis

Evaluation of the mRNA expression level of genes either involved in iron uptake and transport, in iron storage or in iron export (Table 4) was performed by using the TaqMan™ technology. Therefore, RNA was first isolated from cell samples taken during fed-batch experiments with RNeasy® Mini Kit according to the manufacture's instruction from Qiagen. Briefly, cells stored in RNAlater™ RNA Stabilization Reagent solution were further diluted by adding an equal volume of PBS to the solution. Then, the cell samples were centrifuged at 1630 rpm (300 g) for 5 minutes and the supernatant was discarded. Subsequently, cells were lysed and homogenized by adding 600 μl of the provided RLT buffer. Afterwards, 600 μl of 70% ethanol were added to the mixture and the samples were each loaded onto a provided RNeasy spin column placed in a 2 ml collection tube followed by a centrifugation step (9411 rpm (10000 g) for 15 seconds). After discarding the flow-through, 350 μl of the provided RW1 buffer were added onto each column and samples were again centrifuged at 9411 rpm (10000 g) for 15 seconds. Subsequently, an on-column DNase digestion was performed by using a RNase-Free DNase Set. Therefore, 10 μl DNase I stock solution were pre-mixed with 70 μl of the provided RDD buffer before the solution was transferred to the RNeasy spin column followed by an incubation phase of 15 minutes. Then, further 350 μl RW1 buffer were added to the column and samples were centrifuged at

9411 rpm (10000 g) for 15 seconds. Subsequently, the spin column membrane was dried by adding 500 μl RPE buffer and centrifuging at 9411 rpm (10000 g) for 2 minutes, followed by a further centrifugating step at 9411 rpm (10000 g) for 1 minute to fully remove all residuals. After placing the RNeasy spin column into a new RNase-Free Microfuge Tube, the elution step was performed. Therefore, 40 μl RNase-Free water were added to the spin column membrane followed by a centrifugation step (9411 rpm (10000 g) for 1 minute), whereby this elution step was performed twice gaining a final elution volume of 80 μl. The final RNA amount as well as the ratio 260 nm/280 nm were then determined by using the NanoDrop™.

Table 4: Iron-related genes that were analyzed for their mRNA expression level during fed-batch processes.

Listed are the gene names, their respective protein names and a short description of their function in iron homeostasis, whereby they are grouped into iron uptake and transport, iron storage and iron export.

Gene name	Protein encoded by this gene	Function
Iron uptake and transport		
Tfrc	Transferrin receptor 1 (TfR1)	Transport of transferrin (Tf)-bound iron across the cell membrane
Slc11a2	Divalent metal-ion transporter 1 (DMT1)	Transport of non-Tf-bound iron (NTBI) across the cell membrane
Slc39a14	Zrt- and Irt-like protein 14 (ZIP14)	
Cybrd1	Duodenal cytochrome b (DCYTB)	Reduction of ferric to ferrous ions prior to iron uptake
Pcbp1	Poly(rC)-binding protein 1 (PCBP1)	Delivery of iron to the storage protein
Iron storage		
Ftl	Ferritin light chain (ferritin L)	Storage of iron within the cell
Fth1	Ferritin heavy chain (ferritin H)	
Iron export		
Slc40a1	Ferroportin (FPN)	Export of iron from the cytoplasm to the extracellular space

After RNA purification, RNA was converted into complementary DNA (cDNA) by using TaqMan™ Reverse Transcription Reagents, whereby a master mix was pre-pipetted in PCR strips prior to template RNA and DEPC-Treated Water addition to obtain the respective final volume (Table 5). The final mixture was then placed onto a thermocycler and the reaction was initiated (Table 6). Since 1 μg RNA was transcribed, a similar cDNA amount was expected to be obtained.

Table 5: Reagents and volumes required for the reverse transcription of target RNA to cDNA by using TaqMan™ Reverse Transcription Reagents.

Listed are the reagents needed for the reaction and their respective volumes.

Reagent	Volume (μl) for a 20 μl run
Master mix	
10X RT Buffer	2.0
25 mM $MgCl_2$	1.4
10 mM dNTP mix (2.5 mM each)	4.0
RNase inhibitor (20 U/μl)	1.0
MultiScribe™ RT (50 U/μl)	1.0
50 μM random hexamers	1.0
RNA template addition and final volume adjustment	
Template RNA	1 μg or maximal 9.6 μl
DEPC-Treated Water	Up to 20 μl

Table 6: Cycling parameters for the reverse transcription of target RNA to cDNA.

Listed are the four main steps (random hexamers binding, reverse transcription, inactivation and hold) with their respective temperature and time.

Step	Random hexamers binding	Reverse transcription	Inactivation step	Hold
Temperature	25°C	37°C	95°C	4°C
Time	10 minutes	60 minutes	5 minutes	∞

The relative mRNA expression levels were then obtained by applying quantitative polymerase chain reaction (qPCR) using TaqMan™ Fast Universal PCR Master Mix (2X), No AmpErase™ UNG in combination with specific primers (TaqMan™ Gene Expression Assay Mix (20X)) amplifying the gene of interest (GOI). Therefore, a master mix was pre-pipetted and added to a MicroAmp™ Fast Optical 96-Well Reaction Plate before cDNA was added (Table 7). Additionally, for each primer mix, a no-template control and for each template cDNA a no-primer control was prepared to test for DNA and primer contamination within the reagents, respectively. After covering the plate with a MicroAmp™ Optical Adhesive Film, the plate was placed into an Applied Biosystems 7500 Fast Real-Time PCR System and the reaction was initiated (Table 8).

Table 7: Reagents and volumes required for qPCR by using TaqMan™ Fast Universal PCR Master Mix (2X), No AmpErase™ UNG in combination with specific primers (TaqMan™ Gene Expression Assay Mix (20X)).

Listed are the reagents needed for the reaction, namely TaqMan™ Fast Universal PCR Master Mix (2X), No AmpErase™ UNG, specific primers (TaqMan™ Gene Expression Assay Mix (20X)), template cDNA and DEPC-Treated Water, and their respective volumes.

Reagent	Volume (μl) for a 20 μl run
Master mix	
TaqMan™ Fast Universal PCR Master Mix (2X), No AmpErase™ UNG	10.0
TaqMan™ Gene Expression Assay Mix (20X)	1.0
cDNA template addition and final volume adjustment	
Template cDNA	60 ng or maximal 9.0 μl
DEPC-Treated Water	Up to 20 μl

Table 8: Cycling parameters for qPCR using an Applied Biosystems 7500 Fast Real-Time PCR System.

Listed are the three main steps (DNA Polymerase activation + DNA denaturation, DNA denaturation and annealing/extension) with their respective cycle number, temperature and time.

Step	DNA Polymerase activation +DNA denaturation	DNA denaturation	Annealing/extension
Number of cycles	1	40	
Temperature	95°C	95°C	60°C
Time	20 seconds	3 seconds	30 seconds

Data were then analyzed by applying the $2^{-\Delta\Delta Ct}$ method as described by Livak *et al.* 2001.[140] Therefore, obtained cycle threshold (Ct) values of the target gene on day x during the fed-batch process were first normalized against an endogenous control present in the sample on day x that is non-regulated upon any variation during the fed-batch process, namely *Gapdh* (Equation 6A). Similarly, the Ct values for the control condition, namely on day 0 of the fed-batch process, were normalized (Equation 6B). Then, the relative gene expression level of the target gene on day x was calculated by normalizing it against the control (Equation 6C). Finally, the fold change was calculated (Equation 6D), whereby a fold change of at least two-fold was considered as significant for differentially expressed genes.

Equation 6: $2^{-\Delta\Delta Ct}$ method for analyzing the relative mRNA expression level for cell samples taken during a fed-batch process.

A. Normalization of the sample Ct values on day x against an endogenous control (=*Gapdh*) on day x. B. Normalization of the control Ct values on day 0 against an endogenous control (=*Gapdh*) on day 0. C. Calculation of the relative gene expression of the target gene on day x by normalizing it against the control. D. Calculation of the fold change in gene expression. The method was applied according to Livak *et al.* 2001.[140]

A. $$\Delta Ct_{\text{Sample day x}} = Ct\ (\text{target gene})_{\text{Sample day x}} - Ct\ (\text{endogenous control } (=\textit{Gapdh}))_{\text{Sample day x}}$$

B. $$\Delta Ct_{\text{Control}} = Ct\ (\text{target gene})_{\text{Control day 0}} - Ct\ (\text{endogenous control } (=\textit{Gapdh}))_{\text{Control day 0}}$$

C. $$\Delta\Delta Ct = \Delta Ct_{\text{Sample day x}} - \Delta Ct_{\text{Control}}$$

D. $$\text{Fold change} = 2^{-\Delta\Delta Ct}$$

$$(\text{if fold change between 0 and 1: } = -1/(2^{-\Delta\Delta Ct})$$

3.2.8 Data and statistical analysis

Data are expressed as means ± standard deviation (SD), whereby the graphical analysis of the obtained data was performed with GraphPad Prism 9 software. Statistical analysis was done by using the non-parametric Kruskal-Wallis test for multiple-group comparison with subsequent Dunn's test, whereby p-values smaller than 0.05, 0.01 or 0.001 were considered significant.

4 Results and Discussion

4.1 Method development for detecting intracellular iron

4.1.1 Overview

In literature, there are several approaches described for determining either quantitatively the intracellular iron amount or qualitatively the amount of iron present within the LIP by either colorimetric methods or by using fluorescent probes, respectively.[141]

Colorimetric assays are based on the usage of chromogenic chelators able to complex with mostly ferrous ions for which a reducing environment needs to be provided to favor the presence of ferrous ions over the ferric ones. Upon complexation, the metal-ligand complex then turns into a visible color that can be easily detected with spectrometers or microplate readers and the results can be compared to a prepared iron standard.[141] Among the chelators are for instance 4,7-diphenyl-1,10-phenanthroline, also known as bathophenanthroline, disodium;5-[3-pyridin-2-yl-6-(5-sulfonatofuran-2-yl)-1,2,4-triazin-5-yl]furan-2-sulfonate, also known as ferene, or disodium;4-[3-pyridin-2-yl-6-(4-sulfonatophenyl)-1,2,4-triazin-5-yl]benzenesulfonate, also known as ferrozine.[141–144] All of these chelators are bidentate ligands absorbing light, whereby their maxima are in the range between 530 and 600 nm. Although these chelators are also able to complex with other metals, iron is the preferred species.[145]

Contrary to chromogenic chelators, fluorescent probes are the preferred tools for detecting intracellular iron in living cells since no harsh reducing treatments are necessary.[141] Two ways to determine intracellular labile iron include inter alia the usage of either turn-off or turn-on fluorescent probes. Their principle is based on a shift in fluorescence signal upon complexation/reaction with iron.[141] Turn-off fluorescent probes such as 2-[[7'-[[bis(carboxymethyl)amino]methyl]-3',6'-dihydroxy-3-oxospiro[2-benzofuran-1,9'-xanthene]-2'-yl]methyl-(carboxymethyl)amino]acetic acid, also known as calcein, or dipotassium;3-carboxy-4-(2,7-dichloro-3-oxido-6-oxoxanthen-9-yl)-N-(1,10-phenanthrolin-5-yl)benzene-carboximidate, also known as phen green SK, are quenched upon complexation with either ferrous or ferric ions but the fluorescence can be recovered by adding a chelator having a stronger binding affinity to the metal than the initially used fluorescent probe. The degree of fluorescence recovery can thus be used as an indicator for intracellular iron amount.[146,147] In contrast to turn-off fluorescent probes, turn-on fluorescent probes become only fluorescent upon complexation/reaction with a metal.[141] Reported turn-on fluorescent probes specific for ferric ion are for instance a coumarin fluorophore linked to two aza-18-crown-6 moieties[148] or a probe consisting of a 2,2-difluoro-3-aza-1-azonia-2-boranuidatricyclo[7.3.0.03,7]dodeca-1(12),4,6,8,10-pentaene group, also known as BODIPY.[149] 6'-(diethylamino)-N,N-diethyl-3-oxospiro[2-benzofuran-1,9'-xanthene]-3'-amine oxide, also known as RhoNox-1, is an example for a turn-on fluorescent probes specific for ferrous ions due to the

deoxygenation of the tertiary amine N-oxide functional group upon Fe^{2+} mediation leading thus to a fluorescence signal.[150]

More recently, a new approach for quantitating intracellular labile ferrous ion amount was published.[151] The procedure is based on a puromycin molecule conjugated to a trioxolane-based probe resulting in TRX-PURO. Intracellularly, this probe reacts with ferrous ions causing the fragmentation of the trioxolane ring leading to a ketone intermediate that is spontaneously reacting further to puromycin (Figure 7). Free puromycin is then incorporated into nascent polypeptides at the ribosome where it can be detected by using anti-puromycin specific antibodies. The carbamoyl group present at the α-amino group of puromycin within the TRX-PURO prevents the incorporation of puromycin prior to the iron reaction. Thus, the probe represents a further approach for detecting intracellular labile ferrous ions based on immunofluorescence.[151]

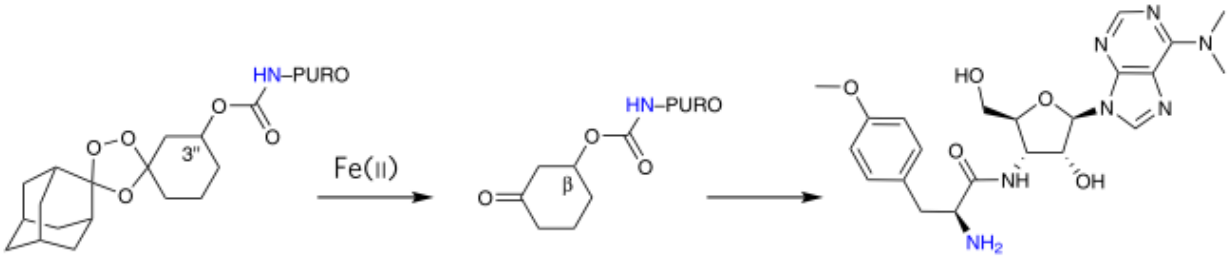

Figure 7: Chemical mechanism of puromycin release from trioxolane conjugated puromycin probe (TRX-PURO).

TRX-PURO consists of puromycin conjugated to a trioxolane-based probe. Upon the presence of ferrous ion, a fragmentation of the trioxolane ring occurs leading to a ketone intermediate that is further reacting and thereby releasing puromycin. The graphical scheme was taken and slightly modified from Spangler *et al.* 2016.[151]

Since no method for detecting intracellular iron amount was available and tested in our laboratory so far, the establishment of a colorimetric assay as well as the testing of several (fluorescent) probes able to detect intracellular iron by using flow cytometry was implemented. For the colorimetric assay, a ferrozine-based approach was used and optimized based on a publication of Riemer *et al.* 2004[152] to quantitate total intracellular iron amount, whereas calcein, RhoNox-1 and TRX-PURO were tested with flow cytometry for detecting intracellular labile iron. The results are presented hereinafter.

4.1.2 Results

4.1.2.1 Development of a ferrozine-based colorimetric assay for determining total intracellular iron amount

The protocol for quantifying intracellular iron with ferrozine described by Riemer *et al.* 2004[152], which is already a modified version of a ferrozine-based approach to detect intracellular iron in biological samples published by Wayne W. Fish[153], is comprising the following steps. First, flash frozen cells were lysed in 200 μl 50 mM NaOH for 2 hours. Then, 100 μl of an iron releasing reagent consisting of a 1:1 solution of 1.4 M HCl and 4.5% (w/v) $KMnO_4$ in Milli-Q® water and 100 μl of 10 mM HCl were added to 100 μl of cell lysate and the complete mixture was incubated at 60°C for 2 hours. This step is necessary

to remove all iron bound to proteins such as ferritin. After the incubation step, the mixture was cooled to RT and subsequently the iron detection step was performed. Therefore, 30 μl of a mixture consisting of 6.5 mM ferrozine, 6.5 mM neocuproine, 2.5 M ammonium acetate and 1 M ascorbic acid were added and incubated for 30 minutes. During this step, ascorbic acid is reducing all remaining ferric ions into the ferrous state able to build a complex with ferrozine, whereas the addition of neocuproine to this solution helps to scavenge copper ions that might compete with the iron ions for ferrozine complex formation. Ammonium acetate works as a buffer within this mixture by maintaining a pH value of around 4.5-5 allowing the iron-ferrozine complex to form.[153] After transferring 280 μl of the solution into a 96-well plate, absorbance was determined with a microplate reader at 550 nm and compared to a standard. The standard was prepared by mixing 100 μl $FeCl_3$ standards, prepared in 10 mM HCl and present within a concentration range of 0 - 300 μM, with 100 μl 50 mM NaOH, 100 μl iron releasing reagent and 30 μl iron detection reagent, whereby the handling of the standard samples was identical to the cell samples.[152]

Based on this protocol, a first test attempt with flash frozen cell pellets of a CHO K1 cell line cultured in Cellvento® 4CHO medium for over 2 weeks was performed. Therefore, flash frozen cell pellets with a cell amount ranging from 0 – 2.0 x10^7 cells were taken and the total intracellular iron amount calculated per cell was compared. The obtained values were expected to be similar due to homogeneity of the cell pool. In contrast to the reference protocol, cell lysis was done in 220 μl 50 mM NaOH before transferring 100 μl of the cell lysate to a new tube for iron releasing step. Furthermore, for each component present within the iron detection reagent, a stock solution in Milli-Q® water was prepared beforehand, whereas the final concentration of ascorbic acid within the iron detection reagent was only 0.9 M instead of 1 M due to solubility issues. For neocuproine, 25% HCl solution was added to the stock solution until fully dissolved. Additionally, 300 μl instead of 280 μl of the final solution were transferred into a transparent, u-shaped 96-well plate for absorbance measurement. For the iron standard, $FeCl_3$ solutions ranging from 0 – 1000 μM were prepared. The procedure was performed for two biological replicates for each condition. Evaluation was done by correcting the absorbance values obtained for each standard and sample with the average absorbance value obtained for the respective control (either no iron or no cells included, respectively). Total intracellular iron amount in fg per cell was calculated by using Equation 7, considering the obtained optical density (OD) value of the sample corrected by the control, the slope of the standard curve, the final cell amount present within the well and the atomic mass of iron.

Equation 7: Determination of total intracellular iron amount per cell upon ferrozine-based assay usage.

The iron amount per cell in fg was obtained by dividing the quotient of the corrected absorbance value of the sample and slope of the iron standard curve by the cell amount present within each well and multiplying the complete expression with the atomic mass of iron.

$$Iron\ amount\ per\ cell\ (fg) = \frac{\frac{Corrected\ OD\ of\ the\ sample\ (OD)}{Slope\ of\ iron\ standard\ curve\ \left(\frac{OD}{nmol}\right)} \cdot 10^{-9}}{Cell\ amount\ within\ well} \cdot 55.845\ \left(\frac{g}{mol}\right) \cdot 10^{15}$$

As shown in Figure 8A, absorbance values obtained for the standard curve were linearly increasing within an iron range up to around 25 nmol/well, whereas a further increase in iron concentration led to a stagnation of the OD with values above 2. Increasing amounts of lysed cells present per well led to an increased OD for the four lowest tested cell amounts, whereas no further increase in OD was detected for the three highest tested cell amounts. Obtained values for OD were significantly lower than the value obtained for the highest iron concentration of the standard solution being still within the linear range (Figure 8B). Average calculated intracellular iron amount per cell for all analyzed cell amounts was determined to be around 9.3 fg, whereas a higher applied cell amount per well gained rather lower values (Figure 8C). However, these lower detected intracellular iron amounts for higher applied cell amounts per well were probably caused by an insufficient cell lysis and homogenization of the cell lysate solution as already observed while performing the assay.

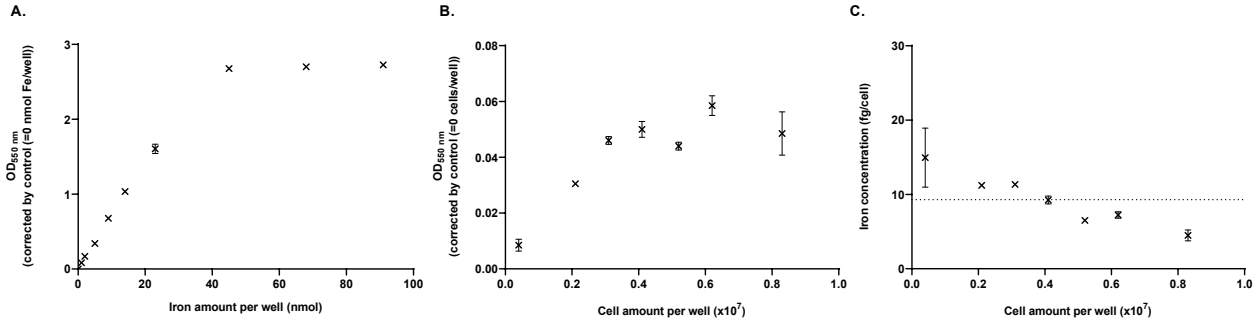

Figure 8: First attempt of the ferrozine-based assay with NaOH used as cell lysis buffer.

Flash frozen cell pellets of a CHO K1 cell line cultured for more than 2 weeks in Cellvento® 4CHO medium with a total cell amount ranging from 0 – 2.0 x10^7 cells were lysed in 220 µl 50 mM NaOH for 2 hours. Subsequently, 100 µl cell lysate solution was mixed with 100 µl 10 mM HCl and 100 µl of a 1:1 solution of 1.4 M HCl and 4.5% (w/v) $KMnO_4$ in Milli-Q® water. The mixture was incubated at 60°C for 2 hours before 30 µl of an iron detection reagent consisting of 6.5 mM ferrozine, 6.5 mM neocuproine, 2.5 M ammonium acetate and 0.9 M ascorbic acid were added and incubated at RT for 30 minutes. Finally, 300 µl of the solution were transferred into a transparent, u-shaped 96-well plate and the absorbance was determined with a microplate reader at 550 nm. For the standard, 100 µl cell lysate solution was replaced by the iron standard solution and 100 µl 10 mM HCl were replaced by 50 mM NaOH. All other steps were identical. A. OD values obtained at 550 nm for increasing iron standard concentrations per well in nmol corrected by the control. B. OD values obtained at 550 nm for increasing cell amounts per well corrected by the control. C. Calculated intracellular iron concentration in fg/cell for increasing cell amounts per well, whereby the absorbance values were corrected by the control obtained upon no cell addition. Horizontal dotted line in panel C. represents the average calculated intracellular iron amount of all analyzed cell amounts. Data are mean ± SD of two biological replicates.

Based on the results presented in Figure 8 and the observations made while performing the assay, the following improvements were done in a second test approach. First, the applied iron concentrations for the standard were decreased to a range between 0.1 - 20 nmol Fe/well with several more points included in between. Second, an alternative cell lysis protocol was tested. Therefore, flash frozen cell pellets were lysed in 220 μl of CytoBuster™ solution for only 1 hour at RT with a subsequent incubation in ultrasound bath at highest power for 2 minutes. Third, the overall volume for each condition was doubled in order to be able to measure technical replicates. Thus, 200 μl cell lysate, 200 μl 10 mM HCl, 200 μl iron releasing reagent and 60 μl iron detection reagent were mixed for the sample conditions, whereas 200 μl

iron standard, 200 µl CytoBuster™, 200 µl iron releasing reagent and 60 µl iron detection reagent were mixed for the iron standards. Time and length of the incubation steps for iron releasing and iron detection steps were not adjusted. Last, a further control was introduced by preparing a further biological replicate for each condition, whereby the iron detection reagent did not contain ferrozine. This implementation was done to evaluate the impact of turbidity caused upon increasing cell amount presence on absorbance and final intracellular iron calculation. Increasing iron amounts per well led to a linear increase in OD resulting in a coefficient of determination (R^2) of 0.9999 for the obtained regression line (Figure 9A). Addition of increasing cell amounts to the well caused a steady increase in OD, however, this was also observed upon the absence of the iron specific chromogenic chelator ferrozine (Figure 9B). Determination of intracellular iron amount varied depending on the control used for correction. Correcting the absorbance values with the no cell control absorbance values resulted in an increase in iron amount per well, whereas the correction with the respective no ferrozine control gained a similar intracellular iron concentration with an average of 16.0 fg/cell, which rather matched the expectations (Figure 9C). In conclusion, the obtained results demonstrated that the chosen range of the standard concentrations was ideal for gaining a linear regression line with a high R^2. Furthermore, cell lysis with CytoBuster™ solution seemed to be more efficient in comparison to NaOH usage due to the linear increase in absorbance even for high cell amounts applied. However, the results also reveal that it is crucial to include a no ferrozine control for each condition when calculating the intracellular iron amount per cell to consider and exclude the turbidity caused by the cells.

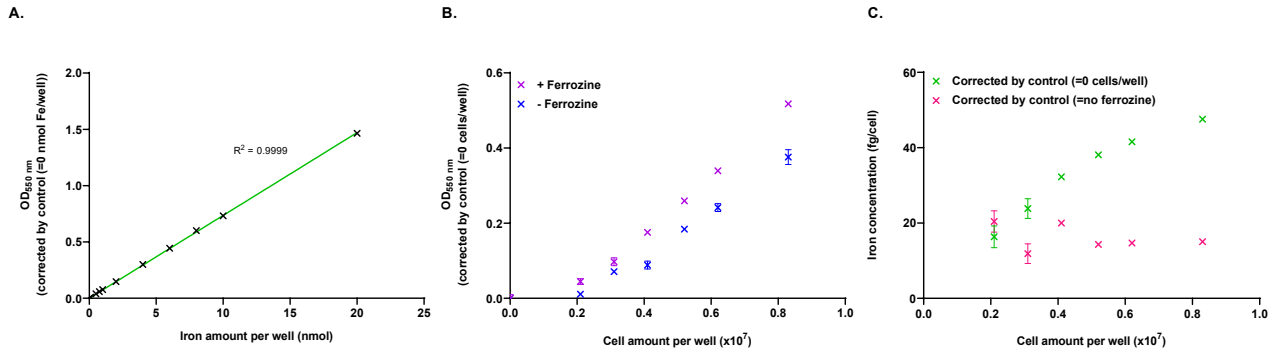

Figure 9: Second attempt of the ferrozine-based assay with CytoBuster™ used as cell lysis buffer.

Flash frozen cell pellets of a CHO K1 cell line cultured for more than 2 weeks in Cellvento® 4CHO medium with a total cell amount ranging from 0 – 2.0 x10^7 cells were lysed in 220 µl CytoBuster™ solution for 1 hour followed by the application to an ultrasound bath at the highest power for 2 minutes. Subsequently, 200 µl cell lysate solution was mixed with 200 µl 10 mM HCl and 200 µl of a 1:1 solution of 1.4 M HCl and 4.5% (w/v) $KMnO_4$ in Milli-Q® water. The mixture was incubated at 60°C for 2 hours before 60 µl of an iron detection reagent consisting of 6.5 mM neocuproine, 2.5 M ammonium acetate, 0.9 M ascorbic acid and optional with 6.5 mM ferrozine were added and incubated at RT for 30 minutes. Finally, 300 µl of the solution were transferred into a transparent, u-shaped 96-well plate and the absorbance was determined with a microplate reader at 550 nm. For the standard, 200 µl cell lysate solution was replaced by the iron standard solution and 200 µl 10 mM HCl were replaced by CytoBuster™. All other steps were identical. A. OD values obtained at 550 nm for increasing iron standard concentrations per well in nmol corrected by the control. B. OD values obtained at 550 nm for increasing cell amounts per well corrected by the control upon the presence or absence of ferrozine within the iron detection reagent. C. Calculated intracellular iron concentration in fg/cell for increasing cell amounts per well, whereby the absorbance values were either corrected by the control obtained upon no cell addition or by the control obtained upon no ferrozine addition. Data are mean ± SD of two technical replicates.

In a next step, the assay was further optimized regarding the used volumes. This was done to be able to obtain the no ferrozine control from the same cell sample that is also used for the actual iron detection, while gaining additionally two technical replicates for each approach. The obtained results for standard curve as well as for intracellular iron amount were similar to the results obtained for the second test attempt, indicating the robustness of the assay (data not shown).

Thus, the final protocol used for further applications was conceptualized (Figure 10). Briefly, cell lysis of flash frozen cells is performed in 220 μl CytoBuster™ solution at RT for 1 hour with a subsequent incubation in the ultrasound bath at highest power for 2 minutes. Then, two times 100 μl of the cell lysate solution are transferred into new tubes and 100 μl 10 mM HCl and 100 μl iron releasing reagent are added into each tube and incubated at 60°C for 2 hours. Subsequently, 30 μl of the iron detection reagent, including ferrozine or not, are added and the mixture is incubated at RT for 30 minutes. From each tube, two times 100 μl are then transferred into a transparent, u-shaped 96-well plate and the OD is measured at 550 nm with a microplate reader. For the control, 100 μl of each iron standard, ranging from 0 - 20 nmol final well concentration, are mixed with 100 μl CytoBuster™, 100 μl iron releasing reagent and 30 μl iron detection reagent including ferrozine. Time and length of the incubation as well as measuring procedure are identical to the sample treatment.

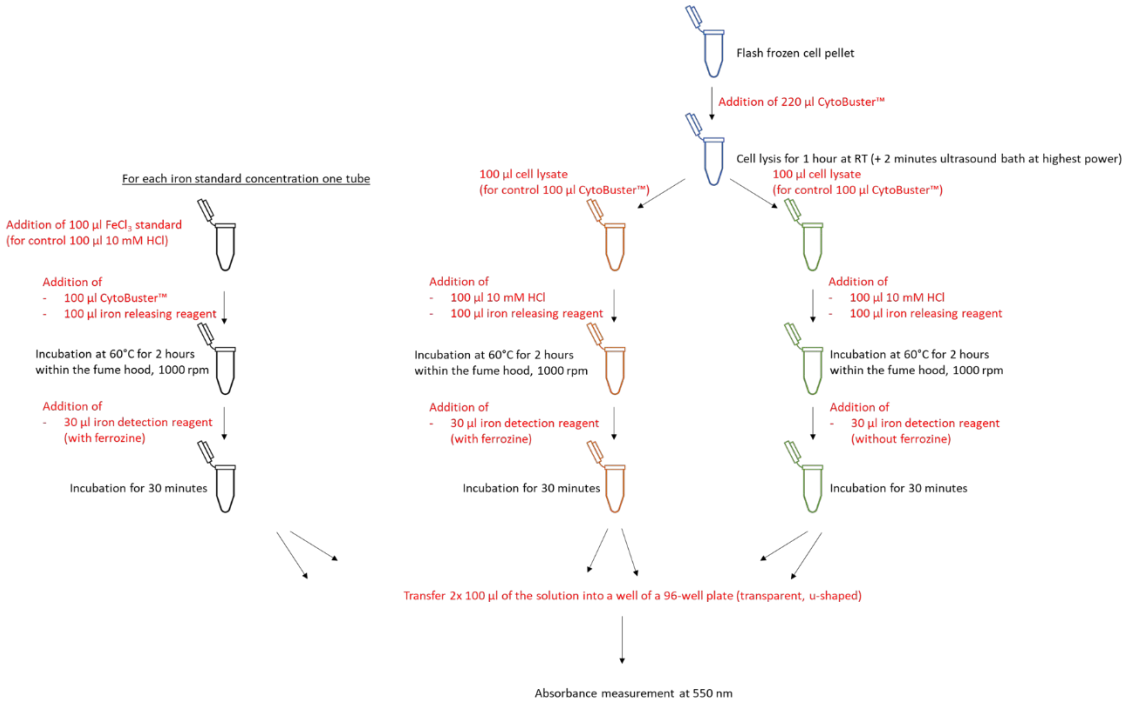

Figure 10: Final schematic workflow of the optimized and established ferrozine-based assay.

Briefly, 220 µl of CytoBuster™ solution are added to flash frozen cells and cell lysis is done at RT for 1 hour with a subsequent incubation of the sample in the ultrasound bath at the highest power for 2 minutes. Then, two times 100 µl are transferred to two new tubes and 100 µl of 10 mM HCl and 100 µl of iron releasing reagent, consisting of a 1:1 solution of 1.4 M HCl and 4.5% (w/v) $KMnO_4$ in Milli-Q® water, are added. The mixture is incubated at 60°C for 2 hours before the iron detection step takes place. Therefore, 30 µl of the iron detection reagent consisting of 6.5 mM neocuproine, 2.5 M ammonium acetate, 0.9 M ascorbic acid and 6.5 mM ferrozine, are added and incubated at RT for 30 minutes. For the ferrozine control, the iron detection reagent does not contain ferrozine. Finally, two times 100 µl of the solution are transferred into a transparent, u-shaped 96-well plate and the absorbance is determined with a microplate reader at 550 nm. For the iron standard, 100 µl cell lysate solution is replaced by the iron standard solution and 100 µl 10 mM HCl is replaced by CytoBuster™. All other steps are identical.

As a last step of the method development, the plausibility and correctness of the assay results were proven by comparing them with another orthogonal method. Therefore, flash frozen cell pellets, consisting of 0.75, 1.00 and 2.00 x10^7 cells and that were taken from the same cell pool as used for all the previous test attempts, were lysed in 220 μl CytoBuster™ solution and total iron amount was determined with HR-ICP-MS. The obtained results in comparison to the results gained from the ferrozine-based assay are presented in Figure 11. Total intracellular iron quantification with HR-ICP-MS resulted in slightly lower values with less pronounced error bars for the technical replicates than obtained upon ferrozine-based assay performance. An average intracellular iron amount of 14.9 and 16.9 fg/cell was calculated from HR-ICP-MS and ferrozine-based assay method, respectively. For further experiments it was decided to perform the assay with a cell amount of 1.00 x10^7 cells per cell pellet since this is an appropriate amount that can be easily removed from any cell culture experiment for intracellular iron analysis.

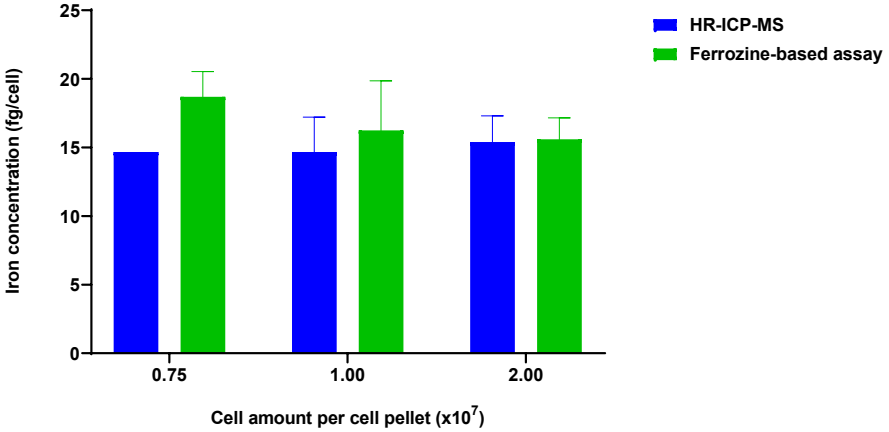

Figure 11: Plausibility check of the intracellular iron amounts obtained with the ferrozine-based assay in comparison to HR-ICP-MS analysis.

Flash frozen cell pellets of a CHO K1 cell line cultured for more than 2 weeks in Cellvento® 4CHO medium with a total cell amount of 0.75, 1.00 and 2.00 x10^7 cells were lysed in 220 µl CytoBuster™ solution for 1 hour followed by the application to an ultrasound bath at the highest power for 2 minutes. The cell lysate was then either used for HR-ICP-MS analysis or it was further proceeded with the ferrozine-based assay as presented in Figure 10. Presented are the calculated intracellular iron concentrations in fg/cell, whereby the absorbance values obtained upon application of the ferrozine-based assay were corrected by the control obtained upon no ferrozine addition. Data are mean ± SD of three (HR-ICP-MS) or two (ferrozine-based assay) technical replicates.

In conclusion, the established colorimetric ferrozine-based assay based on the published procedure by Riemer *et al.* 2004[152] was proven to be a robust method that is easy and straight forward to use while gaining similar results in comparison to destructive HR-ICP-MS procedure, indicating that all iron is fully complexed and thus determined by the ferrozine-based method.

4.1.2.2 Development of a flow cytometry protocol for determining LIP levels

Three different (fluorescent) probes were tested for their suitability to detect intracellular labile iron. Therefore, a flow cytometer, namely the iQue® Screener PLUS from Sartorius, was used which is equipped with three lasers and thirteen fluorescence channels. A further characteristic of the device comprises an air-gap delimited stream allowing the distinction of the different samples that are applied continuously to the device. Depending on the cell concentration per well as well as the selected sip time, which defines the volume aspirated from the well, an estimation of the number of total cells that are applied to the system can be made. A sip time of 1 second corresponds to a volume of around 1.75 μl. Another feature of the device includes the non-requirement for pre-analysis. However, one major difference compared to other flow cytometers available on the market is that there is no possibility to adjust the voltage settings of the photomultiplier. Thus, in case the fluorescence signal is reaching the limit within one channel, a switch into the next higher fluorescence channel needs to be performed to evaluate the data.

Calcein

Calcein is a turn-off fluorescent probe that can be used in combination with a chelator for measuring the LIP. Usage of only calcein results in a quenching of the fluorescence signal upon the presence of iron, whereas the addition of a chelator on top of the probe leads to a dequenching of the signal. This shift in fluorescence intensity can then be used to determine the LIP concentration for different cellular conditions. For instance, Prus *et al.* 2008[154] demonstrated the successful LIP determination of several human hematopoietic cells by using calcein, or rather the acetoxymethyl (AM) derivative of calcein (calcein-AM). Due to the AM group, the cellular uptake of the probe is facilitated but once intracellularly present, only calcein is present due to the hydrolysis of the AM group by esterases. The probe was used in combination with the iron chelators DFP or SIH. The used protocol comprised a washing step prior to the incubation of the cells with 0.25 or 0.50 μM calcein-AM at 37°C for 15 minutes. Then, a further washing step was performed before cells were incubated at RT for 1 hour with 100 μM chelator solution, followed by a further washing step. Finally, fluorescence was measured with flow cytometry.[154]

As a first test attempt for using the calcein-AM probe for a CHO K1 cell line cultured in Cellvento® 4CHO medium, a dose-response of calcein-AM with concentrations ranging from 0.05 - 1.00 μM was performed, whereby cells were additionally incubated with 100 μM of either DFP or BPY chelator solution, a further chelator available in the laboratory at that time. Since the experiment was carried out in a 96-well plate, final cell concentration per well was set to 1000 cells/μl. The protocol included the following steps. First, the desired cell amount of cell suspension was transferred into a new spin tube and cells were washed two times with PBS by centrifugating at 1764 rpm (600 g) for 5 minutes. Cells were then transferred into a 96-well plate and incubated in 100 μl calcein-AM solution at 37°C for 15 minutes. As a control,

cells were incubated in only PBS. Subsequently, cells were washed again two times with PBS by centrifugating at 2442 rpm (600 g) for 5 minutes before 100 μl of the chelator solution (or PBS for the no chelator control) were added and incubation at RT for 1 hour took place. Afterwards, cells were washed again two times with PBS by centrifugating at 2442 rpm (600 g) for 5 minutes before cells were resuspended in PBS for flow cytometry measurement. Chosen sip time was 10 seconds. As shown in the histogram plot in Figure 12A, an increase in fluorescence intensity was observed upon increasing calcein-AM concentrations, however, usage of 0.05 μM calcein-AM led to a higher mean fluorescence intensity (MFI) than observed for 0.10 μM calcein-AM. The overall increase in MFI upon calcein-AM usage compared to the PBS control was more than 34.2-fold and also higher compared to the results presented in the reference paper (difference of around 27-fold).[154] Additional treatment with chelator solution did not result in a dequenching of the fluorescence signal compared to the control without chelator usage (Figure 12B). The overall measured counts of viable cells per well was rather low with values being below 2000 (data not shown).

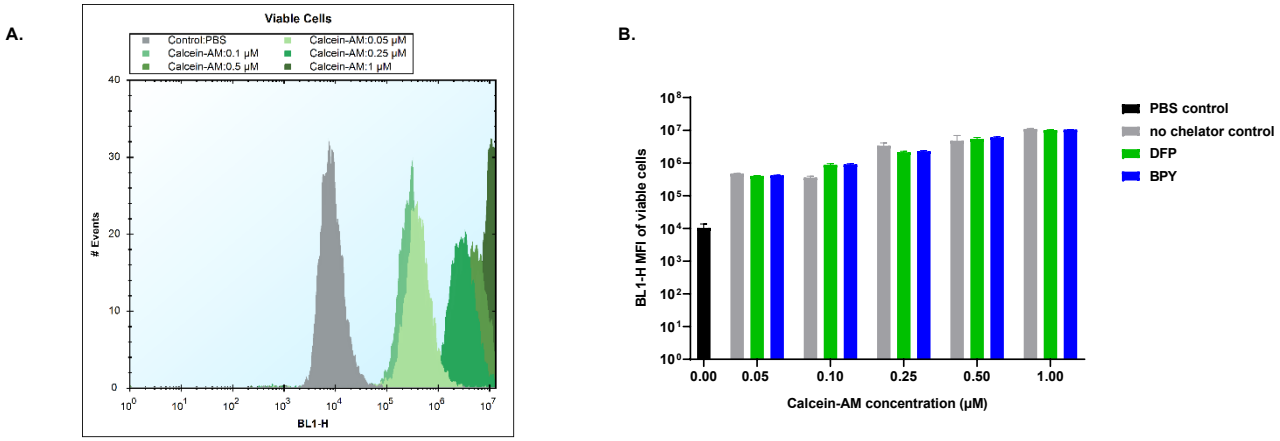

Figure 12: First attempt of determining LIP with increasing calcein-AM concentrations (0.05 – 1.00 µM) and 100 µM DFP or BPY chelator concentration by flow cytometry.

CHO K1 cells cultured in Cellvento® 4CHO medium were washed with PBS prior to calcein-AM incubation (concentrations ranging from 0.05 - 1.00 µM) at 37°C for 15 minutes. After washing the cells again with PBS, cells were treated with 100 µM chelator solution, either DFP or BPY, for 1 hour before being measured with flow cytometry at a sip time of 10 seconds. Final cell concentration per well was 1000 cells/µl. A. Histogram plot for only calcein-AM treated viable cells in dependency of the fluorescence intensity detected within the BL1-H channel in comparison to the PBS control. B. Effect of DFP or BPY chelator treatment on BL1-H MFI of viable cells for cells treated with 0.05, 0.10, 0.25, 0.50 or 1.00 µM calcein-AM in comparison to the PBS and no chelator control. Data are mean ± SD of three technical replicates.

The presented results revealed that the method did not yet work due to the missing shift in fluorescence intensity upon chelator treatment. It was hypothesized that this might have resulted from a relatively low LIP present inside the cells. In combination with high calcein-AM concentrations used, the quenching and dequenching of the fluorescence intensity upon iron complexation might have thus not been detectable. Thus, in a next step, the calcein-AM concentrations were reduced from 0.05 – 1.00 μM to 0.001 - 0.500 μM while chelator concentrations were kept the same. Additionally, the final cell concentration per well was increased to 10000 cells/μl in order to detect a higher number of events per

well while keeping the sip time at 10 seconds. Decreasing the calcein-AM concentration led to a clear decrease in fluorescence intensity in a dose-dependent manner, whereas also the overall difference in MFI compared to the PBS control was reduced upon treating cells with lower calcein-AM concentrations compared to the previously performed experiment resulting thereby in a higher range for increasing fluorescence intensity upon chelator usage (Figure 13A). However, additional treatment of the cells with either DFP or BPY chelator solution did not result in a shift of BL1-H MFI of viable cells compared to the respective calcein-AM control (Figure 13B). A higher cell concentration per well also led to a higher detected count of viable cells per well up to nearly 35000 (data not shown), which represents a more representative number compared to the first experiment with below 2000 counts.

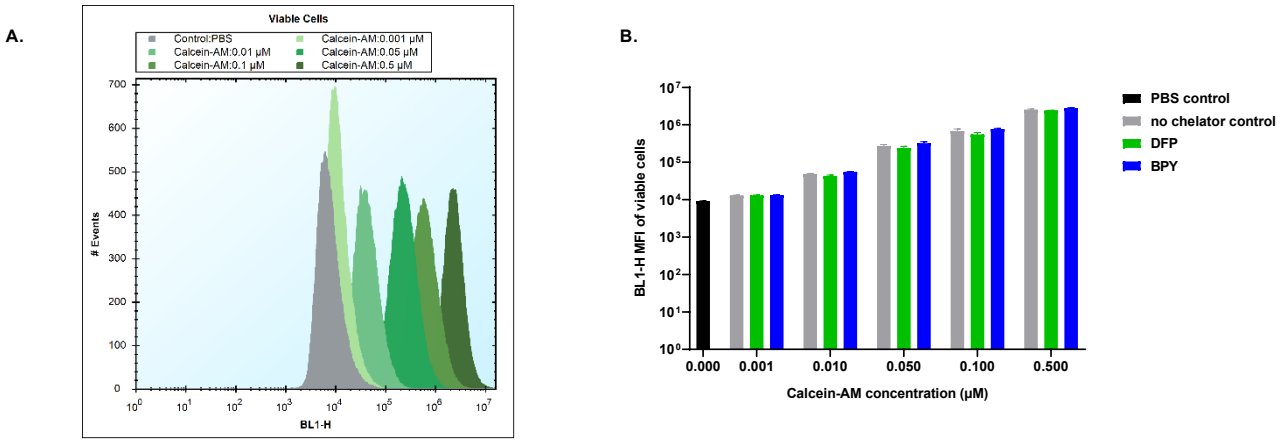

Figure 13: Second attempt of determining LIP with reduced calcein-AM concentrations (0.001 – 0.500 µM) and 100 µM DFP or BPY chelator concentration by flow cytometry.

CHO K1 cells cultured in Cellvento® 4CHO medium were washed with PBS prior to calcein-AM incubation (concentrations ranging from 0.001 - 0.500 µM) at 37°C for 15 minutes. After washing the cells again with PBS, cells were treated with 100 µM chelator solution, either DFP or BPY, for 1 hour before being measured with flow cytometry at a sip time of 10 seconds. Final cell concentration per well was 10000 cells/µl. A. Histogram plot for only calcein-AM treated viable cells in dependency of the fluorescence intensity detected within the BL1-H channel in comparison to the PBS control. B. Effect of DFP or BPY chelator treatment on BL1-H MFI of viable cells for cells treated with 0.001, 0.010, 0.050, 0.100 and 0.500 µM calcein-AM in comparison to the PBS and no chelator control. Data are mean ± SD of three technical replicates.

Based on the obtained results, 0.01 μM calcein-AM concentration was chosen as the concentration used for further testing since this concentration led to a clear visible shift in fluorescence intensity compared to the control, although the determined difference herein (5.3-fold) was smaller than the one presented within the reference paper by Prus *et al.* 2008 (around 27-fold).[154] However, since none of the tested chelators caused a shift in fluorescence intensity and thus resulted in a dequenching of the signal, higher chelator concentrations were tested in a next attempt. Therefore, DFP and BPY chelator concentrations ranging from 100 μM - 10 mM were applied. Additionally, a reduced sip time of 7 seconds was applied to reduce overall measuring time while keeping a final cell concentration per well of 10000 cells/μl. Results indicate that higher applied chelator concentrations led to an elevated MFI observed for viable cells within the BL1-H channel, but with a difference in MFI of only around 1.2- and 1.3-fold for DFP and BPY compared to only calcein-AM application, respectively. However, no clear dose response was

detected and an overall high variability of the BL1-H MFI of viable cells was observed in comparison to the no chelator control (Figure 14). Additionally, no clear shift in MFI within the histogram plot was observed (data not shown) and thus the results were not as pronounced as observed within the reference paper by Prus *et al.* 2008 (difference of more than 4.1-fold upon chelator usage compared to the no chelator control).[154]

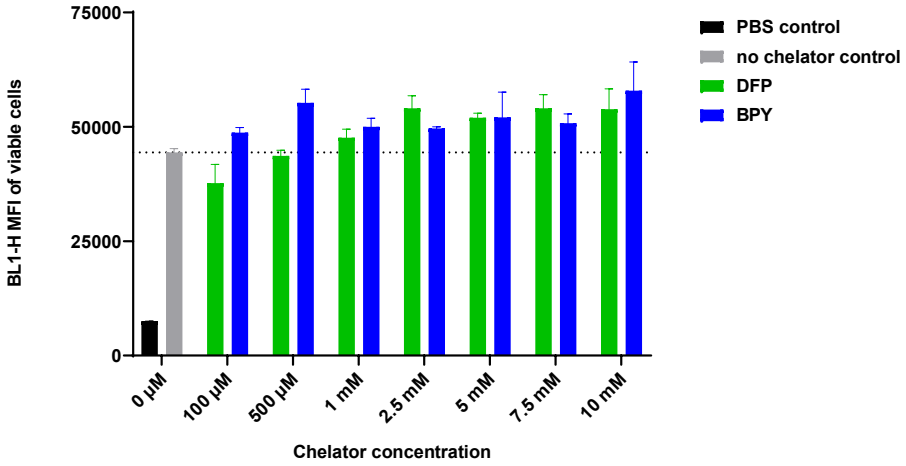

Figure 14: Third attempt of determining LIP with 0.01 µM calcein-AM concentration and increasing DFP or BPY chelator concentrations (100 µM – 10 mM) by flow cytometry.

CHO K1 cells cultured in Cellvento® 4CHO medium were washed with PBS prior to calcein-AM incubation (0.01 µM) at 37°C for 15 minutes. After washing the cells again with PBS, cells were treated with DFP or BPY chelator solution ranging from 100 µM - 10 mM for 1 hour before being measured with flow cytometry at a sip time of 7 seconds. Final cell concentration per well was 10000 cells/µl. Presented are the obtained BL1-H MFI of viable cells of calcein-AM treated cells upon DFP or BPY chelator treatment in comparison to the PBS and no chelator control. The horizontal dotted line represents the BL1-H MFI of viable cells obtained upon only calcein-AM treatment. Data are mean ± SD of three technical replicates.

It was then hypothesized that an increase in iron concentration present within the CCM might help to increase LIP concentration due to an assumed higher iron uptake rate. More precisely, it was assumed that with a higher LIP concentration, a higher quenching of the calcein fluorescence intensity might be obtained providing also a higher dequenching signal upon chelator treatment. Therefore, the iron concentration within Cellvento® 4CHO medium was increased by a factor of more than 50 and cells were cultured in the respective medium for several days. However, this resulted in no difference compared to the already performed experiments (data not shown).

As a further step, it was then decided to test a further chelator, namely SIH, that was similar to DFP already published in literature in combination with calcein-AM for detecting LIP.[154,155] The idea was to see a more pronounced dequenching signal upon chelator treatment compared to the previous two tested chelators. Tested concentrations of SIH were in the range between 1 - 200 μM, whereas all other parameters were not changed compared to the previously performed experiment. The tested low concentration range resulted from solubility issue of the chelator in aqueous solution. The results revealed similarly to the other tested chelators only a slight shift in MFI compared to the no chelator control, whereas the highest shift in MFI was observed upon application of 100 μM SIH with a fold

change of only 1.1 in comparison to a more than 4.1-fold increase upon chelator usage presented in the reference paper.[154] Furthermore, no clear dose response was observed (Figure 15).

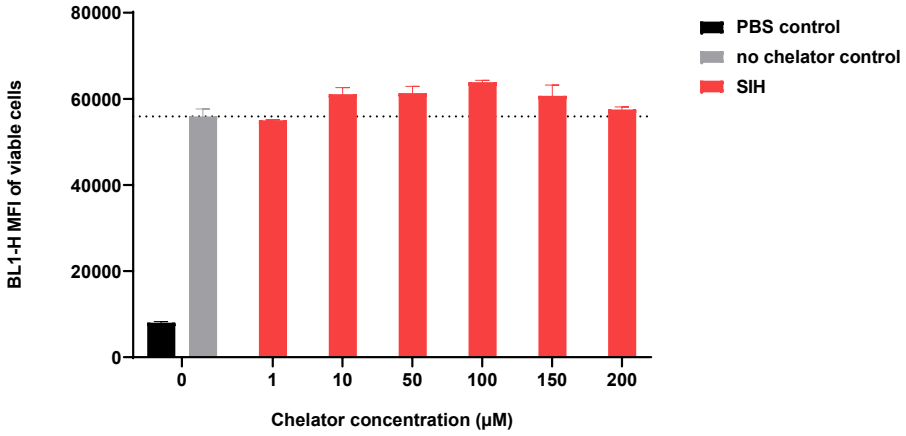

Figure 15: Fourth attempt of determining LIP with 0.01 µM calcein-AM concentration and increasing SIH chelator concentrations (1 – 200 µM) by flow cytometry.

CHO K1 cells cultured in Cellvento® 4CHO medium were washed with PBS prior to calcein-AM incubation (0.01 µM) at 37°C for 15 minutes. After washing the cells again with PBS, cells were treated with SIH chelator solution ranging from 1 - 200 µM for 1 hour before being measured with flow cytometry at a sip time of 7 seconds. Final cell concentration per well was 10000 cells/µl. Presented are the obtained BL1-H MFI of viable cells of calcein-AM treated cells upon SIH chelator treatment in comparison to the PBS and no chelator control. The horizontal dotted line represents the BL1-H MFI of viable cells obtained upon only calcein-AM treatment. Data are mean ± SD of three technical replicates.

Since all the experiments performed with calcein-AM and either DFP, BPY or SIH for determining LIP were not as promising as data published in literature, it was decided to continue the method development with another fluorescent probe. Therefore, a turn-on fluorescent probe, namely RhoNox-1, was selected, for which no additional chelator treatment was needed.

RhoNox-1

For the first test attempt with the turn-on fluorescent probe RhoNox-1, which is able to detect intracellular labile ferrous ions, a RhoNox-1 dose-response was performed. Therefore, RhoNox-1 solutions with concentrations ranging from 0.01 – 50.00 μM were prepared from a 1 mM stock, for which 50 μg RhoNox-1 were dissolved in DMSO and then further diluted in PBS. Additionally, for each prepared RhoNox-1 working solution, a respective DMSO control was prepared to evaluate the impact of DMSO on cell viability during the procedure. Then, the desired amount of CHO K1 cells cultured in Cellvento® 4CHO medium was transferred into a new spin tube and cells were washed two times with PBS by centrifugating at 1764 rpm (600 g) for 5 minutes. Afterwards, cells were transferred into a transparent, u-shaped 96-well plate and 100 μl of the RhoNox-1 solution was added and incubation at 37°C for 1 hour took place. Chosen incubation time was selected according to the probe manufacturer's instructions. Subsequently, cells were washed again two times with PBS by centrifugating at 2442 rpm (600 g) for 5 minutes before cells were resuspended in PBS for flow cytometry analysis. Final cell concentration per

well was set to 10000 cells/μl in combination with a selected sip time of 7 seconds. As shown within the histogram plot in Figure 16A, treating cells with increasing RhoNox-1 concentrations resulted in an increase in BL2-H MFI of viable cells in comparison to the PBS control, whereas a clear separation from the PBS control was observed upon application of 5 μM RhoNox-1. Addition of RhoNox-1 or the respective DMSO control to the cells did not impact the overall counts of viable cells/well in comparison to the control and thus did not affect cell viability during the procedure (Figure 16B).

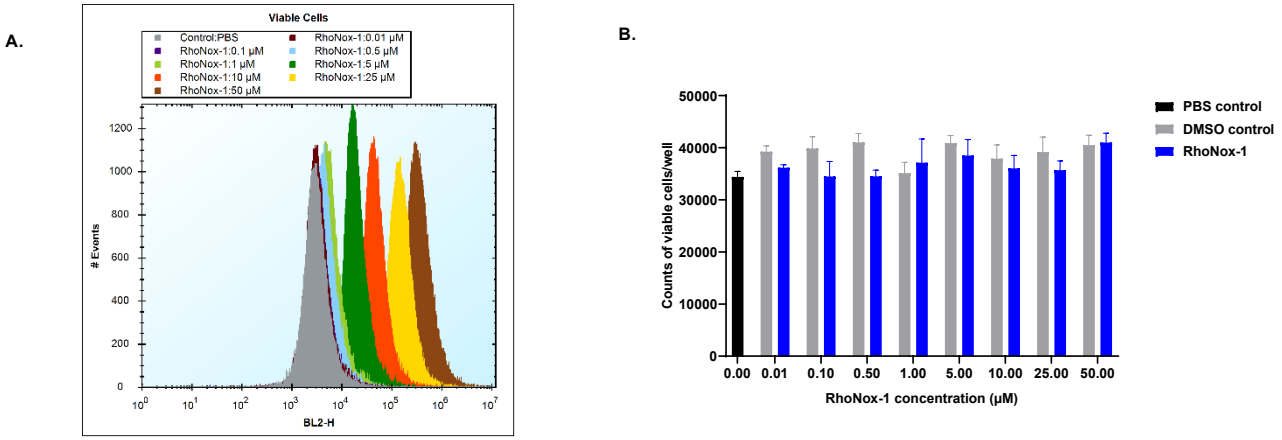

Figure 16: First attempt of determining LIP with increasing RhoNox-1 concentrations (0.01 – 50.00 µM) by flow cytometry.

CHO K1 cells cultured in Cellvento® 4CHO medium were washed with PBS prior to RhoNox-1 treatment with concentrations ranging from 0.01 – 50.00 µM at 37°C for 1 hour. After washing the cells again with PBS, cells were measured with flow cytometry at a sip time of 7 seconds. Final cell concentration per well was 10000 cells/µl. A. Histogram plot for RhoNox-1 treated viable cells in dependency of fluorescence intensity detected within the BL2-H channel in comparison to the PBS control. B. Effect of RhoNox-1 treatment on counts of viable cells/well in comparison to the PBS control, whereby the respective DMSO control for each tested RhoNox-1 concentration is plotted in grey next to it. Data are mean ± SD of four technical replicates.

Although the obtained results were already very promising and 5 μM RhoNox-1 seemed to be ideal for obtaining a clear shift in BL2-H MFI compared to the unstained control, the fluorescence response of RhoNox-1 in dependency of increasing iron concentrations was studied thereafter to investigate the sensitivity of the probe to iron concentration changes. Therefore, 100 μl of increasing amounts of ferrous ions in form of $FeSO_4$ were loaded on a 96-well plate. Then, 100 μl of a 10 μM RhoNox-1 solution were added resulting in a final RhoNox-1 concentration of 5 μM/well. Subsequently, the plate was incubated at 37°C while the fluorescence intensity at 575 nm with excitation wavelength at 540 nm was continuously measured with a multiplate reader for 1 hour. As shown in Figure 17A, a linear increase in fluorescence intensity was observed upon increasing iron concentrations. An increase in incubation time also led to an increase in fluorescence intensity independently of the applied iron concentration, whereby the increase was more pronounced within the first 30 minutes before the signal went into a plateau for the lower tested iron concentrations (Figure 17B). Overall, those results indicated that a RhoNox-1 concentration of 5 μM was sensitive enough to detect changes within the fluorescence intensity for a wide range of ferrous ion concentrations. Furthermore, the results revealed that an incubation time of around 30 minutes was already enough for almost all tested iron concentrations to obtain a full turn-

over of the probe with present ferrous ions. Thus, it was expected that a concentration of 5 μM RhoNox-1 is sufficient to determine LIP concentrations within cells by flow cytometry, since it was further expected that the intracellular LIP concentration in general does not exceed the iron concentration tested herein.

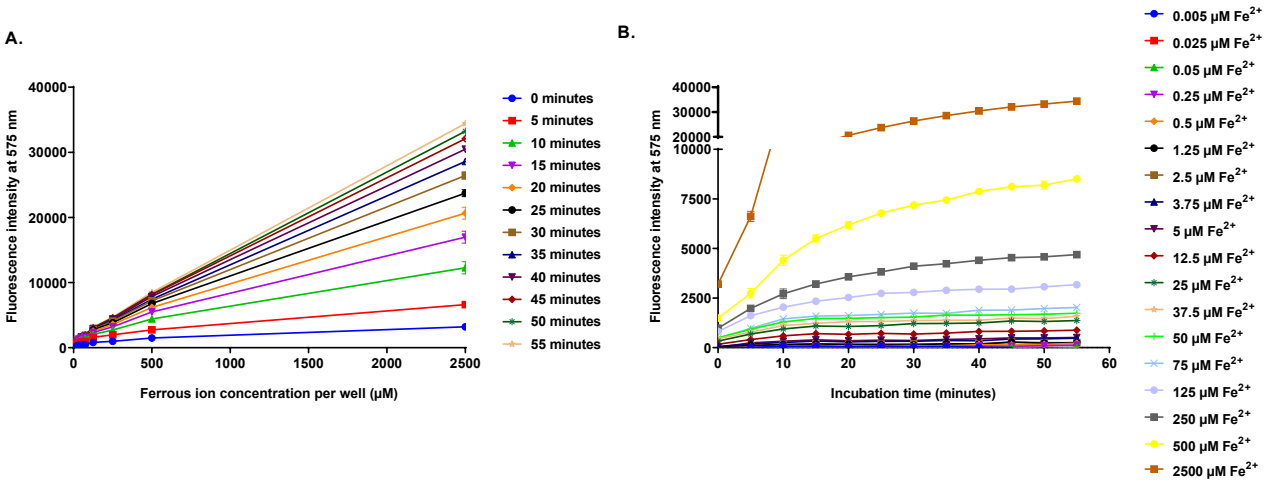

Figure 17: Fluorescence response of RhoNox-1 over time upon increasing ferrous ion concentrations.

100 µl of a 10 mM RhoNox-1 solution were mixed in a 96-well plate with 100 µl ferrous ion solution resulting in final well concentrations between 0.005 - 2500 µM. The plate was then incubated at 37°C for 1 hour while the fluorescence intensity at 575 nm with excitation wavelength at 540 nm was continuously measured with a multiplate reader. A. Fluorescence intensity at 575 nm in dependency of ferrous ion concentration per well for each measured time point. B. Fluorescence intensity at 575 nm in dependency of incubation time for each tested ferrous ion concentration. Data are mean ± SD of four technical replicates and were corrected by the respective negative control containing no iron.

The method development with RhoNox-1 was thus considered to be completed due to the data obtained. The probe was therefore thought to be a promising candidate for detecting changes in LIP during fed-batch processes for CHO cells.

TRX-PURO

Lastly, the TRX-PURO probe was studied as a further alternative to detect LIP with flow cytometry, whereby the probe was kindly provided by Adam R. Renslo lab. The principle of TRX-PURO is based on the idea that after being taken up by the cells, puromycin is released from the probe due to the reaction with labile ferrous ion. Free puromycin is then incorporated into the nascent polypeptides where it can be detected with an anti-puromycin specific antibody.[151] The probe was thus used in combination with an Alexa Fluor® 488 conjugated anti-puromycin antibody enabling an one-step staining protocol. Since the incorporated puromycin is detected intracellularly, cells needed to be additionally fixated and permeabilized. Therefore, the BD Cytofix/Cytoperm™ Fixation/Permeabilization Kit was first tested with a conjugated antibody detecting alpha tubulin within CHO K1 cells to set the parameters for the fixation/permeabilization and staining procedure (data not shown). The final protocol, which was used for all following experiments with the TRX-PURO probe, comprised the following steps. The needed

amount of CHO K1 cells cultured in Cellvento® 4CHO medium was washed two times with PBS by centrifugating at 1764 rpm (600 g) for 5 minutes before transferring them into a 96-well plate. Then, cells were incubated with PBS (control), 100 μl TRX-PURO or puromycin solution, whereby the latter was used as a positive control, within the incubator (37°C, 80% humidity and 5% CO_2) for a fixed time period. Afterwards, cells were washed again two times with PBS by centrifugating at 2442 rpm (600 g) for 5 minutes before the actual fixation/permeabilization and staining protocol started. Therefore, cells were incubated in 100 μl BD Cytofix/Cytoperm solution at 4°C and light-protected for 20 minutes. Subsequently, cells were washed two times with 1X BD Perm/Wash buffer by centrifugating at 2442 rpm (600 g) for 5 minutes before cells were stained with 50 μl antibody solution at 4°C and light-protected for 30 minutes, whereby PBS was used for the unstained control. Afterwards, cells were washed again two times with 1X BD Perm/Wash buffer by centrifugating at 2442 rpm (600 g) for 5 minutes before cells were resuspended in 1X BD Perm/Wash buffer for flow cytometry analysis. Final cell concentration per well was set to 20000 cells/μl in combination with a selected sip time of 7 seconds.

For a first attempt, a dose response for the positive control puromycin was performed for a CHO K1 cell line, named in the following cell line 1, to get familiar with the procedure and test the limitations of the system. Chosen puromycin concentrations dissolved in PBS were in the range of 0.0001 - 100 μM, whereas incubation time was set to 4 hours in accordance to the reference paper by Spangler *et al.* 2016.[151] Selected antibody concentration for the specific antibody as well as for the isotype control was set to 2 μg/ml. An isotype control was applied to detect possible unspecific binding of the anti-puromycin antibody. As shown in Figure 18A, incubation of cells with puromycin resulted in similar counts of viable cells/well, whereas only upon 100 μM puromycin usage slightly lower counts were detected, which was probably caused by the high DMSO amount (10%) present within this condition. Staining with isotype control only led to a slight shift in BL1-H MFI of viable cells in comparison to the unstained control. In contrast, staining with anti-puromycin antibody revealed a significant increase in BL1-H MFI of viable cells upon increasing puromycin concentrations to more than 70000 compared to the PBS control for which a BL1-H MFI of only around 16300 was observed (fold change of 4.5). However, detected BL1-H MFI of viable cells upon 100 μM puromycin usage decreased again compared to 10 μM puromycin treatment (Figure 18B). Results for the histogram plot revealed a broad distribution of anti-puromycin stained cells within the BL1-H channel upon incubation with 10 μM puromycin, whereas the peak width for the other tested puromycin concentrations was rather narrow (Figure 18C). Overall, the results indicated that cells were able to take up puromycin and incorporate it into nascent polypeptides at the ribosomes since a higher BL1-H MFI was observed with increasing puromycin concentrations. Furthermore, results also suggested a signal linearity on a logarithmic scale within 0.1 and 10 μM of puromycin upon anti-puromycin staining, whereas a puromycin concentration of 100 μM

seemed to be too high since cells showed a decreased viability compared to the other tested conditions. Unspecific binding upon usage of anti-puromycin antibody was not observed.

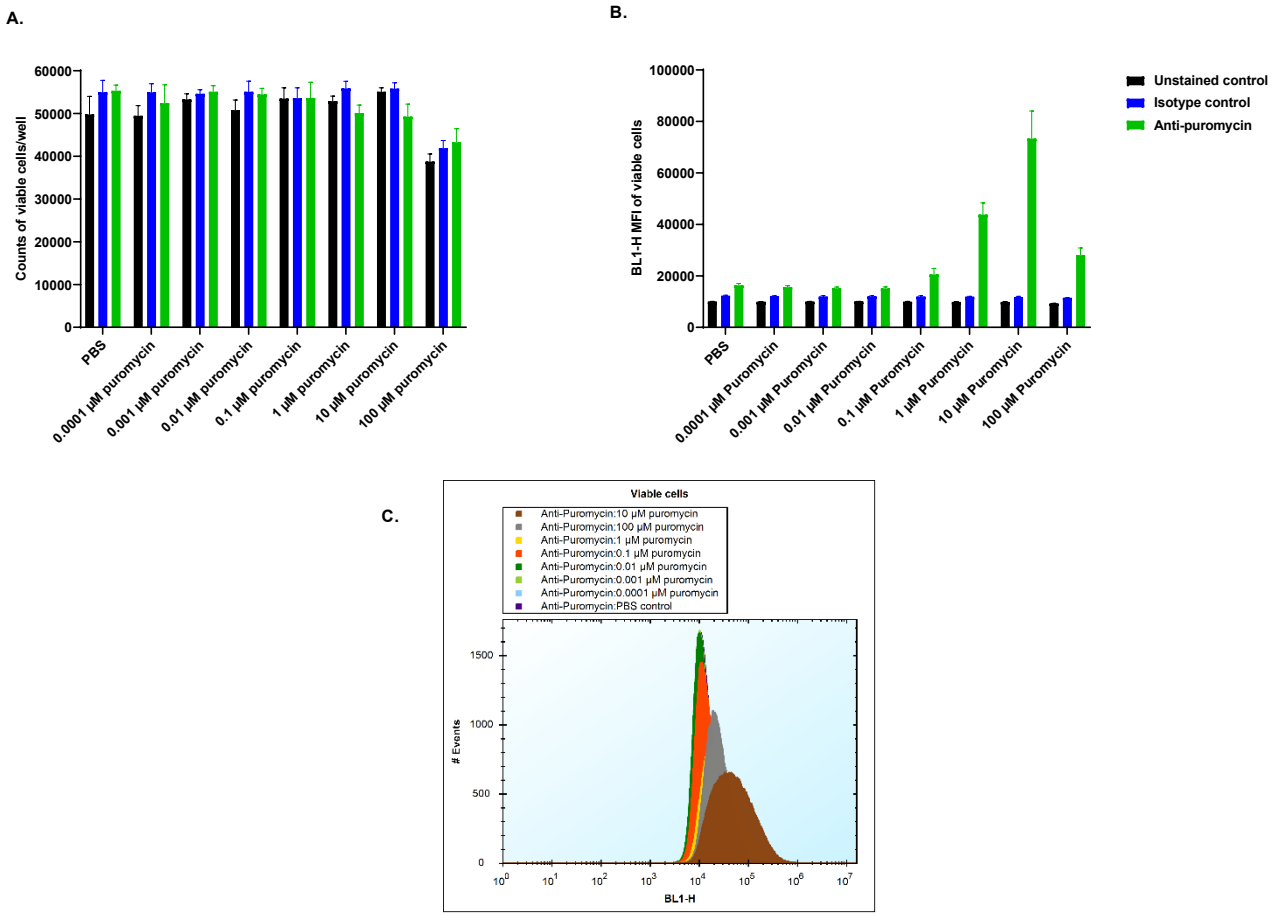

Figure 18: Effect of increasing puromycin concentrations on fluorescence intensity of cell line 1 upon anti-puromycin staining.

CHO K1 cells cultured in Cellvento® 4CHO medium were washed with PBS prior to puromycin treatment with concentrations ranging from 0.0001 - 100 µM for 4 hours at 37°C, 80% humidity and 5% CO_2. After washing the cells again with PBS, cells were fixed and permeabilized at 4°C and light-protected for 20 minutes, followed by the antibody staining at 4°C and light-protected for 30 minutes (Isotype control: Alexa Fluor® 488 conjugated mouse IgG2a kappa 1:250 in 1X BD Perm/Wash buffer, Puromycin: Alexa Fluor® 488 conjugated mouse anti-puromycin 1:250 in 1X BD Perm/Wash buffer). Subsequently, cells were washed again and measured with flow cytometry at a sip time of 7 seconds. Final cell concentration per well was 20000 cells/µl. A. Effect of puromycin treatment on counts of viable cells/well for unstained control, isotype control and anti-puromycin stained samples. B. BL1-H MFI of viable cells for unstained control, isotype control and anti-puromycin stained samples upon puromycin treatment. C. Histogram plot for anti-puromycin stained viable cells upon puromycin treatment in dependency of the fluorescence intensity detected within the BL1-H channel. Data are mean ± SD of four technical replicates.

Although the impact of different incubation times and different antibody concentrations on fluorescence intensity was not yet evaluated, it was decided to continue testing the TRX-PURO probe for cell line 1. Therefore, CHO K1 cells were incubated for 4 hours with increasing concentrations of TRX-PURO diluted in PBS from a 1 mM stock solution in DMSO, whereby TRX-PURO concentrations ranged from 0.01 – 100 μM. Chosen antibody concentrations were the same as previously applied (2 μg/ml). Cell treatment with TRX-PURO concentrations up to 10 μM had no effect on counts of viable cells/well compared to the PBS control, whereas the highest applied TRX-PURO concentration (100 μM) resulted in a drastic loss of cell counts, which was probably induced by the 10% DMSO present within this

condition (Figure 19A). Staining with isotype control caused a slight increase in BL1-H MFI of viable cells compared to the unstained control independently of the used TRX-PURO concentration. BL1-H MFI of viable cells upon anti-puromycin staining increased with increasing TRX-PURO concentrations, with a highest value detected at around 21200 MFI for 100 μM TRX-PURO, however this resulted only in a fold change of less than 1.2 compared to the PBS control (Figure 19B). Within the histogram plot, no clear shift in BL1-H MFI upon treating cells with increasing TRX-PURO concentrations was detected compared to the PBS control, whereby no peak broadening was observed (Figure 19C).

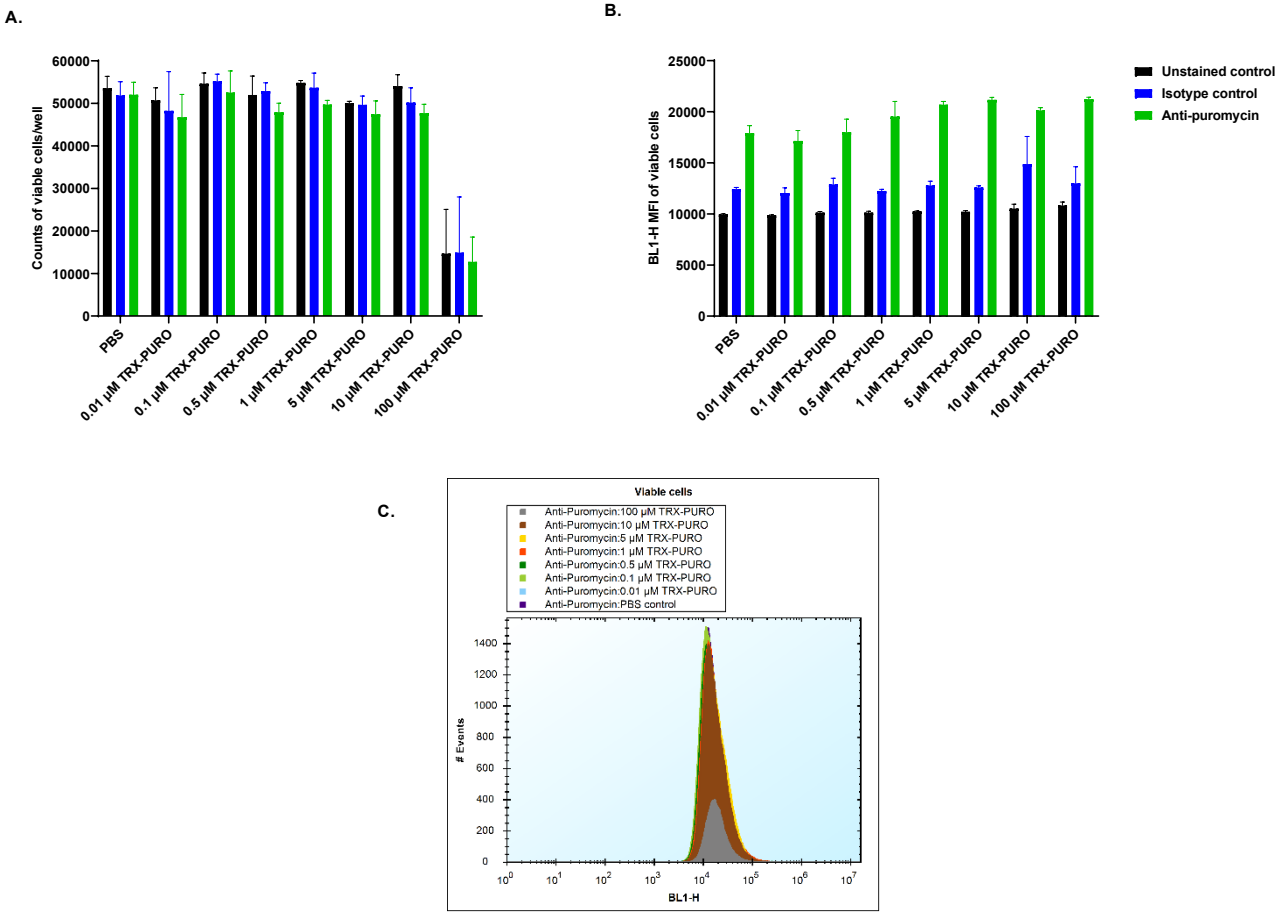

Figure 19: Effect of increasing TRX-PURO concentrations on fluorescence intensity of cell line 1 upon anti-puromycin staining.

CHO K1 cells cultured in Cellvento® 4CHO medium were washed with PBS prior to TRX-PURO treatment with concentrations ranging from 0.01 - 100 µM for 4 hours at 37°C, 80% humidity and 5% CO_2. After washing the cells again with PBS, cells were fixed and permeabilized at 4°C and light-protected for 20 minutes, followed by the antibody staining at 4°C and light-protected for 30 minutes (Isotype control: Alexa Fluor® 488 conjugated mouse IgG2a kappa 1:250 in 1X BD Perm/Wash buffer, Puromycin: Alexa Fluor® 488 conjugated mouse anti-puromycin 1:250 in 1X BD Perm/Wash buffer). Subsequently, cells were washed again and measured with flow cytometry at a sip time of 7 seconds. Final cell concentration per well was 20000 cells/µl. A. Effect of TRX-PURO treatment on counts of viable cells/well for unstained control, isotype control and anti-puromycin stained samples. B. BL1-H MFI of viable cells for unstained control, isotype control and anti-puromycin stained samples upon TRX-PURO treatment. C. Histogram plot for anti-puromycin stained viable cells upon TRX-PURO treatment in dependency of the fluorescence intensity detected within the BL1-H channel. Data are mean ± SD of four technical replicates.

Contrary to the published results by Spangler *et al.* 2016[151], treatment of cell line 1 with either puromycin or TRX-PURO did not result in a similar incorporation rate of puromycin in cells reflected by the significant differences in BL1-H MFI of viable cells and the calculated different fold changes. Although

this was hypothesized to not affect the suitability of TRX-PURO for detecting LIP within cell line 1 by flow cytometry, no further testing with cell line 1 were made at that time. This decision was made due to the recognition of a specific characteristic of cell line 1, which was not considered beforehand. More precisely, it was noticed that cell line 1 expresses the enzyme puromycin N-acetyltransferase, a selection marker used for generating this specific recombinant cell line. It was thus strongly assumed, that the presence of this enzyme might cause the inactivation of puromycin by acetylating the nitrogen atom of its tyrosinyl group and hence preventing the incorporation of puromycin, which is, however, the basis for TRX-PURO application.

Thus, further testing for detecting the LIP with TRX-PURO were only made with another CHO K1 cell line, named in the following as cell line 2, that does not express puromycin N-acetyltransferase.

The first experiment with cell line 2 consisted again of a puromycin dose-response (0.01 - 100 μM), whereby additionally the impact of two different incubation times, namely 4 and 6 hours, on puromycin incorporation was investigated to evaluate time-dependent effects. Chosen antibody concentrations for specific and isotype control were again 2 μg/ml. As shown in Figure 20A, incubation of cells with increasing puromycin concentrations for 6 hours led to clear decreased counts of viable cells/well in comparison to cells incubated only for 4 hours with puromycin. Highest tested puromycin concentrations resulted in a loss of viability for both incubation times, which was again probably caused by the presence of a high DMSO concentration for this condition. Addition of increasing puromycin concentrations to cells caused an increase in BL1-H MFI of viable cells, whereby this increase was even higher for cells incubated for 6 hours with puromycin. Signal linearity on a logarithmic scale was observed between 0.1 and 5 μM puromycin reaching MFI values of more than 80000 and 130000 upon 4- and 6-hours incubation with puromycin and anti-puromycin antibody staining, respectively. The respective differences in MFI upon incubation with 5 μM puromycin compared to the PBS control were determined to be more than 4.6-fold, independently of the incubation time. Contrary to 6-hours incubation time, a decrease in BL1-H MFI of viable cells was detected for cells incubated with 10 and 100 μM puromycin for 4 hours. Application of the isotype control resulted in comparable BL1-H MFI of viable cells compared to the unstained control independently of tested puromycin concentrations or incubation time (Figure 20B). Histogram plots revealed a clear visible shift of MFI upon puromycin incubation, whereas a narrower peak width was observed for 4-hours incubated cells (Figure 20C) in comparison to cells incubated for 6 hours with puromycin (Figure 20D). Altogether, the results demonstrated the successful uptake and incorporation of puromycin in cell line 2 with a clear dose-dependent increase in BL1-H MFI, that was even higher upon a longer incubation time.

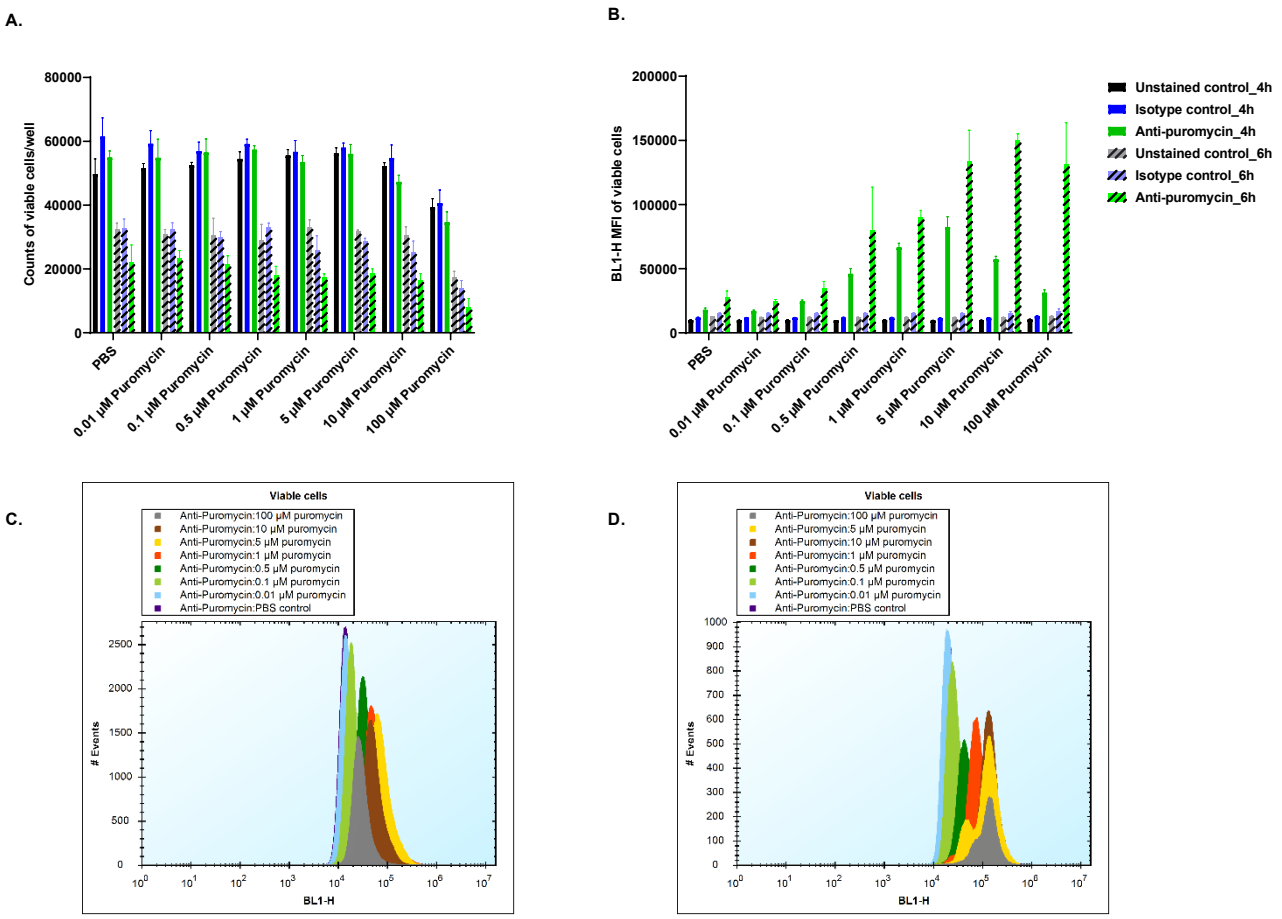

Figure 20: Effect of increasing puromycin concentrations on fluorescence intensity of cell line 2 upon anti-puromycin staining.

CHO K1 cells cultured in Cellvento® 4CHO medium were washed with PBS prior to puromycin treatment with concentrations ranging from 0.01 - 100 µM for either 4 or 6 hours at 37°C, 80% humidity and 5% CO_2. After washing the cells again with PBS, cells were fixed and permeabilized at 4°C and light-protected for 20 minutes, followed by the antibody staining at 4°C and light-protected for 30 minutes (Isotype control: Alexa Fluor® 488 conjugated mouse IgG2a kappa 1:250 in 1X BD Perm/Wash buffer, Puromycin: Alexa Fluor® 488 conjugated mouse anti-puromycin 1:250 in 1X BD Perm/Wash buffer). Subsequently, cells were washed again and measured with flow cytometry at a sip time of 7 seconds. Final cell concentration per well was 20000 cells/µl. A. Effect of puromycin treatment on counts of viable cells/well for unstained control, isotype control and anti-puromycin stained samples. B. BL1-H MFI of viable cells for unstained control, isotype control and anti-puromycin stained samples upon puromycin treatment. C. Histogram plot for anti-puromycin stained viable cells upon 4 hours of puromycin treatment in dependency of the fluorescence intensity detected within the BL1-H channel. D. Histogram plot for anti-puromycin stained viable cells upon 6 hours of puromycin treatment in dependency of the fluorescence intensity detected within the BL1-H channel. Data are mean ± SD of four technical replicates.

Since a decreased isotype antibody concentration (1 μg/ml) did not result in a significant lower BL1-H MFI, this indicated a similar unspecific binding of the isotype control for both concentrations (data not shown). Consequently, the higher antibody concentration was again selected for further experiments (2 μg/ml).

As a next step, the same experiment was repeated but instead of puromycin, cells of cell line 2 were incubated with increasing concentrations of TRX-PURO. Results revealed, similar to the puromycin incubation experiment, a decreased count of viable cells/well for cells incubated for 6 instead of 4 hours with TRX-PURO. Additionally, a significant lower cell count was observed upon incubating cells with 100 μM TRX-PURO compared to the other tested conditions, which was independent of the incubation

time and probably again induced by the DMSO concentration present within these conditions (Figure 21A). An increase in BL1-H MFI of viable cells was observed with increasing TRX-PURO concentrations up to 1 μM, whereas the differences compared to the PBS control were determined to be 1.4-fold and 1.2-fold upon 4- and 6-hours incubation time and anti-puromycin staining, respectively, indicating no time-dependent increase in MFI compared to the control. TRX-PURO concentrations above 1 μM did not cause a further increase in fluorescence signal, which stayed below 26000 and 36000 upon 4 and 6 hours of TRX-PURO incubation, respectively. Interestingly, cells incubated for either 4 or 6 hours with PBS and stained with anti-puromycin antibody showed a similar increased BL1-H MFI of viable cells as cells incubated with TRX-PURO. Unstained cells and cells stained with isotype control resulted in a comparable BL1-H MFI of viable cells (Figure 21B). Histogram plots of viable cells in dependency of the fluorescence intensity observed within the BL1-H channel revealed no peak broadening for any of the tested TRX-PURO concentrations (Figure 21C and D).

Based on those results, the following decisions were made for further experiments performed with cell line 2. Since TRX-PURO incubation for 6 hours resulted in a significant loss in cell viability, an incubation time of 4 hours was suggested to be sufficient for further experiments. Additionally, in order to be able to determine LIP variations among different culture conditions, a TRX-PURO concentration of either 5 or 10 μM was selected since for those concentrations, no further change in fluorescence intensity was observed suggesting an excess of the probe. Moreover, since a linearity of the signal upon puromycin application resulted in a higher MFI compared to TRX-PURO treatment, the already used antibody concentrations were also suggested to be in excess allowing to continue using these concentrations.

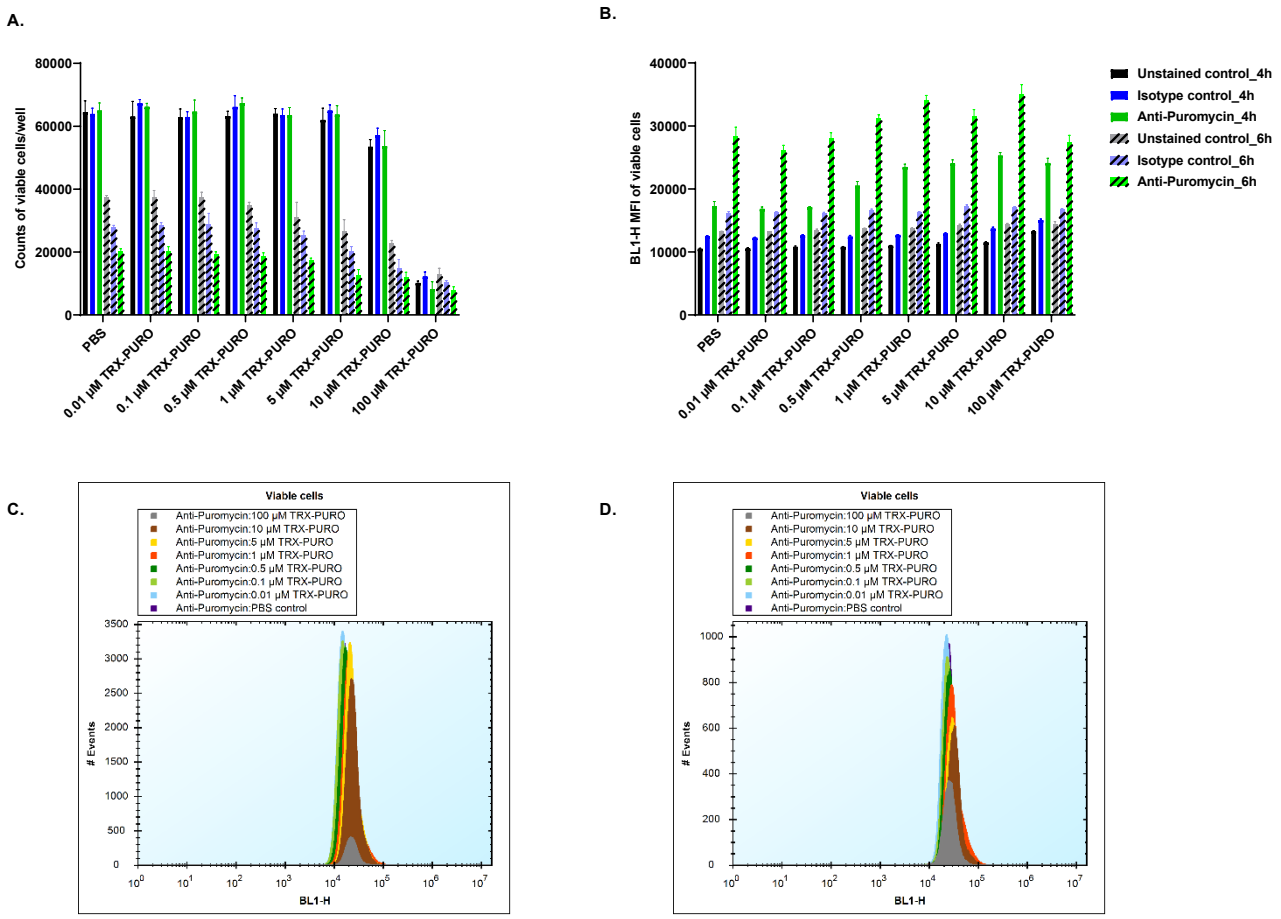

Figure 21: Effect of increasing TRX-PURO concentrations on fluorescence intensity of cell line 2 upon anti-puromycin staining.

CHO K1 cells cultured in Cellvento® 4CHO medium were washed with PBS prior to TRX-PURO treatment with concentrations ranging from 0.01 - 100 µM for either 4 or 6 hours at 37°C, 80% humidity and 5% CO_2. After washing the cells again with PBS, cells were fixed and permeabilized at 4°C and light-protected for 20 minutes, followed by the antibody staining at 4°C and light-protected for 30 minutes (Isotype control: Alexa Fluor® 488 conjugated mouse IgG2a kappa 1:250 in 1X BD Perm/Wash buffer, Puromycin: Alexa Fluor® 488 conjugated mouse anti-puromycin 1:250 in 1X BD Perm/Wash buffer). Subsequently, cells were washed again and measured with flow cytometry at a sip time of 7 seconds. Final cell concentration per well was 20000 cells/µl. A. Effect of TRX-PURO treatment on counts of viable cells/well for unstained control, isotype control and anti-puromycin stained samples. B. BL1-H MFI of viable cells for unstained control, isotype control and anti-puromycin stained samples upon TRX-PURO treatment. C. Histogram plot for anti-puromycin stained viable cells upon 4 hours of TRX-PURO treatment in dependency of the fluorescence intensity detected within the BL1-H channel. D. Histogram plot for anti-puromycin stained viable cells upon 6 hours of TRX-PURO treatment in dependency of fluorescence intensity detected within the BL1-H channel. Data are mean ± SD of four technical replicates.

Following the procedure of the reference paper, it was then decided to pre-incubate the cells for 2 hours in media comprising different iron concentrations prior to TRX-PURO treatment and subsequent fixation/permeabilization and staining. It was expected that a higher iron concentration within the medium leads to a higher LIP similar to the results published by Spangler *et al.* 2016.[151] Chosen iron concentrations were 2 and 10 mg/L (FC) with a selected cell concentration of 2 x10^6 cells/ml during the incubation step. As shown in Figure 22A, only slightly lower counts of viable cells/well were detected for cells pre-incubated in 2 mg Fe/L compared to 10 mg Fe/L, whereas no difference was observed for the different staining conditions or TRX-PURO concentrations applied. Pre-incubation of cells within media containing different iron concentrations resulted in an increased BL1-H MFI of viable cells upon

anti-puromycin staining compared to the PBS control (more than 3.1-fold increase). However, no difference in BL1-H MFI of viable cells was detected upon incubating cells either in 2 or 10 mg Fe/L prior to TRX-PURO treatment, which was independent of the used TRX-PURO concentration (Figure 22B). Overall, those results suggested that pre-incubation of cells within media containing different iron concentrations did not affect LIP concentration for cell line 2, which was contrary to published data by Spangler *et al.* 2016.[151]

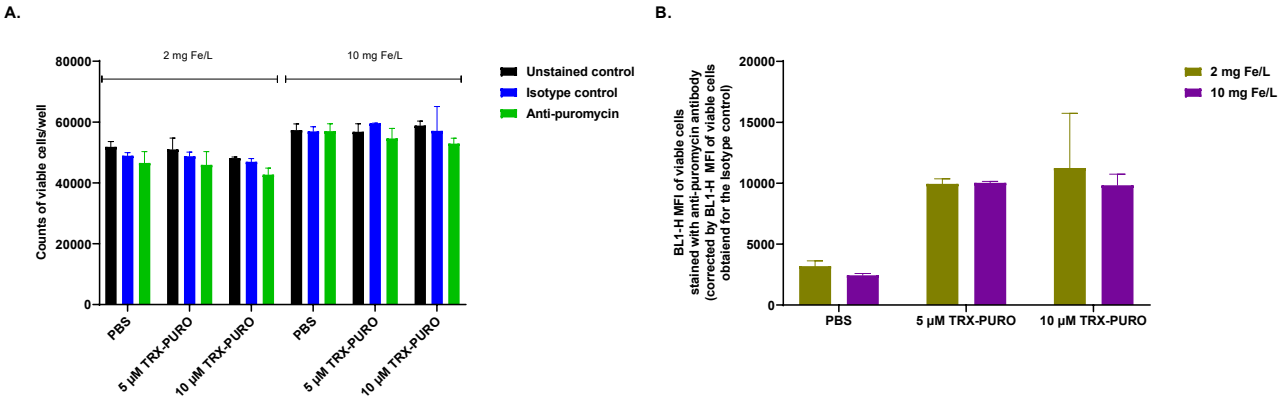

Figure 22: Effect of iron pre-incubation prior to TRX-PURO incubation on fluorescence intensity of cell line 2 upon anti-puromycin staining.

CHO K1 cells cultured in Cellvento® 4CHO medium were incubated for 2 hours in medium containing either 2 or 10 mg Fe/L (FC) before cells were washed with PBS and incubated with either 5 or 10 µM TRX-PURO for 4 hours at 37°C, 80% humidity and 5% CO_2. After washing the cells again with PBS, cells were fixed and permeabilized at 4°C and light-protected for 20 minutes, followed by the antibody staining at 4°C and light-protected for 30 minutes (Isotype control: Alexa Fluor® 488 conjugated mouse IgG2a kappa 1:250 in 1X BD Perm/Wash buffer, Puromycin: Alexa Fluor® 488 conjugated mouse anti-puromycin 1:250 in 1X BD Perm/Wash buffer). Subsequently, cells were washed again and measured with flow cytometry at a sip time of 7 seconds. Final cell concentration per well was 20000 cells/µl. A. Effect of iron pre-incubation prior to TRX-PURO treatment on counts of viable cells/well for unstained control, isotype control and anti-puromycin stained samples. B. BL1-H MFI of viable cells for anti-puromycin stained samples and corrected by the BL1-H MFI of viable cells for the respective isotype control upon iron pre-incubation prior to TRX-PURO treatment. Data are mean ± SD of either four (PBS control) or two technical replicates.

To exclude the possibility that the pre-incubation time was too short, cells were cultured for a longer period of time, namely 3 weeks, within CCM comprising either 2 or 10 mg Fe/L (FC). However, there was still no effect on LIP concentration observed (data not shown). Due to time limitations, it was then decided that a further method development with TRX-PURO was not reasonable without having a more profound literature evaluation done.

In conclusion, the method development for using different (fluorescent) probes, namely calcein and TRX-PURO, for detecting LIP concentrations in CHO K1 cell lines by flow cytometry was not as straightforward and easy as experienced for the colorimetric ferrozine-based assay. A more detailed evaluation of the different methods might be needed to implement a robust method able to reflect LIP concentrations for CHO K1 cell lines. However, it might be possible that, contrary to the data presented within the reference papers, increasing iron concentrations within CCM might not lead to a fluorescently measurable change in LIP concentration of CHO cells due to cell line-dependent effects and limitations.

4.1.3 Discussion

Determining intracellular iron amount is a helpful tool to evaluate and characterize the cellular iron homeostasis. Therefore, within this study, a method for detecting total intracellular iron amount was established and several (fluorescent) probes were tested for their capability to determine LIP concentrations within CHO cells. Whereas the colorimetric ferrozine-based assay was proven to be a reliable and robust method for total intracellular iron amount quantification whose results were cross-checked and verified with another orthogonal method, namely HR-ICP-MS, the results obtained for the tested (fluorescent) probes calcein and TRX-PURO were not as promising as results presented in literature. Results from the tested fluorescent probe RhoNox-1, however, seemed promising.

Total intracellular iron amount within CHO cells was determined to be around 16.9 fg/cell upon ferrozine-based assay usage, which matched to the intracellular iron amount determined with HR-ICP-MS (14.9 fg/cell). Moreover, these values were also in a similar range presented already by Smit *et al.* 1982[156], who analyzed the iron amount within CHO cells and reported an iron content of 42.6 nmol/10^8 cells, which corresponds to 23.8 fg Fe/cell. Thus, the established colorimetric ferrozine-based assay is a valid tool to evaluate total intracellular iron amount, also within the context of iron-related questions within cell culture processes.

In contrast to the ferrozine-based assay, the results obtained with the fluorescent probe calcein to qualitatively determine the LIP revealed differences compared to published data. Incubation of CHO K1 cells with increasing calcein-AM concentrations led to an increase in fluorescence signal, however, none of the tested chelators (DFP, BPY and SIH), which were added on top to the turn-off fluorescent probe, were able to cause a dequenching of the fluorescence signal. One hypothesis is that the chelators might not have passed the cell membrane and thus might not have complexed iron ions that were previously complexed by calcein. The expected fluorescence dequenching might have therefore not occurred. Missing transporter expression or an inaccessible uptake route within CHO cells might have affected the cellular uptake. However, for all three tested iron chelators, the described uptake route in literature is passive diffusion across the cell membrane suggesting a cell line- and transporter-independent uptake mechanism.[82,146,157,158] It was further reported that compounds with a molecular weight below 200 g/mol are likely to pass the cellular membrane via passive diffusion.[159] This is at least applicable for DFP and BPY with a molecular weight of 139.15 and 156.18 g/mol, respectively. A further indication whether a compound is likely to pass the cell membrane or not comprises the n-octanol-water partition coefficient K_{OW} or log K_{OW}. It defines whether a neutral molecule is rather hydrophilic or rather lipophilic and thus having a higher tendency to pass the cellular membrane[160], whereby a log K_{OW} value greater than -0.7 was suggested to facilitate cell membrane penetration.[80,82] Reported log K_{OW} values for DFP and BPY were -0.77 and 1.50, respectively, whereas a predicted log K_{OW} value of 1.5 was calculated for SIH, indicating a more lipophilic property of the chelators and thus strengthening the reported uptake

route.[157,161,162] Additionally, dissolving the chelators in DMSO instead of in Milli-Q® water to facilitate chelator uptake during the experimental approach did also not lead to a fluorescence dequenching (data not shown) suggesting that there might have been other factors affecting the outcome.

One further hypothesis for the absence of the fluorescence dequenching effect upon chelator treatment is based on an assumed low LIP concentration present within CHO cells. In that case, the quenching of the calcein fluorescence signal upon iron complexation might have been already so low that it was not possible for a chelator to cause a higher dequenching signal and thus resulting in a visible shift in fluorescence intensity. Within the cell, the iron concentration present within the LIP is tightly regulated to prevent the formation of oxidative stress that may lead to cellular damages.[109] Thus, the amount of iron present within the LIP represents only a small percentage of the total iron amount present within the cell.[109] However, the LIP concentration may change due to an altered cellular demand, which was mainly observed for several disease states such as inflammation, β-thalassemia, an iron overload disease affecting the blood cells, or cancer.[151,163–167] Especially for cancer cells, having a rapid proliferation rate and thus a high demand of iron, an increased LIP was determined in combination with altered iron uptake and storage protein expression rates.[151,163,165,168,169] Elevated expression of transporters involved in iron uptake were also demonstrated for hepatocyte cells representing the major iron storage location within the organism.[63,167,170] Among the reported cell lines used for detecting and evaluating successfully the LIP by applying the fluorescent probe calcein-AM were inter alia K562 cells[146,154,171], a human cell line derived from myelogenous leukemia, murine erythroid leukemia (MEL) cells[155,172], human blood cells such as erythrocytes[166] or leukocytes[173], and rat hepatocytes[147], which are all cell types prone to have a high LIP due to their high cellular iron demand or iron storage capacity. It is thus likely that the usage of the fluorescent probe calcein to determine the LIP within CHO cells did not result in a visible effect due to an already limited and low amount of iron present within the LIP. However, to exclude method-related issues and thereby verify and prove the suitability and capability of the method used to determine the cellular LIP with calcein in general, another cell line known to have a high LIP content needs to be studied in combination with the probe.

Usage of TRX-PURO as an immunofluorescence approach to determine LIP demonstrated as well differences compared to the data published by Spangler *et al.* 2016.[151] Whereas increasing amounts of puromycin led to a very important increase in MFI, application of TRX-PURO only caused a slight increase in MFI with increasing concentrations independently of the used CHO K1 cell lines. The results thus suggest a different incorporation rate of puromycin at the ribosomes upon usage of either puromycin or TRX-PURO, which is contrary to the results presented in the reference paper. One hypothesis is that puromycin and TRX-PURO might use different uptake routes within CHO cells compared to the cell lines used by Spangler *et al.* 2016[151], namely PC-3 and U-2 OS cells, leading thus to different intracellular concentrations of puromycin and TRX-PURO after the same incubation time. However, since puromycin

and TRX-PURO showed a similar permeability rate upon usage of a parallel artificial membrane permeability assay (PAMPA)[151], the uptake mechanisms seems to be passive diffusion for both compounds and thus suggesting that this uptake route might be also used within CHO cells.

Another hypothesis is that the intracellular cleavage rate of TRX-PURO probe to generate free puromycin was limited due to a rather low iron amount present within the LIP, similarly to what was already suggested previously in the context of calcein. Since the cells used and tested by Spangler *et al.* 2016[151] to evaluate the LIP upon TRX-PURO application were as well cancer cell lines, it is likely that CHO K1 cell lines might not be suitable for determining LIP concentrations due to a smaller amount of iron present within the LIP compared to the other successfully used cell lines.

The hypothesis of a low LIP present within CHO cells is strengthened by the results obtained upon incubating and cultivating cells within CCM containing different iron amounts, for which no change in LIP was observed. On the one hand, this suggests that the iron uptake within CHO cells might be limited, saturated or just so small, so that therefore no change in LIP was observed. In order to study and evaluate the iron uptake rate upon presence of different iron concentrations within CCM, radiolabeled iron such as ^{59}Fe might be used and added to CCM to determine the radioactivity within the cells after a certain incubation time similarly to what was done by Zhang *et al.* 2008[174], who studied the iron uptake within CHO cells upon DMT1 overexpression. Additionally, it might be reasonable to overexpress transporters and proteins involved in iron uptake to analyze whether a higher protein expression level might increase the uptake rate and thereby identify possible uptake limitations. However, this requires a profound understanding of iron uptake pathways used in the tested CHO cells, for instance by applying gene and protein expression analytics. Alternatively, the sensitivity of the method to determine rather low changes in LIP might have been not high enough and therefore did not lead to a detected difference in LIP upon cultivating cells in CCM with different iron amounts. On the other hand, the absent change in LIP upon incubating cells in different iron concentrations might have also been caused by a fast distribution of iron within the cells once taken up. Thus, instead of being present within the LIP for a longer and thus detectable period of time, the iron might have been either directly stored within ferritin or used intracellularly. The amount of iron bound to ferritin might be quantified by using species-specific isotope dilution mass spectrometry (SS-IDMS) or furnace atomic absorption spectrometry[175–177], whereas an enzyme-linked immunosorbent assay (ELISA) might be used to quantify and evaluate a change in only ferritin protein expression, although the amount of ferritin does not automatically allow to draw conclusions about the iron amount stored inside of it.[178] Methods to determine increased synthesis rates of iron-containing proteins such as hemeproteins or iron-sulfur cluster-containing proteins might include iron isotope labeling studies to track the iron intracellularly or classical protein quantitation methods such as ELISA, Western Blot or MS.[179,180]

Besides CHO-related reasons, other method-related reasons might have affected the outcome upon TRX-PURO usage. One major difference between the method applied herein and the method used by Spangler *et al.* 2016[151] includes the CCM composition. Whereas the CHO cells were cultivated in chemically defined CCM, PC-3 and U-2 OS cells were cultivated in media supplemented with fetal bovine serum (FBS), a non-defined CCM additive containing different proteins and small molecules such as Tf and albumin that might chelate iron.[21,151] It is thus likely that the presence of FBS might have positively impacted the efficiency of iron uptake and thus might have led to an increased LIP in PC-3 and U-2 OS cells. However, the addition of increasing FBS concentrations to CCM 2 hours prior to TRX-PURO incubation did not result in a higher fluorescence intensity compared to non-FBS usage (data not shown). Another major difference comprises the antibody detection principle. Within this work, a direct detection principle consisting of a conjugated primary antibody was used to detect incorporated puromycin, whereas a primary-secondary antibody system (indirect approach) was applied within the reference paper.[151] Although the usage of an indirect detection method involves more protocol steps and thus increases the experiment time compared to the direct immunofluorescence staining, this approach is more sensitive and provides a better signal amplification.[181] Therefore, it might be necessary to evaluate the impact of an indirect immunofluorescence staining on incorporated puromycin detection within CHO cells upon TRX-PURO usage.

Overall, the results demonstrate that only the colorimetric ferrozine-based assay was shown to be a valuable tool to determine total iron amounts within CHO cells, whereas flow cytometry protocols depending on a rather high LIP concentration, such as for calcein and TRX-PURO application, might not be suitable for CHO cells that seem to have a rather low LIP. However, a more detailed study about iron homeostasis in CHO cells is essential to evaluate whether other methods need to be applied for studying LIP-dependent effects in CHO cells.

4.2 Effect of iron in fed-batch processes on cell performance, CQAs, intracellular iron levels and mRNA expression levels

4.2.1 Overview

Iron is a needed compound when performing cell culture processes as it supports essential cellular functions. Therefore, CCM consists of at least one iron source to provide the required amount of iron for the cells. However, the iron concentration may vary with different CCM formulations and can thus impact either cell performance, metabolism or CQAs.

One part of this chapter is thus evaluating the impact of iron in fed-batch processes on CHO cell performance and recombinant protein product quality. In particular, the effect of increasing iron amounts in CCM provided either in form of FAC or FC on CHO K1 cell performance and IgG quality attributes was investigated as well as the overall change on total intracellular iron amount by using the previously established colorimetric ferrozine-based assay. Furthermore, the impact on LIP concentration upon applying increasing FC concentrations to the cells was studied by using the RhoNox-1 turn-on fluorescent probe. Moreover, the mRNA expression level of genes involved in iron homeostasis, namely iron uptake and transport, storage and export, was analyzed during a fed-batch process upon usage of increasing iron concentrations (FAC). Additionally, the effect of increasing FC concentrations within CCM on a further cell line producing a fusion protein was studied by evaluating cell performance and CQA data.

A second part of this chapter is studying the impact of several different iron sources, varying in chelation properties and oxidation state, on cell performance, CQAs and intracellular iron amount of a CHO K1 cell line, whereby the final iron concentration applied to CCM was the same for all tested iron sources. Among the tested iron sources were FAC, FC, F(III)SC, F(II)SC, $FeCl_3$, $FeCl_2$ and $FeSO_4$. Additionally, the effect on LIP upon usage of either FC or $FeSO_4$ was studied by using the turn-on fluorescent probe RhoNox-1. Moreover, similarly to the first part, the mRNA expression level of genes involved in iron homeostasis was evaluated during the fed-batch process upon usage of those different iron sources.

4.2.2 Results

4.2.2.1 Effect of increasing iron concentrations

The effects of increasing iron amounts in CCM on cell performance and CQAs have been already published in *Biotechnology Progress* in 2021[136] as part of this PhD thesis project. However, in the following, key findings will be revised and linked to further non-published data. The respective figures taken from the publication are labelled accordingly.

CHO K1 cells

Within the scope of the paper, it was demonstrated that the cell performance of a CHO K1 cell line in Cellvento® 4CHO medium as well as CQAs of the produced mAb are strongly impacted by the manganese impurity level present within the used iron sources when performing a small-scale fed-batch experiment. This was especially observed when adding increasing amounts of either FAC or FC into iron-deficient Cellvento® 4CHO CCM, whereby the used iron source FC comprised a manganese impurity of only 0.36 μg/g FC in comparison to 38 μg Mn/g FAC. The latter was thus contributing to more than 94% of the total manganese concentration present within the CCM only due to its manganese impurity. Since FAC and FC in general are showing a similar chelation strength and ammonium content present in FAC was proven to be not relevant for any of the observed results (data not shown), this direct comparison of FAC and FC was possible. The respective results are presented in Figure 23. Addition of either 10, 50 or 100 mg Fe/L in form of FC resulted in a reduced maximal VCD of 7.4, 28.9 and 3.5%, respectively, compared to the corresponding FAC condition containing a higher manganese impurity level, whereas increasing amounts of iron, independently of manganese impurity, caused a slightly reduced cell growth (Figure 23A). With increasing iron concentrations, a faster decline in viability was observed for both iron sources, however, this effect was even more pronounced upon FC usage, the low manganese-contaminated iron source (Figure 23B). Only slight variations on titer production were observed between the different iron sources (Figure 23C). A similar decrease in iron concentration over time was detected for both tested iron sources, whereas higher starting iron concentrations within the CCM led to a higher absolute decrease (Figure 23D). The results thus revealed that the presence of manganese impurity in iron sources contributed to an overall improved cell performance, whereas increasing iron concentrations alone, which were tested by adding increasing amounts of low manganese-contaminated FC, showed a rather reduced cell growth and faster decline in cell culture viability.

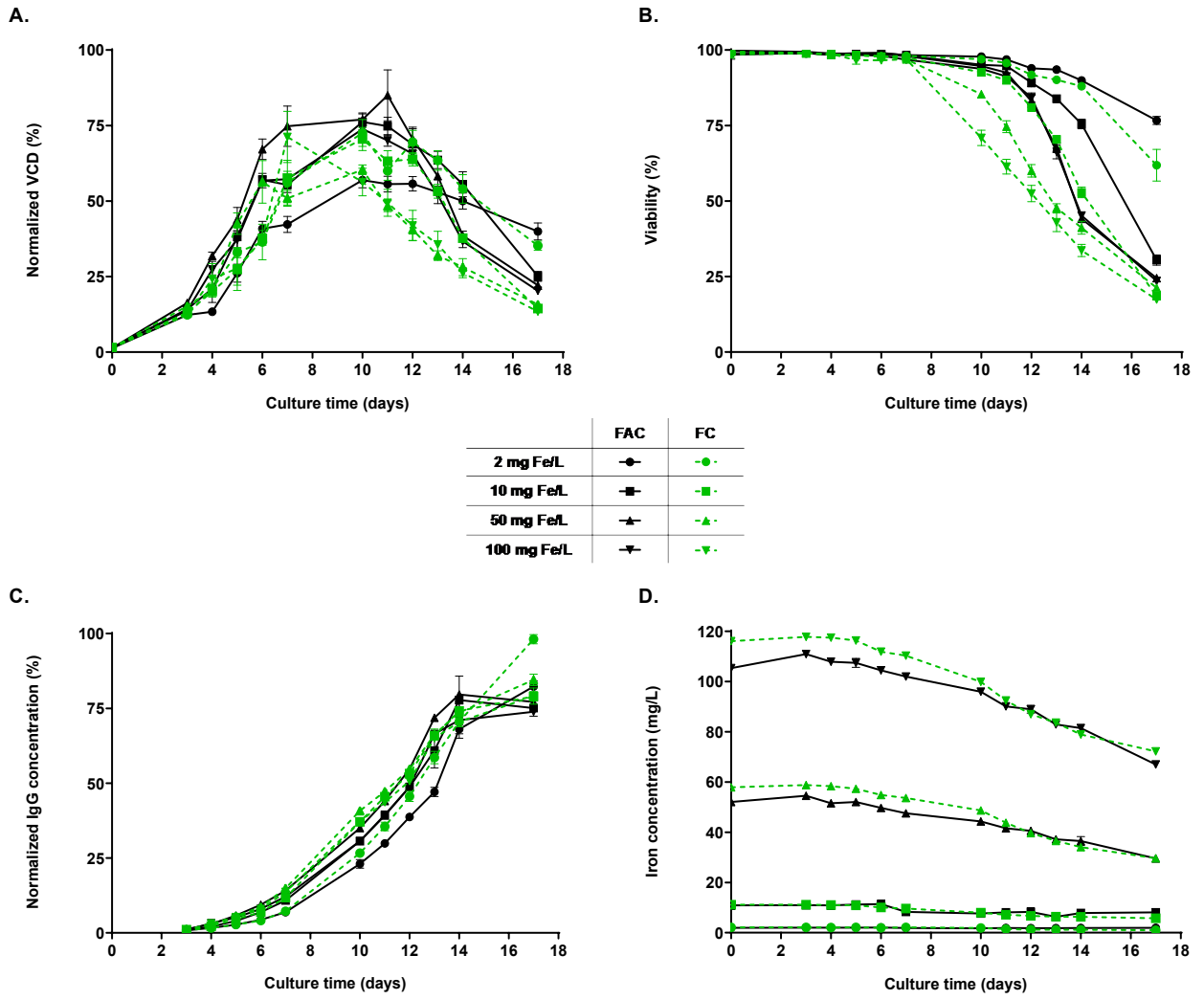

Figure 23: Effect of increasing FAC or FC concentrations in CCM on cell performance of a CHO K1 cell line in a fed-batch process.

CHO K1 cells were cultivated in iron-deficient Cellvento® 4CHO medium supplemented with either 2, 10, 50 or 100 mg Fe/L (FAC or FC). 1.5% (v/v) of Cellvento® 4Feed were added on day 3 and 3% (v/v) on day 5, 7, 10, 12 and 14. Cultivation was performed in 50 ml spin tubes at 37°C, 5% CO_2, 80% humidity and with an agitation speed of 320 rpm. A. VCD in % normalized to the highest value measured using the Vi-CELL^{XR}. B. Viability in % measured using the Vi-CELL^{XR}. C. IgG concentration in % normalized to the highest value measured using the Cedex Bio HT. D. Iron concentration in mg/L measured with Cedex Bio HT. Data are mean ± SD of six biological replicates. The graphical plot was taken and slightly modified from Weiss *et al.* 2021.[136]

Aggregation and glycosylation profiles of the produced mAb on day 10 of the fed-batch process were analyzed by SEC-UV and CGE-LIF, respectively. Obtained aggregation results revealed a dose-dependent increase in HMW species level with increasing iron concentrations which was independent of the used iron source and thus of the present manganese impurity level. The overall detected HMW species level did not exceed a value of 3.1%, implicating a main peak level of more than 96.9% (Figure 24A). Evaluation of the glycosylation profile of the mAb revealed significant differences upon either FAC or FC usage. An increased level of terminal galactosylated species was detected upon increasing FAC concentrations with an absolute increase from 13.3 to 25.6% upon an iron increase from 2 to 100 mg Fe/L, respectively, which inversely correlated with observed decreasing terminal GlcNAc species

levels. In contrast, increasing low manganese-contaminated FC concentrations within CCM caused a slight decrease of terminal galactosylated species with the lowest value detected for 50 mg Fe/L (8.0%). Detected levels of terminal sialylation, mannosylation and non-identifiable species present within the mAb were below 2.5% for both tested iron sources (Figure 24B). This observed increase in terminal galactosylation level was an effect caused by the manganese impurity present in FAC, whereas iron itself rather caused a reduced level of terminal galactosylated species upon increasing iron amounts.

In conclusion, the results revealed that the actual effect of iron in Cellvento® 4CHO was masked upon the presence of manganese impurity since elevated levels of manganese impurity present within the iron source led to contrary effects on cell performance and protein glycosylation compared to solely iron.

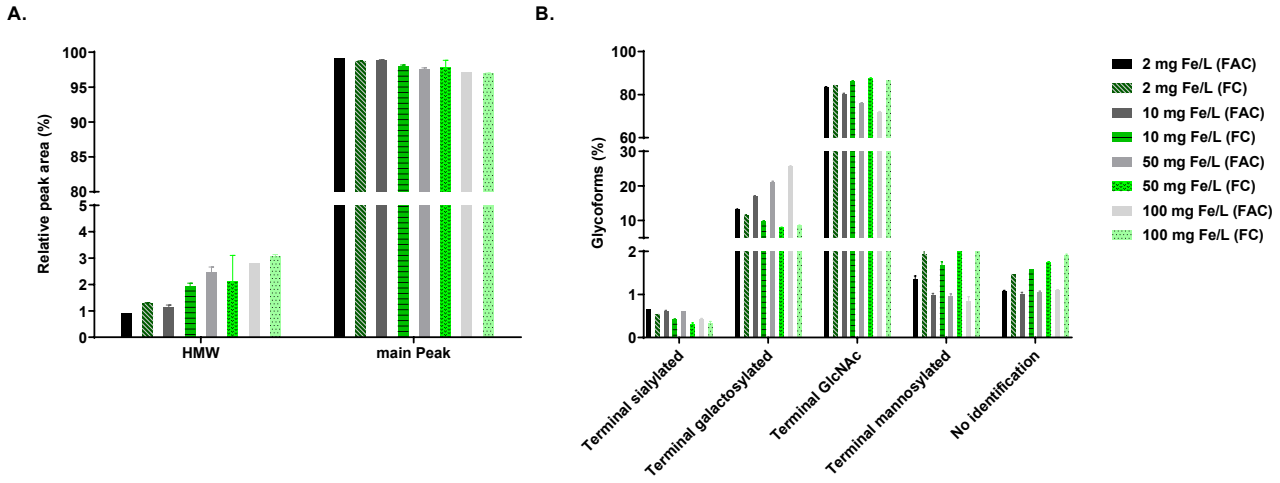

Figure 24: Effect of increasing FAC or FC concentrations in CCM on CQAs of the mAb produced by CHO K1 cell line in a fed-batch process and harvested on day 10.

A. HMW and main peak level in % measured using SEC-UV. B. N-glycosylation forms (terminal sialylated, terminal galactosylated, terminal GlcNAc and terminal mannosylated) in % measured using CGE-LIF. Data are mean ± SD of two replicate pools (each with three biological replicates). The graphical plot was taken and slightly modified from Weiss *et al.* 2021.[136]

In a next step and going beyond the published data, the impact of increasing iron concentrations in Cellvento® 4CHO CCM supplemented either in form of FAC or low manganese-contaminated FC on intracellular iron amount was investigated during the course of the fed-batch experiment for the CHO K1 cell line. Therefore, cell pellets, that were taken during the fed-batch experiment, were analyzed by applying the previously established colorimetric ferrozine-based assay. As shown in Figure 25, intracellular iron concentrations of CHO K1 cell line increased during the course of the fed-batch experiment for increasing iron concentrations independently of the used iron source, whereby this increase was not so pronounced for 2 mg Fe/L. At day 0, an average intracellular iron amount of 55.3 fg/cell was detected, independently of the used iron source and iron concentration, whereby this amount reached values of above 500 fg/cell on day 12 upon an iron concentration of 100 mg/L (FAC or FC) present within the CCM. For 50 and 100 mg Fe/L, lower intracellular iron amounts were determined on day 7 and day 10 upon FC usage compared to FAC, however, on day 12 the respective FC conditions

revealed a higher intracellular iron amount compared to the corresponding FAC conditions. No cell pellet samples were taken on day 14 due to the already reduced cell culture viability for some conditions. Notably, the increase in detected intracellular iron amounts upon usage of 50 and 100 mg Fe/L was steeper after day 7, a time point for which also the decrease in viability became more pronounced for those conditions, as well as an overall decrease in VCD.

Overall, the results indicated that cultivation of CHO K1 cell line in increasing iron concentrations resulted in a time-dependent increase in intracellular iron amount within the cells, whereas no significant difference upon usage of either FAC or FC was observed. Thus, this suggests a manganese-independent iron uptake. However, since a higher increase in iron amounts was observed for the high iron conditions (50 and 100 mg Fe/L) that went faster from the stationary phase into the death phase (starting from day 7 onwards), it seems questionable whether the results of the ferrozine-based assay were representing the actual intracellular iron amounts. A possible co-precipitation of iron with increasing amounts of cell debris might have occurred, and/or iron precipitates might have formed during the course of the fed-batch, which might have then been trapped in the centrifugated cell samples. Thus, the impact of both on the ferrozine-based assay measurement needs to be further investigated.

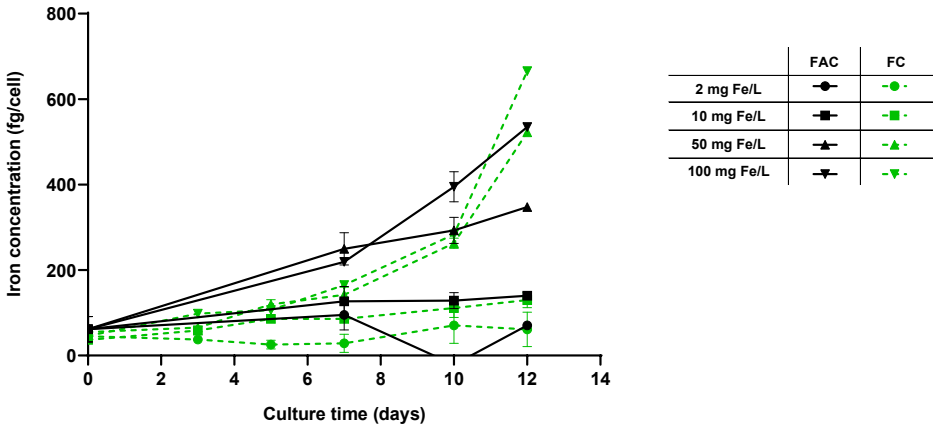

Figure 25: Effect of increasing FAC or FC concentrations in CCM on intracellular iron concentration of CHO K1 cell line in a fed-batch process.

Cell pellet samples were taken on day 0, 7, 10 and 12 for FAC conditions and on day 0, 3, 5, 7, 10 and 12 for FC conditions. Presented are the calculated intracellular iron concentrations in fg/cell, whereby the absorbance values obtained upon application of the ferrozine-based assay were corrected by the control obtained upon no ferrozine addition. Data are mean ± SD of two technical replicates of one pool of three biological replicates.

Ensuing, it was then investigated whether this possible difference in total intracellular iron amount upon supplementation of different iron concentrations into CCM was also observed within a change in LIP. Therefore, LIP was determined during the course of the fed-batch experiment for two selected conditions, namely 2 and 50 mg Fe/L (FC), by using the turn-on fluorescent probe RhoNox-1. Results showed an increase in BL2-H MFI of viable cells over time with an absolute increase in MFI of 40108 and 59448 for 2 and 50 mg Fe/L, respectively, indicating an increase in LIP with time. However, there was no difference in BL2-H MFI of viable cells upon usage of either 2 or 50 mg Fe/L (FC) during the

course of the fed-batch observed, besides on day 10, for which a slightly higher MFI for 50 mg Fe/L was detected (Figure 26). Samples taken on day 12 and 14 of the fed-batch process could not be analyzed due to a fluorescence signal interference in flow cytometer caused by dead cells already present within the samples. Altogether, the results revealed no significant difference in LIP of CHO K1 cells in a fed-batch process upon adding either 2 or 50 mg Fe/L in form of FC to CCM.

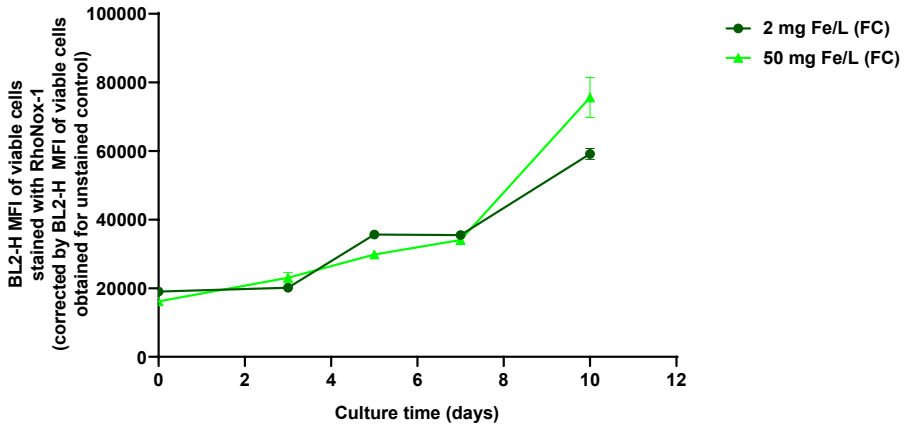

Figure 26: Effect of different FC concentrations in CCM on LIP concentration of CHO K1 cell line in a fed-batch process determined with RhoNox-1 by flow cytometry.

CHO K1 cells of the fed-batch experiment were washed with PBS prior to incubation with 5 µM RhoNox-1 at 37°C for 1 hour. After washing the cells again with PBS, cells were measured with flow cytometry at a sip time of 7 seconds. Final cell concentration per well was 10000 cells/µl. Presented are the obtained BL2-H MFI of viable cells for RhoNox-1 stained samples and corrected by the BL2-H MFI of viable cells for the respective unstained control. Data are mean ± SD of four technical replicates.

In a last step, it was then of great interest whether increasing iron concentrations in a fed-batch process also caused a change in mRNA expression level of genes involved in iron homeostasis, namely *Tfrc* (coding for TfR1), *Slc11a2* (coding for DMT1), *Slc39a14* (coding for ZIP14), *Cybrd1* (coding for DCYTB), *Pcbp1* (coding for PCBP1), *Ftl* (coding for ferritin L), *Fth1* (coding for ferritin H) and *Slc40a1* (coding for FPN), and eventually allowing to draw conclusions about a possible iron uptake mechanism in CHO cells. Therefore, mRNA expression levels were determined during the course of the fed-batch experiment for increasing FAC concentrations and were calculated as fold change by normalizing to an endogenous control (*Gapdh*) and to the control condition, for which day 0 of the fed-batch process was used. The decision for investigating samples of FAC conditions instead of FC was based on the higher obtained cell growth upon increasing FAC concentrations compared to FC, for which thus a higher impact on mRNA expression level was expected. As shown in Figure 27A, *Tfrc* was downregulated on day 7 compared to the control upon usage of 10, 50 or 100 mg Fe/L (FAC), whereas on the following days only a slight decreased expression upon usage of 2 and 50 mg Fe/L (day 10) and a slight increased expression upon usage of 100 mg Fe/L (day 12) was observed. An increased expression level of *Slc11a2* was detected on day 12 for 10 and 100 mg Fe/L (Figure 27B), whereby for the latter condition also a slight increased expression level of *Slc39a14* was observed on day 12 (Figure 27C). Gene expression analysis of *Cybrd1*

revealed an overexpression for all tested conditions on all analyzed days compared to day 0, whereby the increase in expression was the highest on day 12 with 6.1-, 5.7-, 3.3- and 6.9-fold for 2, 10, 50 and 100 mg Fe/L (FAC), respectively (Figure 27D). No change in expression level was observed for *Pcbp1* (Figure 27E). An increase in *Ftl* gene expression was detected for 2 mg Fe/L on day 7 (3.8-fold), for 10, 50 and 100 mg Fe/L on day 10 (2.7-, 8.0- and 4.9-fold, respectively) and for 2, 10, 50 and 100 mg Fe/L on day 12 (4.8-, 2.3-, 10.6- and 7.4-fold, respectively), however, no dose-dependent increase was observed (Figure 27F). In contrast, a dose-dependent as well as a time-dependent increase in mRNA expression level compared to the control was obtained for *Fth1* with a maximum fold change on day 12 of 7.9, 11.3, 12.9 and 14.6 upon usage of 2, 10, 50 and 100 mg Fe/L (FAC), respectively (Figure 27G). *Slc40a1* mRNA expression was increased on day 12 for all tested conditions, whereas the highest tested iron concentration (100 mg Fe/L) induced a 10.7-fold increase (Figure 27H). Overall, the results revealed a clear time-dependent (and dose-dependent) increase in *Ftl* and *Fth1* coding for the storage protein subunits ferritin L and ferritin H, as well as an increased level of *Slc40a1* coding for the iron exporter FPN. Among the tested genes involved in iron uptake and transport, no clear dose-dependent effect on mRNA expression levels was observed. However, clear increased *Cybrd1* mRNA expression levels were detected for all tested iron concentrations on all measured days compared to the control, suggesting an increased ferrireductase DCYTB protein level that might have thus contributed to a possible increased NTBI uptake.

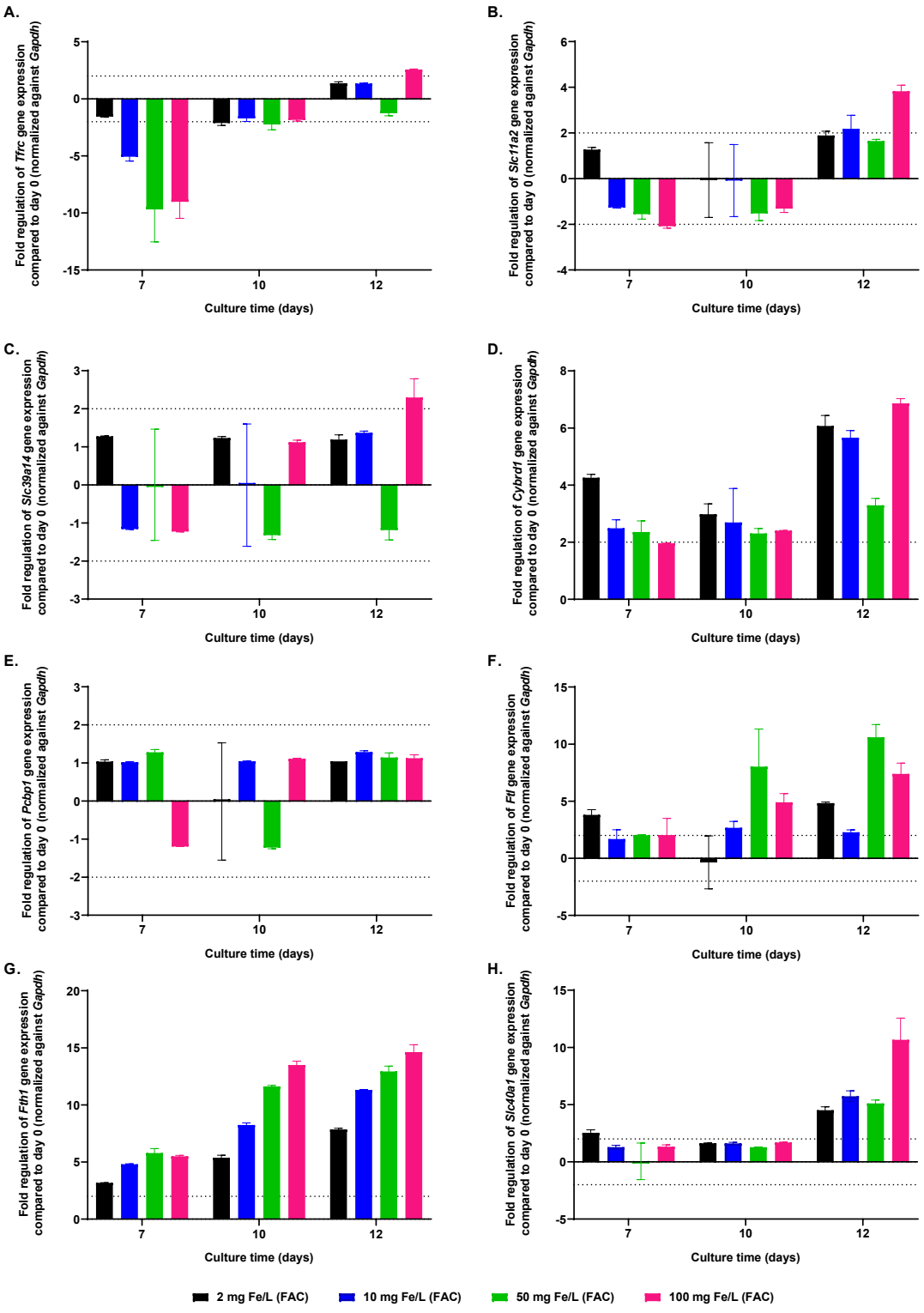

Figure 27: Effect of increasing FAC concentrations in CCM on mRNA expression level of genes involved in iron homeostasis of CHO K1 cell line in a fed-batch process.

Cell pellet samples were taken on day 0, 7, 10 and 12 and mRNA expression levels were evaluated by using the TaqMan™ technology with a preceding RNA purification with RNeasy® Mini Kit. Presented are the mRNA expression levels as fold change normalized to an endogenous control (*Gapdh*) and to the control condition (= day 0). A. *Tfrc* (coding for TfR1). B. *Slc11a2* (coding for DMT1). C. *Slc39a14* (coding for ZIP14). D. *Cybrd1* (coding for DCYTB). E. *Pcbp1* (coding for PCBP1). F. *Ftl* (coding for ferritin L). G. *Fth1* (coding for ferritin H). H. *Slc40a1* (coding for FPN). The horizontal dotted lines at -2 and 2 represent the lower and upper limit of significance for differentially expressed genes, respectively. Data are mean ± SD of two technical replicates of one pool of three biological replicates.

Overall, the results showed that increasing iron amounts in CCM caused a decrease in cell growth and viability of the CHO K1 cell line, as well as a reduced terminal galactosylation level of the studied mAb, which is counteracted upon the presence of manganese impurity present in iron raw material. Additionally, increasing iron concentrations within CCM resulted on the one hand in a decreased iron concentration over time within the supernatant and on the other hand in an increase of intracellular iron levels, which is independent of manganese impurity. However, whether these results were representing the actual intracellular iron amount or were caused by possible iron precipitate formation within CCM that might have impacted the ferrozine-based assay measurement needs to be further investigated. In contrast, no iron concentration-dependent effect on LIP concentration seemed to be present. mRNA expression analysis revealed an increased *Ftl/Fth1* and *Slc40a1* mRNA expression level with increasing culture time (and iron concentration) suggesting an increased ferritin and FPN protein expression level, whereas no dose-dependent effect for any tested gene coding for proteins involved in iron uptake and transport was detected. The obtained mRNA expression level results are thus rather favoring a real difference in intracellular iron amount upon usage of increasing iron concentrations, which was measured with the ferrozine-based assay, than supporting the hypothesis for increased intracellular iron concentrations only due to the formation of possible iron precipitates upon usage of increasing iron concentrations. However, the degree of contribution from possible iron precipitates to the intracellular iron results still needs to be determined.

CHOZN® cells

The effect of increasing iron concentrations, also in dependency of iron raw material impurity, on cell performance and CQAs of a further cell line during a small-scale fed-batch process was also already covered and published within the scope of the paper.[136] Supplementation of increasing FC iron source concentrations to iron-deficient Cellvento® 4CHO CCM revealed, similar to the obtained data for CHO K1 cell line, a manganese-dependent impact on CHOZN® cell performance and CQAs of the fusion protein. This was observed when comparing a low-manganese contaminated FC iron source (FC_{Synt}, 0.36 μg Mn/g FC) with a high manganese-contaminated FC iron source (FC_{Purch}, 530 μg Mn/g FC), whereby those two conditions were additionally compared to manganese-supplemented FC_{Synt} condition to match the same manganese concentration as present within FC_{Purch}. The respective results are presented in Figure 28. Addition of FC_{Purch} or FC_{Synt} + Mn^{2+} to CCM resulted in a higher maximal VCD compared to FC_{Synt}, whereas a higher cell growth was observed for 10 mg Fe/L compared to 50 mg Fe/L independently of the used iron source (Figure 28A). A higher iron concentration present within CCM resulted in a faster decline in viability, whereby this effect was even more pronounced upon low-manganese contaminated FC_{Synt} usage (Figure 28B). Usage of either FC_{Purch} or FC_{Synt} + Mn^{2+} resulted in an increased final titer of 44.0 and 78.0% compared to FC_{Synt} upon usage

of either 10 or 50 mg Fe/L, respectively (Figure 28C). Overall, the results revealed once more that manganese impurity contributed to an overall improved cell performance, whereas increasing iron concentrations alone resulted in a reduced cell growth, faster decline of cell culture viability and lower final titer of fusion protein.

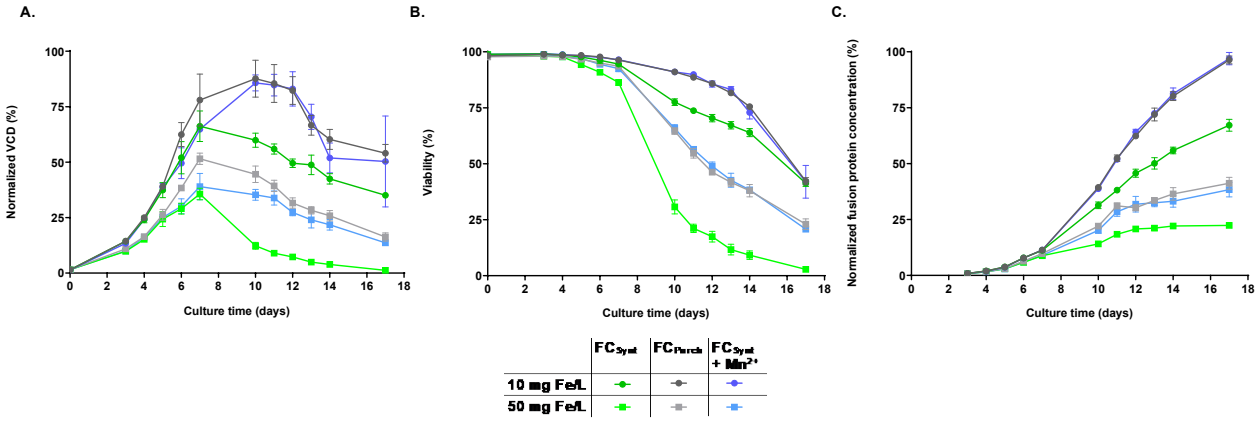

Figure 28: Effect of increasing FC concentrations in CCM on cell performance of a CHOZN® clone in a fed-batch process.

CHOZN® cells were cultivated in iron-deficient Cellvento® 4CHO medium supplemented with either 10 or 50 mg Fe/L (FC_{Synt} (low manganese impurity) and FC_{Purch} (high manganese impurity)). Additionally, a further condition (FC_{Synt} + Mn^{2+}) was added for which manganese was added to FC_{Synt} resulting in the same manganese concentration as present in FC_{Purch}. 1.5% (v/v) of Cellvento® 4Feed were added on day 3 and 3% (v/v) on day 5, 7, 10, 12 and 14. Cultivation was performed in 50 ml spin tubes at 37°C, 5% CO_2, 80% humidity and with an agitation speed of 320 rpm. A. VCD in % normalized to the highest value measured using the Vi-CELL^{XR}. B. Viability in % measured using the Vi-CELL^{XR}. C. Fusion protein concentration in % normalized to the highest value measured using the Cedex Bio HT. Data are mean ± SD of four biological replicates. The graphical plot was taken and slightly modified from Weiss *et al.* 2021.[136]

Aggregation and glycosylation profiles of the produced fusion protein on day 10 of the fed-batch process were analyzed by SEC-UV and UPLC-MS, respectively. Obtained aggregation results revealed a similar HMW species level of around 16.4% for all tested conditions, indicating that neither iron, nor manganese were impacting aggregation levels (Figure 29A). Study of the glycosylation profile of the fusion protein revealed iron- and manganese-dependent effects. Usage of FC_{Purch} or FC_{Synt} + Mn^{2+} resulted in higher terminal sialylated and galactosylated levels compared to low-manganese contaminated FC_{Synt}, whereby this effect was independent of the used iron concentration. Increasing iron concentrations of 10 to 50 mg Fe/L upon FC_{Synt} usage caused an absolute decrease in terminal sialylation level of 8.0%, whereas an absolute increase of 6.2% was observed for terminal galactosylation species. Usage of either 10 or 50 mg Fe/L supplemented in form of FC_{Synt} led to a higher terminal GlcNAc level and slightly elevated terminal mannosylation levels compared to the other two tested conditions (Figure 29B). Overall, the results revealed that manganese present either as impurity or supplemented to CCM caused an increase in terminal sialylation level, whereas increasing iron concentrations alone rather reduced the level of terminal sialylated species. The results thus suggest an opposite effect of iron and manganese on fusion protein glycosylation level.

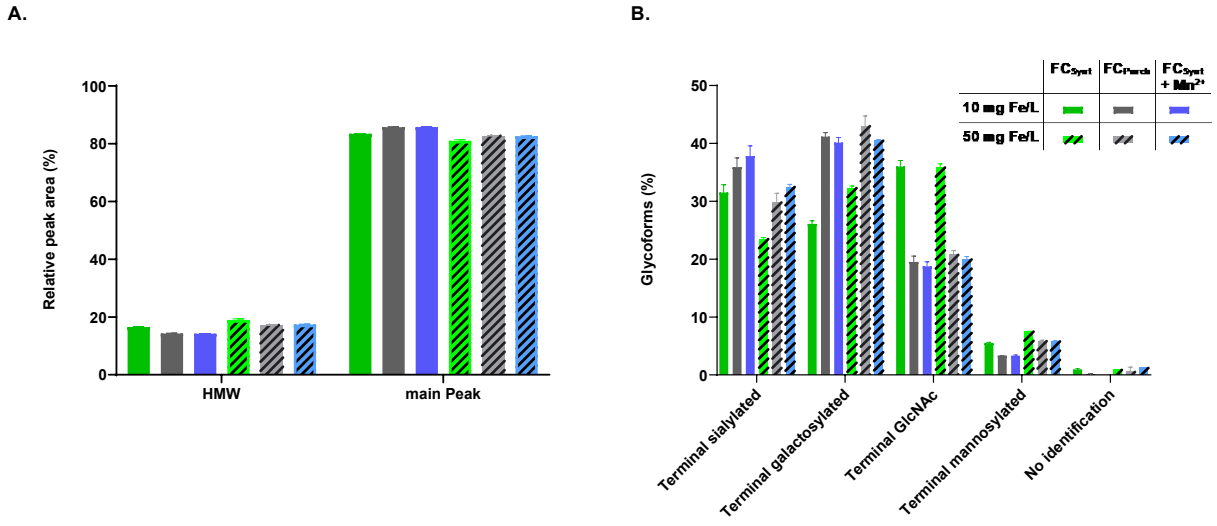

Figure 29: Effect of increasing FC concentrations in CCM on CQAs of the fusion protein produced by a CHOZN® clone in a fed-batch process and harvested on day 10.

A. HMW and main peak level in % measured using SEC-UV. B. N-glycosylation forms (terminal sialylated, terminal galactosylated, terminal GlcNAc and terminal mannosylated) in % measured using UPLC-MS. Data are mean ± SD of two replicate pools (each with two biological replicates). The graphical plot was taken and slightly modified from Weiss *et al.* 2021.[136]

In a further step and going beyond the published data, the impact of iron and its impurities on fusion protein oxidation on day 10 was evaluated by using nanoLC-MS/MS. Therefore, oxidation levels of six different peptides containing methionine or tryptophan residues were calculated by determining the abundances of both oxidized and non-oxidized peptides. As shown in Figure 30, usage of FC_{Purch} or FC_{Synt}, either alone or supplemented with manganese, resulted in similar oxidation levels of the methionine residues M30 and M272 and in similar oxidation levels of the tryptophan residues W65/67, W102, W299 and W333, independently of the used iron concentration. The highest oxidation level was observed for methionine residue M272 with an average value of 10.7%, whereas the oxidation levels of all tested tryptophan residues were below 5.0%. The results thus indicated that neither iron, nor manganese demonstrated an impact on oxidation levels of the fusion protein.

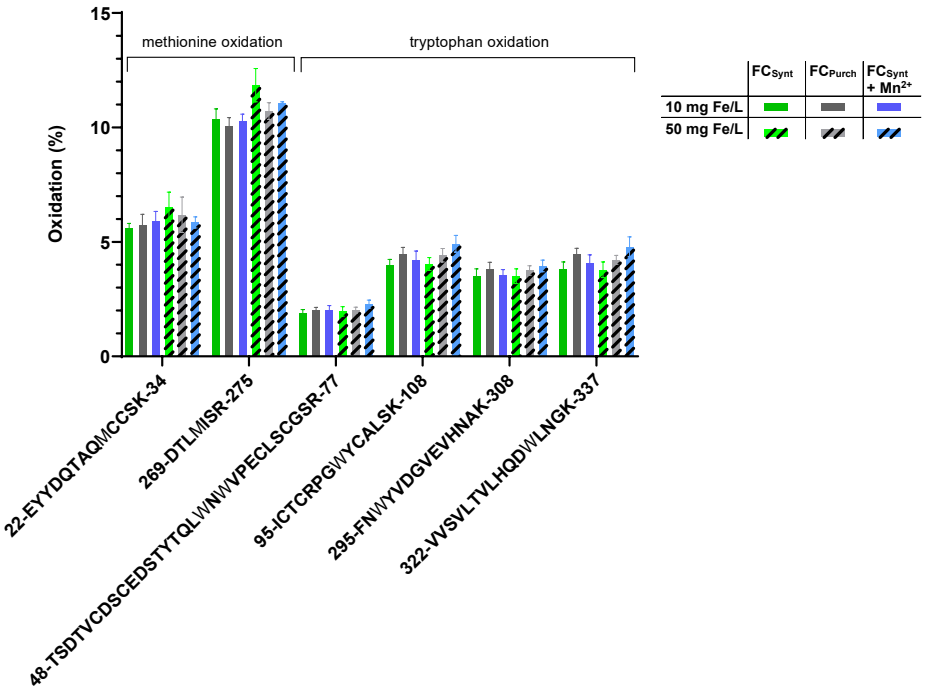

Figure 30: Effect of increasing FC concentrations in CCM on oxidation level of the fusion protein produced by a CHOZN® clone in a fed-batch process and harvested on day 10.

Oxidation level in % for six different peptides measured using nanoLC-MS/MS. Data are mean ± SD of two replicate pools (each with two biological replicates).

Overall, the results showed similar to the observations made for CHO K1 cell line that increasing levels of iron concentration in CCM caused a decrease in cell growth, viability and fusion protein concentration for the tested CHOZN® clone, which was counteracted upon the presence of manganese impurity either present in iron raw material or supplemented to CCM. A contrary effect of iron and manganese was also observed for fusion protein glycosylation, however, in contrast to mAb glycosylation level of CHO K1 cell line, increasing amounts of iron caused an increase in terminal galactosylation and decrease in terminal sialylated species. No effect of either iron or manganese was observed on fusion protein aggregation or oxidation level.

4.2.2.2 Effect of seven different iron sources

The effect of iron on cell performance, CQAs and intracellular iron amount was already studied previously by supplementing either FAC or FC to CCM. However, there are much more iron sources available on the market than the two mentioned. Therefore, a small-scale fed-batch comparability study of seven different iron sources, namely the chelated iron sources FAC, FC, F(III)SC, F(II)SC and the non-chelated iron sources $FeCl_3$, $FeCl_2$ and $FeSO_4$, was performed and their effect on CHO K1 cell line performance, CQAs and intracellular iron level was investigated. Chosen iron concentration supplemented to iron-deficient Cellvento® 4CHO was 50 mg/L since this concentration revealed high cell growth and elevated intracellular iron amounts for the CHO K1 cell line in all previously performed

experiments. Additionally, to mitigate the effect of manganese on cell performance and CQAs, the manganese impurity level present within the iron sources was adjusted to the exact same level. As shown in Figure 31, cell performance was impacted upon usage of different iron sources. Usage of either FAC, FC, F(III)SC, F(II)SC or $FeCl_2$ led to a similar cell growth, whereas a slightly lower maximal VCD was detected upon $FeSO_4$ usage. Addition of $FeCl_3$ to CCM resulted in no cell growth leading to the elimination of this condition on day 10 (Figure 31A). No difference in viability was observed upon usage of the different iron sources, besides for the non-growing $FeCl_3$ condition (Figure 31B). Significant higher final titers compared to $FeSO_4$ condition were detected upon FAC (+33.4%, p-value <0.01, non-parametric Kruskal-Wallis test for multiple-group comparison with subsequent Dunn's test), FC (+28.8%, p-value <0.05) and F(II)SC (+52.4%, p-value <0.001) usage, whereas F(III)SC and $FeCl_2$ gained similar final titers (Figure 31C). Although targeted starting iron concentrations were the same for all used iron sources, detected iron concentrations on day 0 were lower for F(III)SC and $FeCl_3$ conditions, while FAC, FC, F(II)SC and $FeSO_4$ showed a slightly higher starting iron concentration present within the medium. A higher absolute iron decrease during the course of the fed-batch process was observed upon non-chelated $FeCl_2$ and $FeSO_4$ iron source usage, whereas for the $FeCl_3$ condition, a fast drop in iron concentration to below 12 mg/L already on day 3 was observed (Figure 31D). Altogether, the results indicated that usage of different iron sources in CCM led to a comparable cell growth and titer production for most of the tested iron sources with a higher absolute loss in iron concentration observed upon usage of the non-chelated iron sources $FeCl_2$ and $FeSO_4$, whereas usage of $FeCl_3$ did not support cell growth or titer production at all.

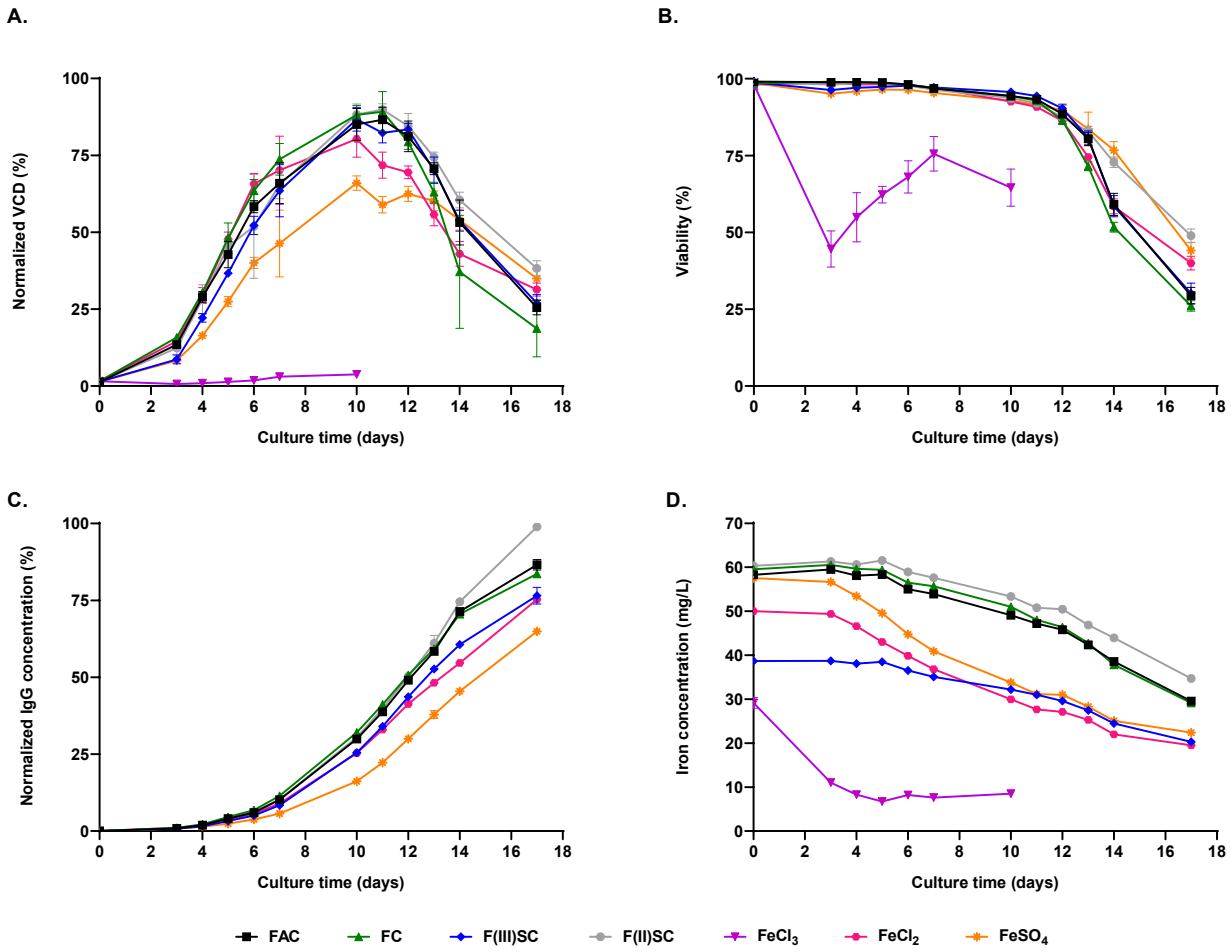

Figure 31: Effect of different iron sources in CCM on cell performance of a CHO K1 cell line in a fed-batch process.

CHO K1 cells were cultivated in iron-deficient Cellvento® 4CHO medium supplemented with 50 mg Fe/L (FAC, FC, F(III)SC, F(II)SC, $FeCl_3$, $FeCl_2$ or $FeSO_4$). 1.5% (v/v) of Cellvento® 4Feed were added on day 3 and 3% (v/v) on day 5, 7, 10, 12 and 14. Cultivation was performed in 50 ml spin tubes at 37°C, 5% CO_2, 80% humidity and with an agitation speed of 320 rpm. A. VCD in % normalized to the highest value measured using the Vi-CELL^{XR}. B. Viability in % measured using the Vi-CELL^{XR}. C. IgG concentration in % normalized to the highest value measured using the Cedex Bio HT. D. Iron concentration in mg/L measured with Cedex Bio HT. Data are mean ± SD of six biological replicates and were already presented in a Master thesis by a supervised student working on this PhD project.[182]

To investigate whether usage of the different iron sources caused an effect on CQAs of the produced mAb, aggregation and glycosylation profile on day 10 of the fed-batch process were analyzed by SEC-UV and CGE-LIF, respectively. The detected level of HMW species was below 5.1% for all tested iron sources, whereby a slightly lower amount of HMWs was observed upon $FeSO_4$ usage (Figure 32A). Glycosylation analysis revealed similar glycosylation profiles for the different used iron sources. An average level of 32.0% and 64.9% was detected for terminal galactosylated and terminal GlcNAc species, respectively, whereas usage of $FeSO_4$ caused slightly altered levels compared to the other tested iron sources. The detected levels for terminal sialylated, terminal mannosylated and non-identifiable species were below 1.4% for all tested iron sources (Figure 32B). Overall, the results demonstrated that CQAs for the mAb were unaffected upon usage of different iron sources within CCM as long as the manganese level within CCM is the same.

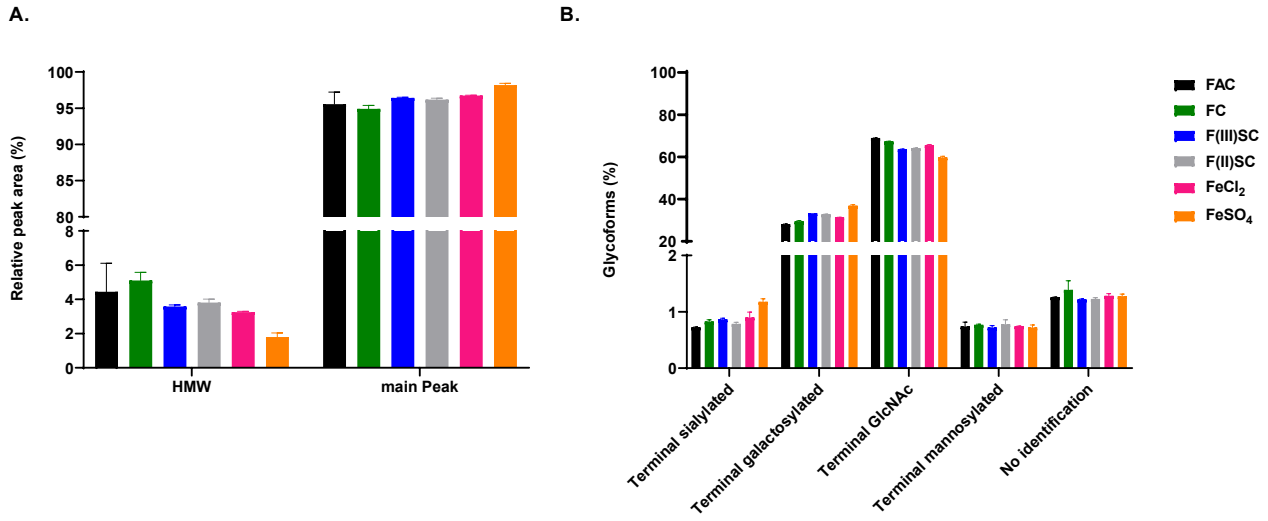

Figure 32: Effect of different iron sources in CCM on CQAs of the mAb produced by CHO K1 cell line in a fed-batch process and harvested on day 10.

A. HMW level in % measured using SEC-UV. B. N-glycosylation forms (terminal sialylated, terminal galactosylated, terminal GlcNAc and terminal mannosylated) in % measured using CGE-LIF. Data are mean ± SD of two replicate pools (each with three biological replicates) and were already presented in a Master thesis by a supervised student working on this PhD project.[182]

Since the iron concentration data revealed different declines in iron concentration measured within the supernatant during the course of the fed-batch, it was of great interest to understand whether such a difference was also observed for intracellular iron amounts. Therefore, the intracellular iron amount of cell pellets taken during the fed-batch experiment was analyzed by the colorimetric ferrozine-based assay. Addition of either FAC, FC or F(II)SC to iron-deficient Cellvento® 4CHO CCM resulted in a steady increase of intracellular iron concentration from around 122.3 fg/cell on day 0 to more than 250 fg/cell measured on day 12. Interestingly, upon F(III)SC usage, a two times higher intracellular iron amount was detected on day 0 and day 3, compared to FAC, FC and F(II)SC. However, on the following days, a similar intracellular iron amount was determined. In contrast, usage of either non-chelated $FeCl_2$ or non-chelated $FeSO_4$ resulted in a drastic increase in intracellular iron amount during the first 5 days of the fed-batch experiment, whereas in the following days a constant intracellular iron amount of around 650 fg/cell was detected (Figure 33). No cell pellet samples were taken on day 14 due to the already reduced cell culture viability.

Overall, the results thus suggested that usage of non-chelated iron sources in CCM caused higher intracellular iron amounts within CHO K1 cells in a fed-batch process in comparison to chelated iron sources. However, whether these data were representing the actual intracellular iron amount seems to be questionable, especially since no difference in cell performance was detected upon usage of either chelated or non-chelated iron sources. Additionally, since the two non-chelated iron sources were missing a chelator normally used to overcome solubility issues of the iron, a possible iron precipitate formation within CCM, that might have led to an overestimation of the intracellular iron amount by

being present within the centrifugated cell samples used for the ferrozine-based assay, needs to be considered and further investigated.

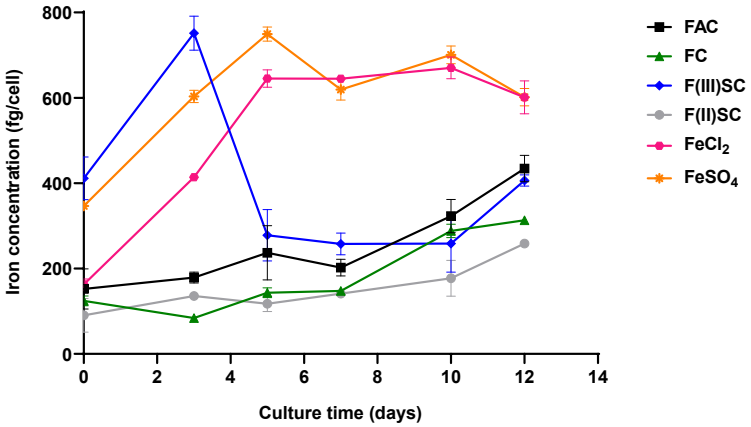

Figure 33: Effect of different iron sources in CCM on intracellular iron concentration of CHO K1 cell line in a fed-batch process.

Cell pellet samples were taken on day 0, 3, 5, 7, 10 and 12. Presented are the calculated intracellular iron concentrations in fg/cell, whereby the absorbance values obtained upon application of the ferrozine-based assay were corrected by the control obtained upon no ferrozine addition. Data are mean ± SD of two technical replicates of one pool of three biological replicates and were already presented in a Master thesis by a supervised student working on this PhD project.[182]

Next, it was of great interest to understand whether the observed possible differences in intracellular iron amount upon usage of either a chelated or non-chelated iron sources was also detected by a change in LIP concentration. Thus, the LIP was determined on several days during a fed-batch experiment with flow cytometry for one representative of each group, namely FC and $FeSO_4$, by using the turn-on fluorescent probe RhoNox-1. As shown in Figure 34, a similar BL2-H MFI of viable cells was detected on day 0 and day 10 for both tested iron sources, however, a higher BL2-H MFI of viable cells was detected on day 3 and day 7 upon usage of $FeSO_4$. Samples taken on day 12 and 14 of the fed-batch process could not be analyzed due to a fluorescence signal interference caused by dead cells already present within the samples. The results thus suggested that usage of a non-chelated iron source caused an increased LIP concentration during the first week of a fed-batch process compared to a chelated iron source.

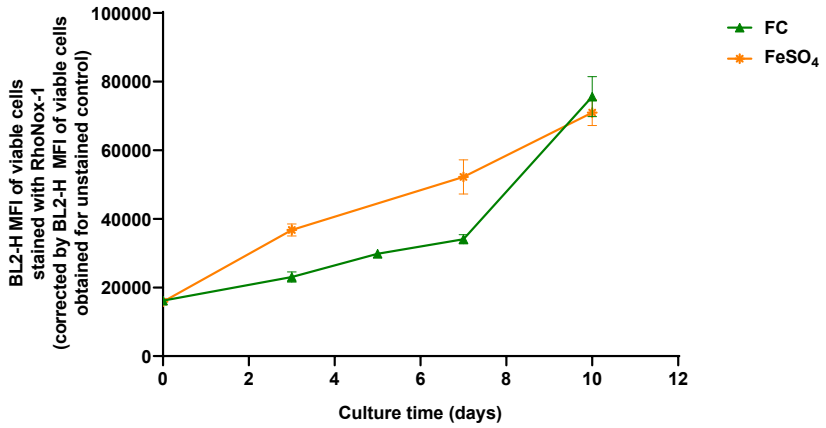

Figure 34: Effect of FC or $FeSO_4$ in CCM on LIP concentration of CHO K1 cell line in a fed-batch process determined with RhoNox-1 by flow cytometry.

CHO K1 cells of the fed-batch experiment were washed with PBS prior to incubation with 5 µM RhoNox-1 at 37°C for 1 hour. After washing the cells again with PBS, cells were measured with flow cytometry at a sip time of 7 seconds. Final cell concentration per well was 10000 cells/µl. Presented are the obtained BL2-H MFI of viable cells for RhoNox-1 stained samples and corrected by the BL2-H MFI of viable cells for the respective unstained control. Data are mean ± SD of four technical replicates.

In a last step, mRNA expression levels of genes involved in iron homeostasis were analyzed, namely *Tfrc* (coding for TfR1), *Slc11a2* (coding for DMT1), *Slc39a14* (coding for ZIP14), *Cybrd1* (coding for DCYTB), *Pcbp1* (coding for PCBP1), *Ftl* (coding for ferritin L), *Fth1* (coding for ferritin H) and *Slc40a1* (coding for FPN), allowing to elaborate further on the impact of different iron sources in CCM. Therefore, mRNA expression levels were determined during the course of the fed-batch experiment upon usage of different iron sources and were calculated as fold change by normalizing to an endogenous control (*Gapdh*) and to the control condition (= day 0). Gene expression analysis of *Tfrc* revealed neither an over-, nor an underexpression on day 3, 5, 10 and 12 compared to the control on day 0, however, a decrease in mRNA expression was observed on day 7 upon FAC, FC, F(II)SC and $FeCl_2$ usage (Figure 35A). No change in mRNA expression level was observed for *Slc11a2* (Figure 35B) and *Slc39a14* (Figure 35C) throughout the fed-batch experiment compared to the control. A time-dependent increase in mRNA expression level from day 7 to day 10 was detected for *Cybrd1*, whereby the highest increase was observed upon FAC and $FeCl_2$ usage with a fold change of 4.7 and 4.6, respectively (Figure 35D). Whereas no fold change in mRNA expression level was obtained for *Pcbp1* throughout the fed-batch experiment (Figure 35E), a time-dependent increase in *Ftl* mRNA expression level was observed with an over 9.7-fold increase on day 12 upon FAC, FC, F(III)SC and $FeCl_2$ usage and an over 3.3-fold increase on day 12 upon F(II)SC and $FeSO_4$ usage compared to the control (Figure 35F). Strangely, a 49.3-fold increase on day 12 was detected for *Ftl* upon $FeCl_2$ usage. A similar time-dependent increase compared to *Ftl* was detected for *Fth1* mRNA expression level, whereby the highest fold change compared to the control was observed upon FAC, FC and $FeCl_2$ usage with 20.2-, 23.2- and 22.6-fold, respectively, compared to the control (Figure 35G). Only slight changes in mRNA expression levels were detected for *Slc40a1* (Figure 35H).

Altogether, the results revealed a clear time-dependent increase in *Ftl* and *Fth1* coding for the storage protein ferritin L and ferritin H, respectively, with the highest levels detected upon usage of FAC, FC and $FeCl_2$ usage suggesting thus a possible higher iron uptake efficiency for those iron sources due to elevated storage protein levels. A time-dependent increase of *Cybrd1* coding for the ferrireductase DCYTB was detected for all tested iron sources suggesting a possible increased NTBI uptake with time. For all other tested genes neither a time-dependent, nor a chelated or non-chelated iron source-dependent effect was observed.

In conclusion, the results showed that usage of different iron sources in CCM caused only slight differences in cell performance and CQAs of the produced mAb for similar manganese levels, whereas non-chelated iron sources seemed to induce a higher iron uptake due to higher detected intracellular iron amounts. However, the impact of a possible iron precipitate formation within CCM upon non-chelated iron source usage on the ferrozine-based assay measurement needs to be further investigated. An increased intracellular iron amount upon non-chelated iron source usage was also demonstrated upon LIP determination, however, further data points may be needed to confirm the effect of non-chelated iron sources on increased LIP concentrations compared to chelated iron sources. mRNA expression level analysis revealed an increased *Ftl* and *Fth1* expression level with increasing culture time suggesting an increased ferritin and FPN protein expression level, whereas no difference in mRNA expression level of genes involved in iron uptake or transport was observed upon usage of either chelated or non-chelated iron sources. However, since mRNA expression levels data revealed no difference upon usage of chelated or non-chelated iron source usage contrary to the intracellular iron amounts, those results are rather in favor of the possible impact of iron precipitate formation on the intracellular iron amount measurement with the ferrozine-based assay. Otherwise, a correlation with storage protein gene expression level might have been observed, similarly to what was observed in the previous chapter for increasing iron amounts.

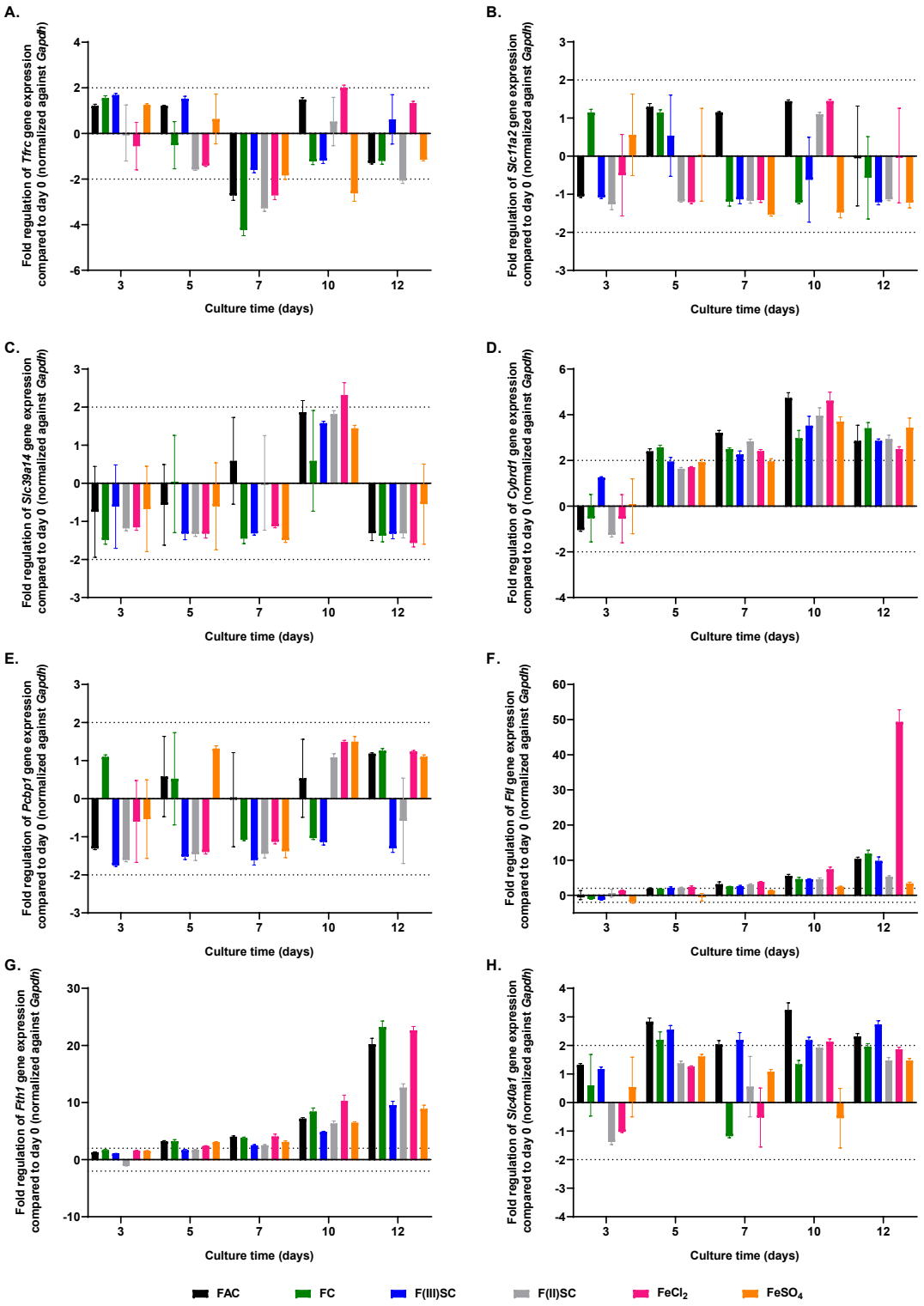

Figure 35: Effect of different iron sources in CCM on mRNA expression level of genes involved in iron homeostasis of CHO K1 cell line in a fed-batch process.

Cell pellet samples were taken on day 0, 3, 5, 7, 10 and 12 and mRNA expression levels were evaluated by using the TaqMan™ technology with a preceding RNA purification with RNeasy® Mini Kit. Presented are the mRNA expression levels as fold change normalized to an endogenous control (*Gapdh*) and to the control condition (= day 0). A. *Tfrc* (coding for TfR1). B. *Slc11a2* (coding for DMT1). C. *Slc39a14* (coding for ZIP14). D. *Cybrd1* (coding for DCYTB). E. *Pcbp1* (coding for PCBP1). F. *Ftl* (coding for ferritin L). G. *Fth1* (coding for ferritin H). H. *Slc40a1* (coding for FPN). The horizontal dotted lines at -2 and 2 represent the lower and upper limit of significance for differentially expressed genes, respectively. Data are mean ± SD of four technical replicates of one pool of three biological replicates and were already presented in a Master thesis by a supervised student working on this PhD project.[182]

4.2.3 Discussion

Iron is an essential compound needed for cell culture processes since iron supports, maintains and regulates several cellular functions. However, an excess of iron may lead to the formation of ROS resulting in oxidative stress for the cells.[62] Thus, within this part of the study, the impact of iron in CCM on cell performance, CQAs, intracellular iron amount and mRNA expression level of genes involved in iron homeostasis was analyzed. More particularly, the impact of increasing iron amounts as well as the effect of different iron sources, namely either chelated or non-chelated, ferrous or ferric sources, supplemented to CCM were studied. On the one hand, the results revealed that increasing amounts of iron added to CCM caused differences in cell growth, viability and glycosylation profile, whereby the effect of iron alone was masked upon manganese impurity when present within the used iron source. Furthermore, increasing amounts of iron seemed to lead to an increase of total intracellular iron, whereas no concentration-dependent differences were observed on LIP. Moreover, an increased *Ftl*, *Fth1* and *Slc40a1* mRNA expression level was observed with increasing culture time, whereby for the latter two even a dose-dependent increase was observed suggesting an increase in intracellular iron. On the other hand, usage of different iron sources supplemented at the same concentration to CCM resulted in only slight differences in cell performance and negligible small differences on CQAs, however, upon $FeCl_3$ usage neither cell growth, nor mAb production was observed. Moreover, varying levels of total intracellular iron amounts and LIP were observed upon usage of chelated and non-chelated iron sources suggesting a chelation-dependent uptake efficiency, however, a possible impact of iron precipitate formation upon non-chelated iron source usage on intracellular iron amount measurement was not fully excluded. mRNA expression level analysis disclosed a time-dependent increase in *Ftl* and *Fth1* gene expression, whereas no difference upon usage of chelated or non-chelated iron source usage was observed.

Effect of increasing iron concentrations

The effect of increasing iron amounts and the impact of manganese impurity present in iron raw material impurity on cell performance and glycosylation was already discussed within the scope of the published paper[136] but the main hypotheses will be shortly revised herein. Upon increasing amounts of manganese, supplemented to CCM either in form of impurities or by $MnCl_2$, prolonged viabilities and higher titers were observed. Since manganese is a known cofactor for mitochondrial superoxide dismutase 2 (SOD2), an enzyme involved in stress response and antioxidant defense by dismutating ROS created during mitochondrial respiration and thereby preventing the cells from apoptosis[183–185], manganese might have contributed to an increased cellular antioxidant capacity of the cells. In contrast, a decreasing cell growth, titer and a faster drop in viability was observed upon increasing amounts of low impurity iron supplemented to CCM suggesting an iron-mediated cell death. This seems to be likely since several ROS-

producing enzymes such as cytochrome P450, xanthine oxidase, or enzymes involved in the mitochondrial electron transport chain, incorporate iron or iron-sulfur clusters to perform their function.[186] Thus, the data suggest an opposite effect of iron and manganese on cellular oxidative stress regulation resulting in contrary effects on cell performance. Since iron was recently reported to be able to inactivate antioxidant SOD2 activity by shifting the enzyme's function to a peroxidase activity upon iron binding[187–190], iron and manganese might have specifically caused an opposite effect on the antioxidant defense capacity of SOD2 within the cells.

A similar different effect of manganese and iron was observed for recombinant protein glycosylation. Increasing amounts of manganese resulted in an increased terminal galactosylation level for the mAb, whereas increasing amounts of low impurity iron resulted in a slight decrease in terminal galactosylated species. Manganese is a known cofactor for β-1,4-galactosyltransferase, however, it was demonstrated that the enzyme has two metal binding sites. Upon binding of further metals such as cobalt or zinc, the formation of an enzyme-metal complex was observed leading to a reduced β-1,4-galactosyltransferase activity.[58,191] Thus, within this study, it is possible that also iron might have formed such an inhibitory enzyme-metal complex and thereby might have altered the enzyme's activity.

Similar to the results obtained for mAb glycosylation levels, contrary effects of manganese and iron were observed for recombinant fusion protein glycosylation. Upon increasing manganese amounts, an increased level of terminal galactosylation and terminal sialylation level was detected, whereas increasing concentrations of low impurity iron source resulted as well in an increased level of terminal galactosylation species but in a decrease in terminal sialylation species. The results thus suggest that iron might have inhibited sialyltransferase activity similarly to what was hypothesized for galactosyltransferase, whereby the inhibitory potential on sialyltransferase seems to be more effective for sialyltransferase compared to galactosyltransferase. However, the decrease in terminal sialylation level upon increasing iron concentrations might have also resulted from a decrease in cell culture viability, which was already reported to cause cell lysis and thereby enhancing the release of sialidase enzymes into the extracellular space.[192]

Overall, the results thus demonstrate the importance of decoupling both elements from each other to control and adjust each element concentration independently resulting thereby in consistent and reproducible cell culture processes.

Within this study and going beyond the published data, the impact of iron on a further CQA, namely oxidation, was investigated for the fusion protein. Thereby, neither iron, nor the presence of manganese impurity caused an effect on oxidation levels. However, this is contrary to described results for iron. For instance, elevated levels of iron in CHO CCM were reported to cause protein oxidation and thereby leading to an increased color formation and an increased level of acidic charge variants.[130,131] Moreover, iron was shown to cause methionine oxidation within proteins and peptides[47], and parathyroid

hormone (PIH) oxidation levels at methionine or tryptophan residues were also demonstrated to be affected upon iron presence.[193] Additionally, mAb degradation was reported as a result of iron-mediated oxidation, which was mitigated upon iron chelator addition.[194] Thus, one hypothesis for the observed absent effect of iron on oxidation is that iron chelators present within the used CCM herein might have also prevented or significantly reduced protein oxidation at an extracellular level. Alternatively, in case the oxidation took place intracellularly, the amount of iron present within the LIP might have been too low even upon increasing iron concentrations present in CCM and thus did not lead to a dose-dependent increase in oxidation level. Such a low LIP present within CHO cells was already suggested and discussed in the previous chapter. Moreover, it might be likely that the proteins studied for their oxidation level in literature were more sensitive to oxidation compared to the fusion protein studied herein. Another hypothesis is that iron might have caused protein oxidation but at residues other than the investigated methionine and tryptophan ones. For instance, oxidation at either cysteine, histidine or tyrosine might have occurred. However, the effect of iron on those residues needs to be further investigated.

Studying the effect of increasing iron concentrations within CCM on intracellular iron levels indicated increasing total intracellular iron amounts with increasing culture process time, which inversely correlated to the obtained decreasing iron concentrations measured within the supernatant. The results thus seem to indicate that higher iron concentrations present within the CCM induce a higher iron uptake rate of the cells. Moreover, since no iron-dependent increase in LIP concentration was observed, the results further seem to suggest that the iron once taken up by the cells is either directly used or stored within ferritin. Such an assumption was already made within the previous chapter and respective suggestions in order to study this effect were proposed. Major suggested methods to study the fate of iron once taken up by the cells included iron isotope labeling, SS-IDMS, MS and ELISA.[174–180] However, since a higher increase in total intracellular iron amount was observed for higher iron concentrations although those conditions went faster into the death phase, which was observed by a faster decline in cell culture viability and decreasing VCD, it might be that the ferrozine-based assay measurement was impacted by other cell culture-dependent effects. A possible impact of iron precipitates that might have been trapped within the cell pellets used for analysis seems to be likely. Possible reasons for iron precipitate formation even upon chelator usage were reported to include pH- or light-dependent effects due to different chelate formations or photo-reductive dissociation, respectively, and thereby increasing the dissociation constant of a tested Fe-EDTA complex.[195] Furthermore, a degradation of the ligand followed by an iron release from the complex was described upon hydroxyl radical attack on FC.[196] Since the amount of hydroxyl radicals is increasing in cell culture processes due to an increase in oxidative stress[197,198], it is thus likely that iron chelators might have degraded by those hydroxyl radicals leading therefore to uncomplexed iron that might have then formed iron precipitates. Moreover, since a faster decrease in VCD and viability was observed upon usage of higher iron concentrations within CCM, a possible higher oxidative stress level might have been already present which might have thus led to a

higher iron precipitate formation compared to lower tested iron concentrations. However, the occurrence of iron precipitates in CCM during the course of the fed-batch process as well as the impact of possible iron precipitates on ferrozine-based assay measurements needs to be further investigated. Ideas and suggestions for the removal of possible iron precipitates from cell samples as well as a more detailed discussion about iron precipitation in CCM will be presented below within the "Effect of seven different iron sources" discussion part.

The effect of increasing iron amounts in CCM was additionally studied for mRNA expression levels of genes involved in iron homeostasis and the obtained data favor a dose-dependent increase in intracellular iron amount upon usage of increasing iron amounts within CCM. On the one hand, results indicated a time- and dose-dependent increase in *Fth1* gene expression, whereas for *Ftl* only a time-dependent increase in mRNA expression level was detected in comparison to the control. Since *Ftl* and *Fth1* genes code for the ferritin L and ferritin H subunits, respectively, this increased expression with time suggests an increased ferritin expression level during the course of the fed-batch process, whereby the dose-dependent increase in *Fth1* gene expression level might be likely induced by increasing intracellular iron amounts due to elevated iron uptake upon increasing iron concentrations present within CCM. This might have been similarly to what was reported by Glahn *et al.* 1998[199] who detected an elevated ferritin formation upon higher iron availability for colorectal adenocarcinoma cells 2 (Caco-2). However, whether a higher ferritin expression also correlates to a proportional increased iron storage within ferritin for the tested CHO cells used within this study needs to be further investigated. Possible methods to determine the iron amount bound to ferritin might include SS-IDMS or furnace atomic absorption spectrometry as already suggested within the scope of the method development chapter.[175–177] On the other hand, results also suggest a different proportion of ferritin L and H subunit composition of ferritin due to the detected higher calculated fold change for *Fth1* in comparison to *Ftl*. Whereas a higher L subunit proportion was reported to be mainly involved in long-term iron storage, a higher H subunit proportion was demonstrated to be present in case of iron usage for cellular metabolism.[68,91] Since increasing iron concentrations within CCM also led to an increased cell growth, this might strengthen the hypothesis of a primary usage of iron for cellular metabolism instead of long-term storage. With progress of the fed-batch process, also an increased *Slc40a1* gene expression level was detected suggesting an increased iron export via FPN. This elevated export might have thereby contributed to a faster removal of iron present within the LIP that is able to create ROS on top of the already increased oxidative stress level created during the course of a fed-batch process.[197,198] Tested genes involved in iron uptake or transport revealed no dose-dependent effect, however, further time points earlier within the fed-batch process might be needed to investigate, in order to observe possible effects. An identification of a possible uptake mechanism and a conclusion regarding proteins mainly involved herein can thus not be made. However, since mRNA expression levels do not

automatically reflect and correlate to protein expression levels, protein expression analyses, for example by using Western Blot[180], need to be performed for all tested genes, which might be essential in order to obtain a deeper insight on CHO iron homeostasis, especially on possible iron uptake routes, and to confirm the possible differences in ferritin L and H subunit composition of ferritin.

Effect of seven different iron sources

Supplementation of different iron sources to CCM to study the effect on CHO cell performance revealed a reduced cell growth and titer formation upon $FeSO_4$ usage compared to FAC, FC, F(III)SC, F(II)SC and $FeCl_2$. One hypothesis for this effect is that the increased sulfate concentration within CCM upon $FeSO_4$ addition might have impacted the cell performance. However, adding Na_2SO_4 to CCM on top of $FeCl_2$, another non-chelated ferrous source, to test the impact of sulfate on cell performance proved that other factors than sulfate were responsible for an altered cell performance (data not shown). A further hypothesis is that impurities, other than manganese, present or absent within the $FeSO_4$ iron raw material but absent or present within the other used iron sources might have contributed to an overall decreased cell performance upon $FeSO_4$ usage. A closer look at the impurity profiles of all used iron sources (data not shown) revealed that only chromium was highly abundant in all iron sources but absent in $FeSO_4$. However, chromium was reported to cause oxidative stress, toxicity and carcinogenicity to cells due to its redox cycling properties.[200–202] Thus, it seems rather unlikely that the iron source showing no chromium impurity was causing a decreased cell performance compared to the other chromium-containing iron sources. However, besides trace element impurities, raw materials might also contain organic impurities such as residual solvents used for the synthesis or production process of the iron sources.[203] It is thus likely that volatile impurities present in $FeSO_4$ iron source might have contributed to the observed effect on cell performance, which needs to be further investigated for instance by applying headspace gas chromatography.[203,204]

An even higher impact on cell performance compared to $FeSO_4$ was observed upon $FeCl_3$ usage since for this iron source neither cell growth, nor mAb production was detected. Additionally, for this condition, a fast decline in iron concentration within the supernatant was determined compared to other tested conditions, whereby iron uptake as a reason for declining iron concentrations within the supernatant seems to be rather unlikely due to the absent cell growth. The results thus suggest a possible unavailability of iron for the cells, for instance due to iron precipitation within CCM. Those colloidal particles might have been then trapped within the cell pellet after centrifugation of the cell samples and might have been therefore undetectable within the supernatant. The CCM is an aqueous solution that is titrated to neutral pH, mostly by adding NaOH or Na_2CO_3.[26] However, at this pH value, non-chelated ferric ions are mainly present as insoluble $Fe(OH)_3$.[71,73,205,206] To overcome such an insolubility, appropriate chelators are normally used to stabilize the iron and keep it in solution.[74,75] One hypothesis is thus that the amount of chelators present within the CCM used within this study might have been

either too low or, alternatively, not selective or not efficient/fast enough to appropriately stabilize the added ferric ions once added to the already hydrated CCM. However, recently performed stability studies within our laboratory showed that also non-chelated $FeCl_2$ and $FeSO_4$ precipitated out of CCM solution, albeit with a slower precipitation rate compared to $FeCl_3$ (data not shown), and therefore rather suggesting a too low or not selective enough chelator presence within CCM instead of a too slow chelate formation.

Data obtained for total intracellular iron amount upon ferrozine-based assay application revealed significant differences between chelated and non-chelated iron sources. Whereas for the chelated iron sources FAC, FC, F(III)SC and F(II)SC a similar slight increase in total intracellular iron amount was detected until the end of the fed-batch process, usage of non-chelated iron sources resulted in a fast increase of intracellular iron amounts during the first 5 days of the fed-batch experiment with constant values being observed in the following process days. This steady intracellular iron amount, however, was identified to be a result of high absorbance values detected outside of the linear range of the standard curve leading therefore to invalid intracellular iron amounts. Nevertheless, at a first glance, the results suggest a difference in uptake efficiency for CHO cells upon usage of either chelated or non-chelated iron sources. Since no difference in cell performance was observed, the results thus further suggest that the iron once taken up by the cells might have not been used for cellular metabolism but rather stored intracellularly. However, this needs to be further investigated by studying the intracellular iron usage and distribution in more detail as already suggested previously.[174–180] At a second glance and with regards to the proposed iron precipitation upon $FeCl_3$ usage, the observed difference between chelated and non-chelated iron sources might have also arisen from a faster iron precipitate formation upon usage of non-chelated iron sources. Collected cell samples might have then also included those colloidal particles due to the applied centrifugation steps during sample preparation leading thus to an overestimation of the actual intracellular iron amount measured with the ferrozine-based assay. Contrary to the immediate precipitation of ferric ions in aqueous solution at neutral pH, ferrous ions are initially soluble before they also form insoluble ferric species upon the presence of oxygen[71,73], whereby the rate of ferrous oxidation was reported to be decisive for the precipitation formation.[207] It is thus likely that the addition of the non-chelated ferrous sources to CCM initially might have resulted in the preservation of soluble ferrous ions, but with progress of the fed-batch process, the rate of ferrous oxidation rate might have increased leading to iron precipitation. One compound that is well described in literature able to oxidize ferrous ion to ferric ion is H_2O_2, with the reaction being better known as the Fenton reaction.[69,71] Increasing levels of H_2O_2 in CCM were reported to be a result of increasing oxidative stress levels within the cells causing the formation of cell membrane permeable H_2O_2.[197] Furthermore, there are several compounds in the CCM such as vitamins, ascorbate, flavonoids and thiols that were reported to undergo oxidation due to instability issues and thereby generating H_2O_2.[197,208,209] Moreover, H_2O_2 was also demonstrated to be generated in CCM upon exposure to daylight fluorescent light sources.[208,210] It

is therefore likely that increasing H_2O_2 levels within the CCM during the course of the fed-batch process might have caused the oxidation of non-chelated ferrous ions resulting finally in iron precipitation.

A possible precipitate formation might have also affected the outcome observed for LIP measurement, whereby a higher LIP was detected upon non-chelated iron source usage ($FeSO_4$) compared to chelated iron source usage (FC). Although cell debris and dead cells were excluded from the analysis due to the applied gating strategy, usage of the whole cell dye RhoNox-1 might have also labeled present iron precipitates trapped in the cell samples upon non-chelated iron source usage leading to an increase in baseline intensity and high carry over.[211] Alternatively, RhoNox-1 might have also been turned-on by iron precipitates trapped within the cell pellet prior to cell uptake and thereby causing a higher fluorescence intensity of the gated cells that did therefore not reflect the actual intracellular iron situation. A repetition of the intracellular LIP measurement for both, $FeSO_4$ and FC, might be therefore needed. Overall, it seems to be essential to remove possible formed iron precipitates from cell samples prior to intracellular iron measurements to obtain valid results representing the actual intracellular iron amount. An appropriate method for the removal of iron precipitates upon cell sample preparation might include the usage of filters with a pore size that is able to let through possible formed iron precipitates but retentate the cells that can be then recollected. Alternatively, a laminar wash system might be used that was recently reported to effectively remove cell debris and dead cells from suspension cell cultures.[212] Otherwise, fluorescence activated cell sorting (FACS) might be suitable to separate and thus differentiate between cells and possible formed precipitates.[213]

Similarly to the results obtained upon usage of increasing iron concentrations within CCM, mRNA expression analysis of *Ftl* and *Fth1* revealed an increased gene expression level with time in comparison to the control on day 0 of the fed-batch process, whereby also the fold-change for *Fth1* was higher compared to *Ftl*. The results thus also suggest the primary usage of iron for cellular metabolism instead of a long-term iron storage upon usage of different iron sources due to a higher ferritin H proportion present in ferritin. [68,91] A difference between the usage of chelated and non-chelated iron sources in CCM on mRNA expression level of all tested genes was not detected, which thus rather suggests a faster iron precipitate formation upon non-chelated iron source usage than providing proof for a difference in iron uptake efficiency between chelated and non-chelated iron sources. However, only the analysis of protein expression levels might reveal possible differences upon chelated or non-chelated iron source usage since mRNA expression levels do not automatically reflect protein expression levels.

One further aspect observed within this study is related to the oxidation state of the iron ions present within the used iron sources. Since especially none of the tested chelated ferrous or ferric sources (FAC, FC, F(III)SC and F(II)SC) caused a significant difference on cell performance, detected intracellular iron amount or mRNA expression level of genes involved in iron uptake, it seems that the iron uptake in CHO cells might be independent of the iron oxidation state. However, nothing is known about the iron

oxidation state of the iron sources once added to CCM. Some data suggest a possible redox-cycling capability of iron-citrate complexes[71,214–216], and also studies performed within our laboratory indicated a predominant ferrous state upon FAC addition to cell culture feed (data not shown). Additionally, it is also possible that other iron complexes might have formed once the iron source was added to CCM and therefore other characteristics and properties might have been present and decisive. Studying the fate of iron in CCM seems thus to be critical to evaluate on the one hand the present iron complexes and forms within CCM, and on the other hand the oxidation state of those present iron species. This might help to investigate to which extend the iron state and form in CCM is impacting and determining the uptake mechanism in CHO cells.

4.3 Impact of iron raw material impurity on cell performance and CQAs

4.3.1 Overview

The impact of iron raw materials and its impurities on CHO cell performance and recombinant protein product quality within the chemically defined Cellvento® 4CHO and 4Feed fed-batch platform was already intensively investigated within the scope of the PhD thesis and the results have already been published in *Biotechnology Progress* in 2021.[136] Shortly, it was demonstrated that the addition of either FAC or FC into CCM, which are showing a similar chelation strength, resulted in different effects on cell performance and glycosylation profile of the recombinant produced proteins, whereby the differences were independent of ammonium introduced by FAC. ICP-MS analysis revealed major differences within the impurity content of those two iron sources, whereby manganese impurity present in FAC was identified to be responsible for increased cell growth, titer, and prolonged viability, as well as altered glycosylation levels compared to FC usage. The results thus demonstrated the major impact iron raw material impurities can have on cell performance and CQA and emphasized the need for low impurity iron sources to efficiently decouple the effects of iron and its trace element impurities.[136]

Following the results of the paper, the impact of iron raw material impurity on cell performance and CQAs was further investigated within another medium platform, namely EX-CELL® Advanced CHO Fed-Batch-Medium and the results are presented hereinafter. In particular, two FAC iron sources differing significantly in their impurity profiles have been studied and compared within small-scale fed-batch experiments for a CHOZN® clone producing a fusion protein, whereby the content of this chapter is currently submitted/under review for publication.

4.3.2 Results

Within Cellvento® 4CHO and 4Feed fed-batch platform, manganese impurity present within the iron source was identified to be the root cause for an overall improved cell performance as well as an altered fusion protein glycosylation profile of a CHOZN® cell line.[136] To test whether manganese or other impurities might be also responsible for an altered cell performance and differences of CQAs within another medium platform, two FAC iron sources differing significantly in several element impurity levels were compared upon supplementation to iron-deficient EX-CELL® Advanced CHO Fed-Batch-Medium.

Table 9 summarizes the impurity levels of those two tested FAC iron sources (FAC_1 and FAC_2), which were determined with ICP-MS analysis. Presented are all elemental impurities showing values above 4 μg/g for at least one iron source. Whereas some elements such as potassium (K), zinc (Zn) or gallium (Ga) were only detected in FAC_2, other presented elements were detected in both iron sources. Higher trace element impurity levels were observed in FAC_2 for magnesium (Mg), aluminum (Al), calcium (Ca), titanium (Ti) and vanadium (V), whereas manganese (Mn), nickel (Ni), copper (Cu),

molybdate (Mo) and tin (Sn) levels were higher in FAC_1. A quite similar impurity level was observed for chromium (Cr) and cobalt (Co).

Table 9: Impurity profile of iron sources FAC_1 and FAC_2.

The impurity characterization was performed by ICP-MS, whereby the quantification was carried out by either a semiquantitative elemental screening method using a quadrupole-based ICP-MS or HR-ICP-MS utilizing an external calibration. Only elements showing values above 4 µg/g for at least one iron source are presented. Mg: magnesium, Al: aluminum, K: potassium, Ca: calcium, Ti: titanium, V: vanadium, Cr: chromium, Mn: manganese, Co: cobalt, Ni: nickel, Cu: copper, Zn: zinc, Ga: gallium, Mo: molybdate, Sn: tin. All obtained calibration curves yielded a correlation coefficient of at least >0.995. *Values gained with HR-ICP-MS. The table is currently submitted/under review for publication.

µg/g	Mg	Al	*K	*Ca	*Ti	*V	Cr	Mn	Co	Ni	Cu	Zn	Ga	Mo	Sn
FAC_1	48	34	<5.0	100	32	60	7.5	56	20	50	60	<1.0	<5.0	21	4.5
FAC_2	150	110	5.3	200	120	140	8.5	38	21	40	4	190	10	1.2	0.75

Since the two FAC iron sources gained so different impurity profiles, they were thought to be suitable candidates to study the impact of iron raw material impurity in EX-CELL® Advanced CHO Fed-Batch-Medium platform. Therefore, FAC_1 and FAC_2 were supplemented to iron-deficient EX-CELL® Advanced CHO Fed-Batch-Medium at a chosen iron concentration of 16 mg/L, and a small-scale fed-batch experiment in spin tubes was performed. Usage of FAC_2 resulted in a significant lower maximal VCD of approximately 30% compared to FAC_1 (Figure 36A), as well as in a faster decline of cell culture viability (Figure 36B). Titer profiles were similar up to day 7 of the fed-batch process, however, fusion protein concentration increased further upon FAC_1 usage, reaching a more than two times higher final titer as obtained with FAC_2 (Figure 36C). N-glycosylation analysis of the fusion protein by UPLC-MS revealed only slight differences. An absolute higher terminal sialylated and galactosylated level of only 3.4 and 2.7%, respectively, was obtained upon FAC_1 supplementation compared to FAC_2 usage, whereas slightly higher terminal GlcNAc and terminal mannosylated levels were observed for FAC_2 in comparison to FAC_1 (Figure 36D). Moreover, both iron sources caused no difference in aggregation profile of the recombinantly produced fusion protein (data not shown).

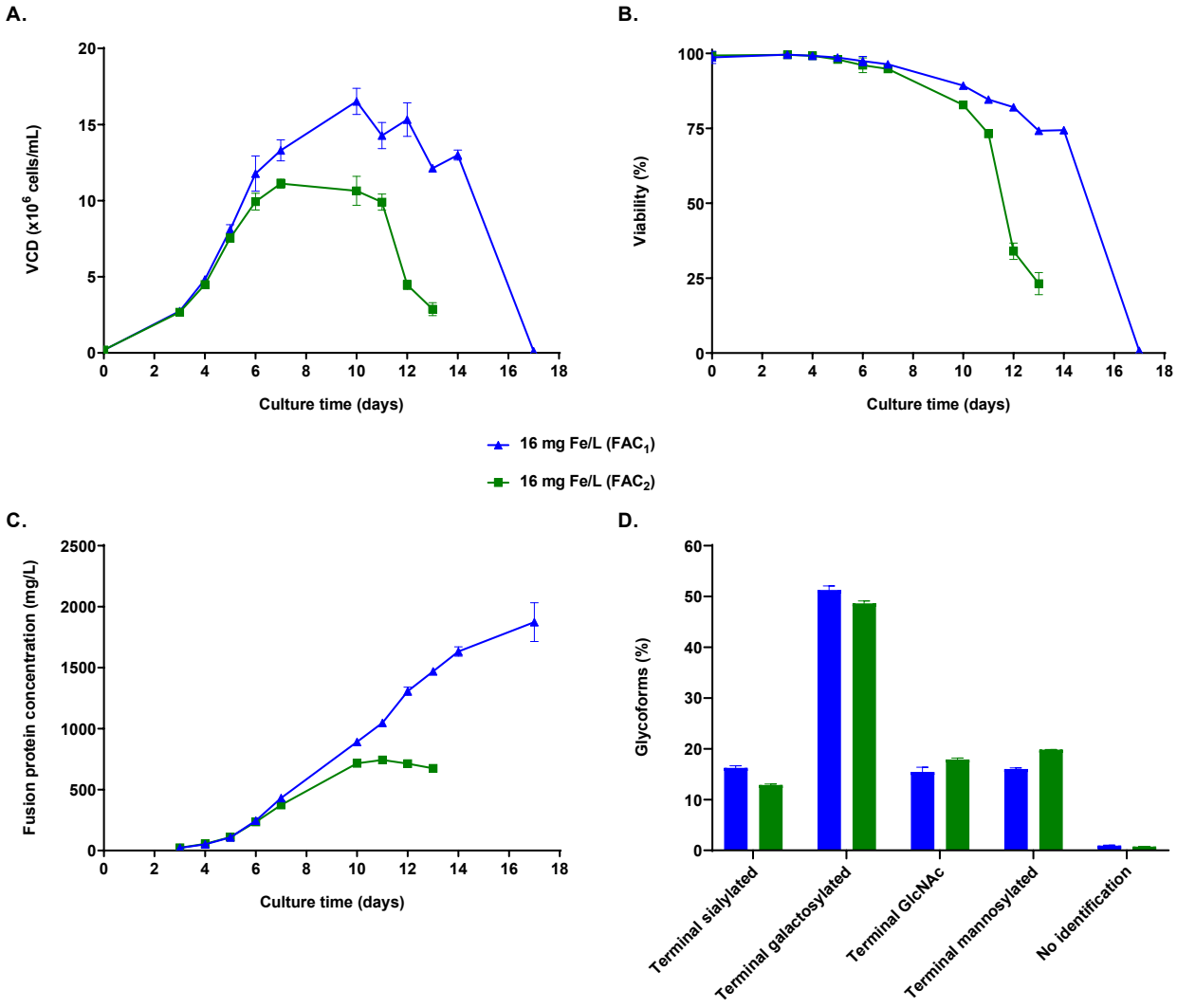

Figure 36: Effect of two different iron sources, FAC_1 and FAC_2, on cell performance of CHOZN® cell line and on glycosylation profile of fusion protein.

CHOZN® cells were cultivated in iron-deficient EX-CELL® Advanced Fed-Batch-Medium supplemented with 16 mg Fe/L (FAC_1 or FAC_2). 5% (v/v) of EX-CELL® Advanced CHO Feed 1 were added on day 3, 5, 7, 10, 12 and 14. Cultivation was performed in 50 ml spin tubes at 37°C, 5% CO_2, 80% humidity and with an agitation speed of 230 rpm. N-glycosylation profile of fusion protein was determined on day 10 of fed-batch process. A. VCD in $x10^6$ cells/ml measured using the Vi-CELL^{XR}. B. Viability in % measured using the Vi-CELL^{XR}. C. Fusion protein concentration in mg/L measured using the Cedex Bio HT. D. N-glycosylation forms (terminal sialylated, terminal galactosylated, terminal GlcNAc and terminal mannosylated) of fusion protein in % measured using UPLC-MS. Data are mean ± SD of four (A., B. and C.) or two (D.) biological replicates. Parts of this graphical plot are currently submitted/under review for publication.

Since manganese was already proven to positively impact cell culture growth and productivity within the Cellvento® 4CHO platform, it was hypothesized that the higher manganese impurity present in FAC_1 (56 μg Mn/g FAC_1) compared to FAC_2 (38 μg Mn/g FAC_2) might be responsible for the observed improved cell growth, prolonged viability, increased titer as well as slightly increased terminal galactosylated and sialylated level. Thus, a further fed-batch experiment was performed, wherein the manganese level of FAC_1 and FAC_2 was adjusted to the same level. However, besides the slight adjustment to a similar level of terminal galactosylation and sialylated species present within the fusion

protein, no improvement in cell performance upon manganese supplementation to FAC_2 was observed (data not shown). This was probably due to a similar high contribution of manganese impurity present within both iron sources to the total manganese concentration in the CCM (>97%). It was thus suggested that impurities other than manganese might have been responsible for the observed effects on only cell performance within EX-CELL® Advanced CHO Fed-Batch-Medium platform. More particularly, it was hypothesized that either impurities that are more abundant in FAC_1 but less present in FAC_2, or impurities that are more abundant in FAC_2 but present at a lower level in FAC_1 might have impacted the outcome.

A closer look at the impurity profiles of FAC_1 and FAC_2 revealed that the number of elements having a higher impurity level within FAC_1 than within FAC_2, including Ni, Cu, Mo and Sn, was fewer than vice versa. Furthermore, since Cu, Mo and Sn element impurity levels were more than five times higher in FAC_1 than in FAC_2, further investigations only focused on the mentioned three elements. Thus, in a next step, the impurity levels of Cu, Mo and Sn supplemented in form of copper (II) sulfate pentahydrate, sodium molybdate (VI) dihydrate and tin (II) chloride dihydrate, respectively, were individually adjusted for FAC_2 to the same level as present in FAC_1 and a further small-scale fed-batch experiment of the CHOZN® cell line within EX-CELL® Advanced CHO Fed-Batch-Medium in spin tubes was performed. Additionally, the combined effect of all three elemental impurities when supplemented to FAC_2 on cell performance was investigated. As shown in Figure 37, cell performance upon usage of FAC_2 was significantly affected upon adjustment of elemental impurity levels. For instance, supplementation of copper to FAC_2 iron source, either alone or in combination with molybdate and tin, led to a similar VCD profile as already observed upon usage of FAC_1. Addition of solely molybdate or tin to FAC_2 iron source resulted in a similar low cell growth compared to FAC_2 only (Figure 37A). Viability for cells cultivated either in only FAC_2 iron source or in FAC_2 iron source supplemented with either molybdate or tin resulted in a faster decline compared to the other tested conditions, whereas the addition of copper to FAC_2 maintained viability above 60% until the end of the fed-batch in comparison to the observed cell death upon usage of FAC_1 on day 17 (Figure 37B). Significant higher final titers were determined upon usage of FAC_2 iron source supplemented with copper compared to either only FAC_2 or FAC_2 conditions containing additionally molybdate or tin. A higher final titer was even observed for FAC_2 supplemented with copper compared to FAC_1 with an average absolute difference of 365 mg/L (Figure 37C). Usage of FAC_1 or FAC_2 supplemented with copper resulted in a lower lactate accumulation within the supernatant compared to the other tested conditions (Figure 37D). No copper-, molybdate- or tin-related effects upon addition to FAC_2 on CQAs, namely aggregation and glycosylation level, were observed (data not shown).

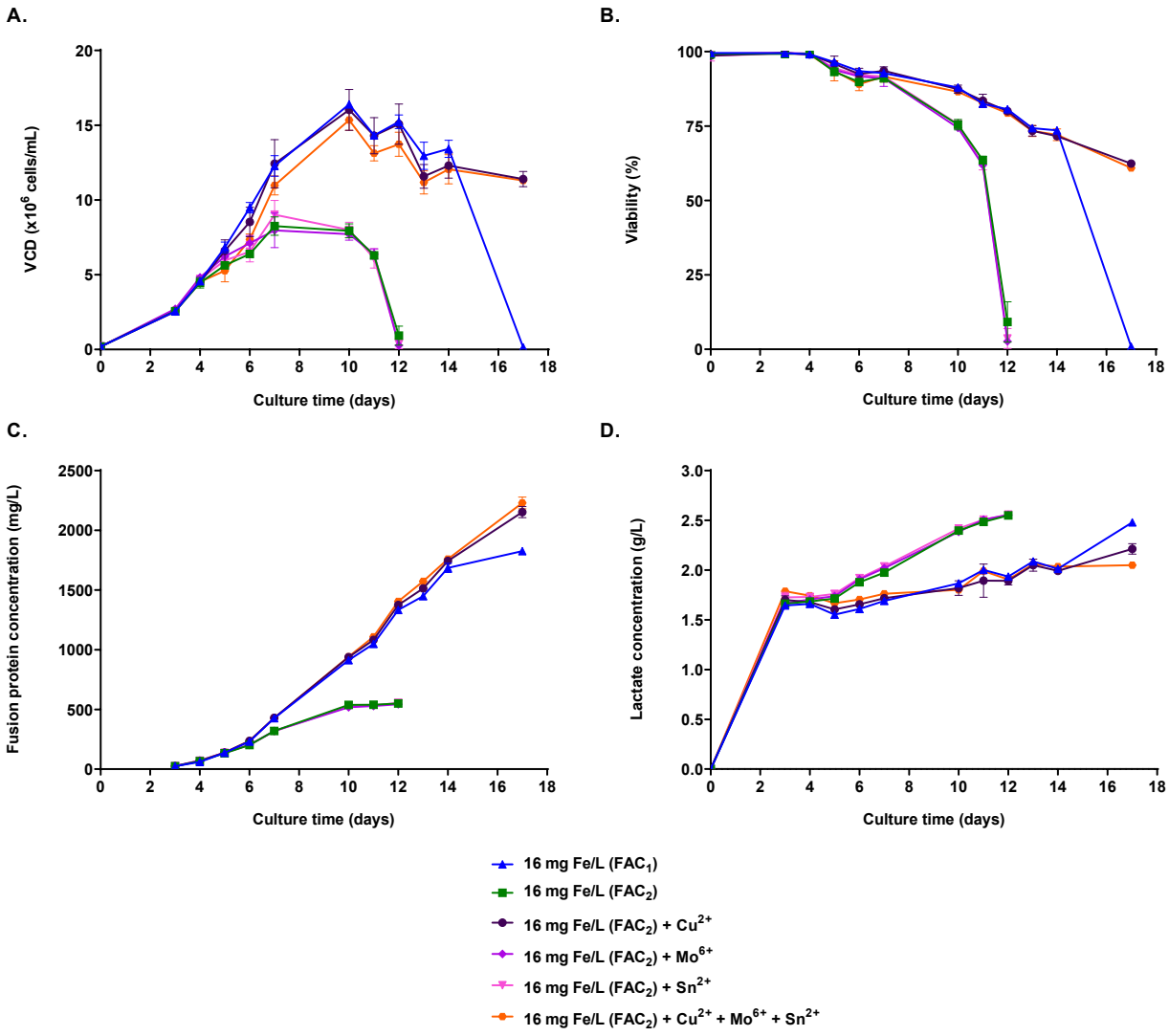

Figure 37: Effect of copper, molybdate or tin supplementation to FAC_2 iron source in CCM on cell performance of CHOZN® cell line in comparison to FAC_1 iron source.

CHOZN® cells were cultivated in iron-deficient EX-CELL® Advanced Fed-Batch-Medium supplemented with 16 mg Fe/L (FAC_1 or FAC_2), whereby copper, molybdate, tin, or the combination of all three of them was added additionally to FAC_2 to achieve the same element concentrations as present in FAC_1. 5% (v/v) of EX-CELL® Advanced CHO Feed 1 were added on day 3, 5, 7, 10, 12 and 14. Cultivation was performed in 50 ml spin tubes at 37°C, 5% CO_2, 80% humidity and with an agitation speed of 230 rpm. A. VCD in $x10^6$ cells/ml measured using the Vi-CELL^{XR}. B. Viability in % measured using the Vi-CELL^{XR}. C. Fusion protein concentration in mg/L measured using the Cedex Bio HT. D. Lactate concentration in g/L measured using the Cedex Bio HT. Data are mean ± SD of four biological replicates. The graphical plot is currently submitted/under review for publication.

Overall, the results show that contrary to the observations made within Cellvento® 4CHO platform, rather copper instead of manganese impurity present within the iron source is contributing to an overall increased cell performance of the tested CHOZN® cell line in EX-CELL® Advanced CHO Fed-Batch-Medium. This was especially observed upon usage of iron sources with different copper impurities contributing significantly differently to the total copper concentration present within the CCM (FAC_1: more than 69%; FAC_2: less than 13%). Thus, the results demonstrate once more the need for low

impurity iron sources to be able to adjust and control the level of iron and other elements independently from each other resulting in consistent and stable cell culture processes.

4.3.3 Discussion

Iron raw material impurities, especially manganese, were already identified as major contributors for altered cell performance and protein glycosylation level within Cellvento® 4CHO CCM platform.[136] This part of the study thus aimed to identify whether iron raw material impurities also affect cell performance and CQAs of a CHOZN® clone within another CCM platform. Therefore, two FAC iron sources differing significantly in their impurity profiles were added to iron-deficient EX-CELL® Advanced CHO Fed-Batch-Medium and small-scale fed-batch experiments were performed. The results revealed that contrary to the observations made within Cellvento® 4CHO CCM platform, copper rather than manganese impurity was significantly improving overall cell performance with a reduced lactate production, whereas no impact on CQAs was observed.

Copper was already reported in literature to increase cell growth and titer upon supplementation to CCM by reducing the overall lactate accumulation within cell culture.[60,217] The underlying mechanism was hypothesized to involve a more efficient energy metabolism via the oxidative phosphorylation pathway upon copper presence due to a higher oxidative metabolic capacity of the cells.[218,219] In contrast, upon copper limitation, an energy generation primarily via glycolysis with no further continuation into the citric acid cycle was suggested leading to a higher lactate accumulation within cell culture.[218,219] It was further suggested that this difference in energy metabolism might be related to copper-dependent enzymes involved in the mitochondrial electron transport chain.[218] One copper metalloenzyme taking part in the oxidative phosphorylation is for instance cytochrome c oxidase, which is responsible for the last electron transfer to the final electron acceptor, namely oxygen, as part of the mitochondrial respiratory chain.[220] A limitation of copper was thus expected to affect cytochrome c oxidase protein level, similarly to what was reported in a study investigating the effect of copper deficiency on the protein expression level of various complexes involved in the mitochondrial oxidative phosphorylation in rat heart tissue.[221] Thus, within this study, copper might have increased the protein expression level of cytochrome c oxidase leading to an enhanced oxidative capacity of the cells and thereby improving overall cell performance by reducing the lactate accumulation within cell culture.

Another explanation for the observed increased cell growth and production of the fusion protein might be the role of copper in antioxidant defense in a similar manner as it was already suggested for manganese. Copper is a known cofactor for copper/zinc superoxide dismutase 1 (SOD1), an enzyme involved in protecting cells from ROS produced during cellular respiration.[222–224] By dismutating superoxide anions, SOD1 is preventing cellular lipid peroxidation or DNA damages and is thus a critical enzyme of the cellular antioxidant defense system.[224]

Although copper impurity in FAC_1 was identified to contribute to an increased overall cell performance, the addition of copper to FAC_2 iron source to match the same copper concentration as present in FAC_1 still resulted in cell performance differences that were especially observed at the end of the fed-batch process. More precisely, usage of FAC_2 iron source supplemented with copper resulted in a prolonged viability and higher final titer of fusion protein compared to FAC_1, whereas the addition of FAC_1 to CCM even led to cell death on day 17. Thus, this suggests that there might have been further trace element impurity differences between FAC_1 and FAC_2 that were affecting cell culture performance. A known trace element that has been disclosed in US Patent No. 6974681B1 for its positive effect on cell growth and viability is vanadium.[225] However, other publications have reported a cytotoxicity within CHO cells upon excessive vanadium presence.[226,227] A further trace element reported to increase productivity within CHO cells was zinc[228], for which also an involvement in oxidative stress regulation was demonstrated due to its cofactor function in SOD1 enzyme.[229,230] An improved cell performance may thus be likely similarly to what was suggested for copper. Since the impurity levels of vanadium and zinc were determined to be more than two times higher in FAC_2 than in FAC_1, those two trace elements seem thus to be likely candidates responsible for the observed differences in cell culture performance upon usage of either FAC_1 or FAC_2 supplemented with copper. However, usage of a low impurity FAC iron source showing neither a vanadium, nor a zinc impurity also resulted in a similar prolonged viability and higher final titer as observed for the vanadium- and zinc-contaminated FAC_2 iron source (data not shown). Moreover, since the low impurity FAC iron source did also not show high levels of other impurity levels, the results rather suggest that there might have been either impurities present within FAC_1 leading to a faster decline in cell culture viability and lower final titer, or that there might have been other factors than raw material impurity, such as organic impurities[203], affecting the outcome. However, both hypotheses need to be further investigated.

Since the results demonstrated the impact of iron raw material impurities on cell culture performance, this highlights the need for low impurity iron sources to be able to adjust and control each element concentration independently. One described root cause for iron raw material impurities includes the usage of undefined starting materials that may not be intended for biopharmaceutical applications. However, variabilities during the manufacturing process itself including the usage of impure solvents, contaminated equipment or leaching packaging may as well lead to raw material impurities.[231,232] It is therefore essential to apply appropriate control systems during the manufacturing process of synthesized raw materials to minimize the variability due to trace elements.[233] Those control steps may be applied during the engineering process, however, also quality control steps such as ICP-MS methods may help to characterize the starting raw materials and thereby allowing a better risk assessment of their supposed impact on cell culture performance.[59,231,233] Nevertheless, decreasing the risk of variability by developing new low impurity iron sources might be more effective and must be considered as a valid alternative.

5 Conclusion and future perspectives

In the presented work, the impact of iron on CHO cell metabolism, on CQAs of recombinantly produced proteins, on intracellular iron levels and on mRNA expression levels of several genes involved in iron homeostasis was analyzed. Thereby, iron raw material impurities, namely manganese and copper, were identified to significantly contribute to an overall improved cell performance and altered glycosylation profile of the investigated recombinant proteins within Cellvento® 4CHO and EX-CELL® Advanced CHO Fed-Batch-Medium platforms, respectively, whereas increasing levels of iron alone rather caused a decrease in cell growth, viability and titer. The use of low impurity iron raw material is therefore crucial to control the effect of iron and its impurities independently and to support and guarantee consistent and reproducible cell culture processes. Since biosimilars need to match CQAs within a very narrow range similar to the original product, this may be particularly relevant within this market sector.

In addition, data of a fed-batch comparability study of seven different iron sources added to CCM demonstrated differences in measured iron concentrations within the supernatant and the cell pellets taken during the course of the fed-batch process upon usage of either chelated or non-chelated iron sources, whereas no difference in mRNA expression of the tested genes involved in iron uptake was observed. At a first glance, the data suggest a difference in uptake efficiency for CHO cells upon usage of either chelated or non-chelated iron sources, however, recent data obtained within our laboratory suggest a faster iron precipitate formation within CCM upon usage of non-chelated iron sources. Studying the fate of iron in CCM and identifying the present iron forms and complexes seem thus to be crucial to understand iron-related uptake mechanisms, which may be further supported by studying protein expression levels of transporters and molecules involved in iron uptake and metabolism. This may be also useful for evaluating and characterizing LIP levels within CHO cells in more detail and be able to compare and relate it to other cell lines and types. Furthermore, the successful removal of iron precipitates seems to be essential for intracellular iron studies and may thus help to develop and generate a more profound knowledge of iron homeostasis in CHO cells with appropriate methods to be used.

6 References

1. Jozala AF, Geraldes DC, Tundisi LL, et al. Biopharmaceuticals from microorganisms: from production to purification. *Brazilian J Microbiol*. 2016;47 Suppl 1(Suppl 1):51-63. doi:10.1016/j.bjm.2016.10.007
2. Kunert R, Reinhart D. Advances in recombinant antibody manufacturing. *Appl Microbiol Biotechnol*. 2016;100(8):3451-3461. doi:10.1007/s00253-016-7388-9
3. Walsh G. Biopharmaceutical benchmarks 2014. *Nat Biotechnol*. 2014;32(10):992-1000. doi:10.1038/nbt.3040
4. Grilo AL, Mantalaris A. The Increasingly Human and Profitable Monoclonal Antibody Market. *Trends Biotechnol*. 2019;37(1):9-16. doi:10.1016/j.tibtech.2018.05.014
5. Nelson AL, Dhimolea E, Reichert JM. Development trends for human monoclonal antibody therapeutics. *Nat Rev Drug Discov*. 2010;9(10):767-774. doi:10.1038/nrd3229
6. Kesik-Brodacka M. Progress in biopharmaceutical development. *Biotechnol Appl Biochem*. 2018;65(3):306-322. doi:10.1002/bab.1617
7. Rita Costa A, Elisa Rodrigues M, Henriques M, Azeredo J, Oliveira R. Guidelines to cell engineering for monoclonal antibody production. *Eur J Pharm Biopharm*. 2010;74(2):127-138. doi:10.1016/j.ejpb.2009.10.002
8. Lalonde M-E, Durocher Y. Therapeutic glycoprotein production in mammalian cells. *J Biotechnol*. 2017;251:128-140. doi:10.1016/j.jbiotec.2017.04.028
9. Durocher Y, Butler M. Expression systems for therapeutic glycoprotein production. *Curr Opin Biotechnol*. 2009;20(6):700-707. doi:10.1016/j.copbio.2009.10.008
10. Lai T, Yang Y, Ng SK. Advances in Mammalian Cell Line Development Technologies for Recombinant Protein Production. *Pharmaceuticals*. 2013;6(5):579-603. doi:10.3390/ph6050579
11. Kim JY, Kim YG, Lee GM. CHO cells in biotechnology for production of recombinant proteins: Current state and further potential. *Appl Microbiol Biotechnol*. 2012;93(3):917-930. doi:10.1007/s00253-011-3758-5
12. Li F, Vijayasankaran N, Shen AY, Kiss R, Amanullah A. Cell culture processes for monoclonal antibody production. *MAbs*. 2010;2(5):466-479. doi:10.4161/mabs.2.5.12720
13. Reinhart D, Damjanovic L, Kaisermayer C, et al. Bioprocessing of Recombinant CHO-K1, CHO-DG44, and CHO-S: CHO Expression Hosts Favor Either mAb Production or Biomass Synthesis. *Biotechnol J*. 2019;14(3):e1700686. doi:10.1002/biot.201700686
14. Fan L, Frye CC, Racher AJ. The use of glutamine synthetase as a selection marker: recent advances in Chinese hamster ovary cell line generation processes. *Pharm Bioprocess*. 2013;1(5):487-502. doi:10.4155/pbp.13.56

15. Urlaub G, Chasin LA. Isolation of Chinese hamster cell mutants deficient in dihydrofolate reductase activity. *Proc Natl Acad Sci*. 1980;77(7):4216-4220. doi:10.1073/pnas.77.7.4216
16. Shukla AA, Thömmes J. Recent advances in large-scale production of monoclonal antibodies and related proteins. *Trends Biotechnol*. 2010;28(5):253-261. doi:10.1016/j.tibtech.2010.02.001
17. Chu L, Robinson DK. Industrial choices for protein production by large-scale cell culture. *Curr Opin Biotechnol*. 2001;12(2):180-187. doi:10.1016/S0958-1669(00)00197-X
18. Butler M. Animal cell cultures: recent achievements and perspectives in the production of biopharmaceuticals. *Appl Microbiol Biotechnol*. 2005;68(3):283-291. doi:10.1007/s00253-005-1980-8
19. Brühlmann D, Jordan M, Hemberger J, Sauer M, Stettler M, Broly H. Tailoring recombinant protein quality by rational media design. *Biotechnol Prog*. 2015;31(3):615-629. doi:10.1002/btpr.2089
20. Kretzmer G. Industrial processes with animal cells. *Appl Microbiol Biotechnol*. 2002;59(2-3):135-142. doi:10.1007/s00253-002-0991-y
21. Yao T, Asayama Y. Animal-cell culture media: History, characteristics, and current issues. *Reprod Med Biol*. 2017;16(2):99-117. doi:10.1002/rmb2.12024
22. Arora M. Cell Culture Media: A Review. *Mater Methods*. 2013;3:175. doi:10.13070/mm.en.3.175
23. Gstraunthaler G. Alternatives to the use of fetal bovine serum: serum-free cell culture. *ALTEX*. 2003;20(4):275-281. doi:10.14573/altex.2003.4.257
24. Brunner D, Frank J, Appl H, Schöffl H, Pfaller W, Gstraunthaler G. Serum-free cell culture: the serum-free media interactive online database. *ALTEX*. 2010;27(1):53-62. doi:10.14573/altex.2010.1.53
25. van der Valk J, Brunner D, De Smet K, et al. Optimization of chemically defined cell culture media – Replacing fetal bovine serum in mammalian in vitro methods. *Toxicol Vitr*. 2010;24(4):1053-1063. doi:10.1016/j.tiv.2010.03.016
26. Vijayasankaran N, Li J, Shawley R, et al. Animal Cell Culture Media. In: *Encyclopedia of Industrial Biotechnology: Bioprocess, Bioseparation, and Cell Technology*. Hoboken, NJ, USA: John Wiley & Sons, Inc.; 2010. doi:10.1002/9780470054581.eib030
27. Reinhart D, Damjanovic L, Kaisermayer C, Kunert R. Benchmarking of commercially available CHO cell culture media for antibody production. *Appl Microbiol Biotechnol*. 2015;99(11):4645-4657. doi:10.1007/s00253-015-6514-4
28. Vidarsson G, Dekkers G, Rispens T. IgG Subclasses and Allotypes: From Structure to Effector Functions. *Front Immunol*. 2014;5:520. doi:10.3389/fimmu.2014.00520
29. Brekke OH, Sandlie I. Therapeutic antibodies for human diseases at the dawn of the twenty-first century. *Nat Rev Drug Discov*. 2003;2(1):52-62. doi:10.1038/nrd984

30. Schroeder Jr. HW, Cavacini L. Structure and function of immunoglobulins. *J Allergy Clin Immunol*. 2010;125(2 Suppl 2):S41-S52. doi:10.1016/j.jaci.2009.09.046
31. Natsume A, Niwa R, Satoh M. Improving effector functions of antibodies for cancer treatment: Enhancing ADCC and CDC. *Drug Des Devel Ther*. 2009;3:7-16. doi:10.2147/DDDT.S4378
32. Alt N, Zhang TY, Motchnik P, et al. Determination of critical quality attributes for monoclonal antibodies using quality by design principles. *Biologicals*. 2016;44(5):291-305. doi:10.1016/j.biologicals.2016.06.005
33. Schofield T, Robbins D, Miró-Quesada G. Critical Quality Attributes, Specifications, and Control Strategy. In: *Quality by Design for Biopharmaceutical Drug Product Development*. New York, NY: Springer; 2015. doi:10.1007/978-1-4939-2316-8_21
34. Vázquez-Rey M, Lang DA. Aggregates in monoclonal antibody manufacturing processes. *Biotechnol Bioeng*. 2011;108(7):1494-1508. doi:10.1002/bit.23155
35. Roberts CJ. Therapeutic protein aggregation: mechanisms, design, and control. *Trends Biotechnol*. 2014;32(7):372-380. doi:10.1016/j.tibtech.2014.05.005
36. Li W, Prabakaran P, Chen W, Zhu Z, Feng Y, Dimitrov DS. Antibody Aggregation: Insights from Sequence and Structure. *Antibodies*. 2016;5(3):19. doi:10.3390/antib5030019
37. Paul AJ, Handrick R, Ebert S, Hesse F. Identification of process conditions influencing protein aggregation in Chinese hamster ovary cell culture. *Biotechnol Bioeng*. 2018;115(5):1173-1185. doi:10.1002/bit.26534
38. Dengl S, Wehmer M, Hesse F, Lipsmeier F, Popp O, Lang K. Aggregation and Chemical Modification of Monoclonal Antibodies under Upstream Processing Conditions. *Pharm Res*. 2013;30(5):1380-1399. doi:10.1007/s11095-013-0977-8
39. Vasconcellos LRC, Dutra FF, Siqueira MS, et al. Protein aggregation as a cellular response to oxidative stress induced by heme and iron. *Proc Natl Acad Sci*. 2016;113(47):E7474-E7482. doi:10.1073/pnas.1608928113
40. Zhang Y-B, Howitt J, McCorkle S, Lawrence P, Springer K, Freimuth P. Protein aggregation during overexpression limited by peptide extensions with large net negative charge. *Protein Expr Purif*. 2004;36(2):207-216. doi:10.1016/j.pep.2004.04.020
41. Liberek K, Lewandowska A, Ziętkiewicz S. Chaperones in control of protein disaggregation. *EMBO J*. 2008;27(2):328-335. doi:10.1038/sj.emboj.7601970
42. Arosio P, Barolo G, Müller-Späth T, Wu H, Morbidelli M. Aggregation Stability of a Monoclonal Antibody During Downstream Processing. *Pharm Res*. 2011;28(8):1884-1894. doi:10.1007/s11095-011-0416-7
43. Torosantucci R, Schöneich C, Jiskoot W. Oxidation of Therapeutic Proteins and Peptides: Structural and Biological Consequences. *Pharm Res*. 2014;31(3):541-553. doi:10.1007/s11095-

013-1199-9

44. Folzer E, Diepold K, Bomans K, et al. Selective Oxidation of Methionine and Tryptophan Residues in a Therapeutic IgG1 Molecule. *J Pharm Sci*. 2015;104(9):2824-2831. doi:10.1002/jps.24509
45. Li S, Schöneich C, Borchardt RT. Chemical instability of protein pharmaceuticals: Mechanisms of oxidation and strategies for stabilization. *Biotechnol Bioeng*. 1995;48(5):490-500. doi:10.1002/BIT.260480511
46. Wang W. Instability, stabilization, and formulation of liquid protein pharmaceuticals. *Int J Pharm*. 1999;185(2):129-188. doi:10.1016/S0378-5173(99)00152-0
47. Mozziconacci O, Ji JA, Wang YJ, Schöneich C. Metal-catalyzed oxidation of protein methionine residues in human parathyroid hormone (1-34): Formation of homocysteine and a novel methionine-dependent hydrolysis reaction. *Mol Pharm*. 2013;10(2):739-755. doi:10.1021/mp300563m
48. Abès R, Teillaud J-L. Impact of Glycosylation on Effector Functions of Therapeutic IgG. *Pharmaceuticals*. 2010;3(1):146-157. doi:10.3390/ph3010146
49. Ohtsubo K, Marth JD. Glycosylation in Cellular Mechanisms of Health and Disease. *Cell*. 2006;126(5):855-867. doi:10.1016/J.CELL.2006.08.019
50. Bondt A, Rombouts Y, Selman MHJ, et al. Immunoglobulin G (IgG) Fab Glycosylation Analysis Using a New Mass Spectrometric High-throughput Profiling Method Reveals Pregnancy-associated Changes. *Mol Cell Proteomics*. 2014;13(11):3029-3039. doi:10.1074/mcp.M114.039537
51. Hossler P, Khattak SF, Li ZJ. Optimal and consistent protein glycosylation in mammalian cell culture. *Glycobiology*. 2009;19(9):936-949. doi:10.1093/glycob/cwp079
52. Zacchi LF, Schulz BL. N-glycoprotein macroheterogeneity: biological implications and proteomic characterization. *Glycoconj J*. 2016;33(3):359-376. doi:10.1007/s10719-015-9641-3
53. Jenkins N, Parekh RB, James DC. Getting the glycosylation right: Implications for the biotechnology industry. *Nat Biotechnol*. 1996;14(8):975-981. doi:10.1038/nbt0896-975
54. Gawlitzek M, Estacio M, Fürch T, Kiss R. Identification of cell culture conditions to control N -glycosylation site-occupancy of recombinant glycoproteins expressed in CHO cells. *Biotechnol Bioeng*. 2009;103(6):1164-1175. doi:10.1002/bit.22348
55. Goochee CF, Monica T. Environmental Effects on Protein Glycosylation. *Nat Biotechnol*. 1990;8(5):421-427. doi:10.1038/nbt0590-421
56. Nyberg GB, Balcarcel RR, Follstad BD, Stephanopoulos G, Wang DIC. Metabolic effects on recombinant interferon-gamma glycosylation in continuous culture of Chinese hamster ovary cells. *Biotechnol Bioeng*. 1999;62(3):336-347. doi:10.1002/(SICI)1097-0290(19990205)62:3<336::AID-BIT10>3.0.CO;2-N
57. Prabhu A, Gadre R, Gadgil M. Zinc supplementation decreases galactosylation of recombinant IgG

in CHO cells. *Appl Microbiol Biotechnol*. 2018;102(14):5989-5999. doi:10.1007/s00253-018-9064-8

58. Powell JT, Brew K. Metal ion activation of galactosyltransferase. *J Biol Chem*. 1976;251(12):3645-3652. doi:10.1016/S0021-9258(17)33393-8
59. Mohammad A, Agarabi C, Rogstad S, et al. An ICP-MS platform for metal content assessment of cell culture media and evaluation of spikes in metal concentration on the quality of an IgG3:κ monoclonal antibody during production. *J Pharm Biomed Anal*. 2019;162:91-100. doi:10.1016/j.jpba.2018.09.008
60. Yuk IH, Russell S, Tang Y, et al. Effects of copper on CHO cells: Cellular requirements and product quality considerations. *Biotechnol Prog*. 2015;31(1):226-238. doi:10.1002/btpr.2004
61. Crabb E, Moore EA. *Metals and Life*. Cambridge, UK: The Royal Society of Chemistry; 2010.
62. Dlouhy AC, Outten CE. The Iron Metallome in Eukaryotic Organisms. *Met Ions Life Sci*. 2013;12:241-278. doi:10.1007/978-94-007-5561-1_8
63. Anderson GJ, Vulpe CD. Mammalian iron transport. *Cell Mol Life Sci*. 2009;66(20):3241-3261. doi:10.1007/s00018-009-0051-1
64. Dev S, Babitt JL. Overview of iron metabolism in health and disease. *Hemodial Int*. 2017;21(Suppl 1):S6-S20. doi:10.1111/hdi.12542
65. Cameron AE, Wichers E. Report of the International Commission on Atomic Weights* (1961). *J Am Chem Soc*. 1962;84(22):4175-4197. doi:10.1021/ja00881a001
66. Holleman AF, Wiberg N, Wiberg E. *Lehrbuch Der Anorganischen Chemie*. 102nd ed. Berlin, Germany: Walter de Gruyter; 2007. doi:10.1515/9783110206845
67. Aisen P, Enns C, Wessling-Resnick M. Chemistry and biology of eukaryotic iron metabolism. *Int J Biochem Cell Biol*. 2001;33(10):940-959. doi:10.1016/s1357-2725(01)00063-2
68. Bou-Abdallah F. The iron redox and hydrolysis chemistry of the ferritins. *Biochim Biophys Acta*. 2010;1800(8):719-731. doi:10.1016/j.bbagen.2010.03.021
69. Fenton HJH. LXXIII.—Oxidation of tartaric acid in presence of iron. *J Chem Soc, Trans*. 1894;65:899-910. doi:10.1039/CT8946500899
70. Haber F, Weiss J. The catalytic decomposition of hydrogen peroxide by iron salts. *Proc R Soc London Ser A - Math Phys Sci*. 1934;147(861):332-351. doi:10.1098/rspa.1934.0221
71. Koppenol WH, Hider RH. Iron and redox cycling. Do's and don'ts. *Free Radic Biol Med*. 2019;133:3-10. doi:10.1016/j.freeradbiomed.2018.09.022
72. Brantley T, Moore B, Grinnell C, Khattak S. Investigating trace metal precipitation in highly concentrated cell culture media with Pourbaix diagrams. *Biotechnol Bioeng*. 2021;118(10):3888-3897. doi:10.1002/bit.27865
73. Hem JD, Cropper WH. Survey of ferrous-ferric chemical equilibria and redox potentials. In: *Water*

Supply Paper. Washington, USA: U.S. G.P.O.; 1959:524-548. doi:10.3133/wsp1459A

74. Pierre JL, Fontecave M, Crichton RR. Chemistry for an essential biological process : the reduction of ferric iron. *BioMetals*. 2002;15(4):341-346. doi:10.1023/a:1020259021641
75. Haas KL, Franz KJ. Application of Metal Coordination Chemistry To Explore and Manipulate Cell Biology. *Chem Rev*. 2009;109(10):4921-4960. doi:10.1021/cr900134a
76. Crichton RR, Pierre JL. Old iron, young copper: from Mars to Venus. *Biometals*. 2001;14(2):99-112. doi:10.1023/a:1016710810701
77. Lawrance GA. *Introduction to Coordination Chemistry*. Chichester, UK: John Wiley & Sons, Ltd; 2010. doi:10.1002/9780470687123
78. Crabb E, Moore E, Smart L. *Concepts in Transition Metal Chemistry*. Cambridge, UK: The Royal Society of Chemistry; 2010.
79. Diehl H. The Chelate Rings. *Chem Rev*. 1937;21(1):39-111. doi:10.1021/cr60068a003
80. Liu ZD, Hider RC. Design of iron chelators with therapeutic application. *Coord Chem Rev*. 2002;232(1-2):151-171. doi:10.1016/S0010-8545(02)00050-4
81. Pearson RG. Hard and Soft Acids and Bases. *J Am Chem Soc*. 1963;85(22):3533-3539. doi:10.1021/ja00905a001
82. Hider R. Recent developments centered on orally active iron chelators. *Thalass Reports*. 2014;4(2):2261. doi:10.4081/thal.2014.2261
83. Sánchez M, Sabio L, Gálvez N, Capdevila M, Dominguez-Vera JM. Iron chemistry at the service of life. *IUBMB Life*. 2017;69(6):382-388. doi:10.1002/iub.1602
84. Evstatiev R, Gasche C. Iron sensing and signalling. *Gut*. 2012;61(6):933-952. doi:10.1136/gut.2010.214312
85. Collman JP, Boulatov R, Sunderland CJ, Fu L. Functional Analogues of Cytochrome c Oxidase, Myoglobin, and Hemoglobin. *Chem Rev*. 2004;104(2):561-588. doi:10.1021/cr0206059
86. Liu J, Chakraborty S, Hosseinzadeh P, et al. Metalloproteins Containing Cytochrome, Iron–Sulfur, or Copper Redox Centers. *Chem Rev*. 2014;114(8):4366-4469. doi:10.1021/cr400479b
87. Lill R. Function and biogenesis of iron–sulphur proteins. *Nature*. 2009;460(7257):831-838. doi:10.1038/nature08301
88. Meyer J. Iron–sulfur protein folds, iron–sulfur chemistry, and evolution. *JBIC J Biol Inorg Chem*. 2008;13(2):157-170. doi:10.1007/s00775-007-0318-7
89. Sheftel A, Stehling O, Lill R. Iron-sulfur proteins in health and disease. *Trends Endocrinol Metab*. 2010;21(5):302-314. doi:10.1016/j.tem.2009.12.006
90. Ponka P. Cellular iron metabolism. *Kidney Int*. 1999;55(Suppl. 69):S2-S11. doi:10.1046/j.1523-1755.1999.055Suppl.69002.x
91. Richardson DR, Ponka P. The molecular mechanisms of the metabolism and transport of iron in

normal and neoplastic cells. *Biochim Biophys Acta*. 1997;1331(1):1-40. doi:10.1016/S0304-4157(96)00014-7

92. Kawabata H. Transferrin and transferrin receptors update. *Free Radic Biol Med*. 2019;133:46-54. doi:10.1016/j.freeradbiomed.2018.06.037
93. Garrick MD, Singleton ST, Vargas F, et al. DMT1: Which metals does it transport? *Biol Res*. 2006;39(1):79-85. doi:10.4067/S0716-97602006000100009
94. Zhao N, Gao J, Enns CA, Knutson MD. ZRT/IRT-like Protein 14 (ZIP14) Promotes the Cellular Assimilation of Iron from Transferrin. *J Biol Chem*. 2010;285(42):32141-32150. doi:10.1074/jbc.M110.143248
95. Byrne SL, Krishnamurthy D, Wessling-Resnick M. Pharmacology of iron transport. *Annu Rev Pharmacol Toxicol*. 2013;53:17-36. doi:10.1146/annurev-pharmtox-010611-134648
96. Qian ZM, Tang PL. Mechanisms of iron uptake by mammalian cells. *Biochim Biophys Acta*. 1995;1269(3):205-214. doi:10.1016/0167-4889(95)00098-X
97. Hider RC. Nature of nontransferrin-bound iron. *Eur J Clin Invest*. 2002;32(Suppl. 1):50-54. doi:10.1046/j.1365-2362.2002.0320s1050.x
98. Lane DJR, Merlot AM, Huang ML-H, et al. Cellular iron uptake, trafficking and metabolism: Key molecules and mechanisms and their roles in disease. *Biochim Biophys Acta*. 2015;1853(5):1130-1144. doi:10.1016/j.bbamcr.2015.01.021
99. Das SK, Oudit GY. Voltage-gated Ca2+ channels as key mediators of iron-transport and iron-overload cardiomyopathy: L-type vs. T-type Ca+ channels. *Eur J Haematol*. 2012;88(6):476-477. doi:10.1111/J.1600-0609.2012.01782.X
100. Knutson MD. Non-transferrin-bound iron transporters. *Free Radic Biol Med*. 2019;133:101-111. doi:10.1016/j.freeradbiomed.2018.10.413
101. Cooper CE, Lynagh GR, Hoyes KP, Hider RC, Cammack R, Porter JB. The relationship of intracellular iron chelation to the inhibition and regeneration of human ribonucleotide reductase. *J Biol Chem*. 1996;271(34):20291-20299. doi:10.1074/jbc.271.34.20291
102. Hider RC, Kong XL. Glutathione: a key component of the cytoplasmic labile iron pool. *BioMetals*. 2011;24(6):1179-1187. doi:10.1007/s10534-011-9476-8
103. Philpott CC, Ryu M-S. Special delivery: distributing iron in the cytosol of mammalian cells. *Front Pharmacol*. 2014;5:173. doi:10.3389/fphar.2014.00173
104. MacKenzie EL, Iwasaki K, Tsuji Y. Intracellular Iron Transport and Storage: From Molecular Mechanisms to Health Implications. *Antioxid Redox Signal*. 2008;10(6):997-1030. doi:10.1089/ars.2007.1893
105. Arosio P, Elia L, Poli M. Ferritin, cellular iron storage and regulation. *IUBMB Life*. 2017;69(6):414-422. doi:10.1002/iub.1621

106. Harrison PM, Arosio P. The ferritins: molecular properties, iron storage function and cellular regulation. *Biochim Biophys Acta*. 1996;1275(3):161-203. doi:10.1016/0005-2728(96)00022-9
107. Linder MC. Mobilization of Stored Iron in Mammals: A Review. *Nutrients*. 2013;5(10):4022-4050. doi:10.3390/nu5104022
108. La A, Nguyen T, Tran K, et al. Mobilization of iron from ferritin: New steps and details. *Metallomics*. 2018;10(1):154-168. doi:10.1039/c7mt00284j
109. Gonciarz RL, Collisson EA, Renslo AR. Ferrous Iron-Dependent Pharmacology. *Trends Pharmacol Sci*. 2021;42(1):7-18. doi:10.1016/j.tips.2020.11.003
110. Wills ED. Lipid peroxide formation in microsomes. General considerations. *Biochem J*. 1969;113(2):315-324. doi:10.1042/bj1130315
111. Perron NR, Brumaghim JL. A Review of the Antioxidant Mechanisms of Polyphenol Compounds Related to Iron Binding. *Cell Biochem Biophys*. 2009;53(2):75-100. doi:10.1007/s12013-009-9043-x
112. Hirschhorn T, Stockwell BR. The development of the concept of ferroptosis. *Free Radic Biol Med*. 2019;133:130-143. doi:10.1016/j.freeradbiomed.2018.09.043
113. Hadian K, Stockwell BR. SnapShot: Ferroptosis. *Cell*. 2020;181(5):1188-1188.e1. doi:10.1016/j.cell.2020.04.039
114. Stockwell BR, Friedmann Angeli JP, Bayir H, et al. Ferroptosis: A Regulated Cell Death Nexus Linking Metabolism, Redox Biology, and Disease. *Cell*. 2017;171(2):273-285. doi:10.1016/j.cell.2017.09.021
115. Ward DM, Kaplan J. Ferroportin-mediated iron transport: expression and regulation. *Biochim Biophys Acta*. 2012;1823(9):1426-1433. doi:10.1016/j.bbamcr.2012.03.004
116. Abboud S, Haile DJ. A novel mammalian iron-regulated protein involved in intracellular iron metabolism. *J Biol Chem*. 2000;275(26):19906-19912. doi:10.1074/jbc.M000713200
117. Yin Z, Jiang H, Lee E-SY, et al. Ferroportin is a manganese-responsive protein that decreases manganese cytotoxicity and accumulation. *J Neurochem*. 2010;112(5):1190-1198. doi:10.1111/j.1471-4159.2009.06534.x
118. Knovich MA, Storey JA, Coffman LG, Torti S V., Torti FM. Ferritin for the clinician. *Blood Rev*. 2009;23(3):95-104. doi:10.1016/j.blre.2008.08.001
119. Anderson CP, Shen M, Eisenstein RS, Leibold EA. Mammalian iron metabolism and its control by iron regulatory proteins. *Biochim Biophys Acta*. 2012;1823(9):1468-1483. doi:10.1016/j.bbamcr.2012.05.010
120. Peyssonnaux C, Nizet V, Johnson RS. Role of the hypoxia inducible factors HIF in iron metabolism. *Cell Cycle*. 2008;7(1):28-32. doi:10.4161/cc.7.1.5145
121. Wang J, Pantopoulos K. Regulation of cellular iron metabolism. *Biochem J*. 2011;434(3):365-381.

doi:10.1042/BJ20101825

122. Rouault TA. The role of iron regulatory proteins in mammalian iron homeostasis and disease. *Nat Chem Biol*. 2006;2(8):406-414. doi:10.1038/nchembio807
123. Nemeth E, Tuttle MS, Powelson J, et al. Hepcidin regulates cellular iron efflux by binding to ferroportin and inducing its internalization. *Science*. 2004;306(5704):2090-2093. doi:10.1126/science.1104742
124. Chen S-W. Materials and methods for enhanced iron uptake in cell culture. US Patent 2012/0264208 A1. 2012.
125. Krüger O, Oellers K, Kober L. Mammalian culture media with polyamine and iron. US Patent 8637312 B2. 2014.
126. Suhr-Jessen P. Iron chelate culture medium additive. WO Patent 1993000423A1. 1993.
127. Bai Y, Wu C, Zhao J, Liu Y-H, Ding W, Ling WLW. Role of iron and sodium citrate in animal protein-free CHO cell culture medium on cell growth and monoclonal antibody production. *Biotechnol Prog*. 2011;27(1):209-219. doi:10.1002/btpr.513
128. Yeung CK, Glahn RP, Miller DD. Inhibition of Iron Uptake from Iron Salts and Chelates by Divalent Metal Cations in Intestinal Epithelial Cells. *J Agric Food Chem*. 2005;53(1):132-136. doi:10.1021/jf049255c
129. Xu J, Rehmann MS, Xu X, et al. Improving titer while maintaining quality of final formulated drug substance via optimization of CHO cell culture conditions in low-iron chemically defined media. *MAbs*. 2018;10(3):488-499. doi:10.1080/19420862.2018.1433978
130. Xu J, Jin M, Song H, et al. Brown drug substance color investigation in cell culture manufacturing using chemically defined media: A case study. *Process Biochem*. 2014;49(1):130-139. doi:10.1016/j.procbio.2013.10.015
131. Vijayasankaran N, Varma S, Yang Y, et al. Effect of cell culture medium components on color of formulated monoclonal antibody drug substance. *Biotechnol Prog*. 2013;29(5):1270-1277. doi:10.1002/btpr.1772
132. Joppe K, Roser A-E, Maass F, Lingor P. The Contribution of Iron to Protein Aggregation Disorders in the Central Nervous System. *Front Neurosci*. 2019;13:15. doi:10.3389/fnins.2019.00015
133. Tweeddale HJ, Hawkins CL, Janmie JF, Truscott RJW, Davies MJ. Cross-linking of lens crystallin proteins induced by tryptophan metabolites and metal ions: implications for cataract development. *Free Radic Res*. 2016;50(10):1116-1130. doi:10.1080/10715762.2016.1210802
134. Clincke M-F, Guedon E, Yen FT, Ogier V, Goergen J-L. Effect of iron sources on the glycosylation macroheterogeneity of human recombinant IFN-γ produced by CHO cells during batch processes. *BMC Proc*. 2011;5(Suppl 8):P114. doi:10.1186/1753-6561-5-S8-P114
135. Wentz AE, Hemmavanh D, Matuck JG. Use of metal ions for modulation of protein glycosylation

profiles of recombinant proteins. US Patent 9598667B2. 2017.

136. Weiss CH, Merkel C, Zimmer A. Impact of iron raw materials and their impurities on CHO metabolism and recombinant protein product quality. *Biotechnol Prog*. 2021;37(4):e3148. doi:10.1002/btpr.3148

137. Ehret J, Zimmermann M, Eichhorn T, Zimmer A. Impact of cell culture media additives on IgG glycosylation produced in Chinese hamster ovary cells. *Biotechnol Bioeng*. 2019;116(4):816-830. doi:10.1002/bit.26904

138. Laborda F, Medrano J, Castillo JR. Quality of quantitative and semiquantitative results in inductively coupled plasma mass spectrometry. *J Anal At Spectrom*. 2001;16:732-738. doi:10.1039/b101814k

139. Chen H, Dabek-Zlotorzynska E, Rasmussen PE, Hassan N, Lanouette M. Evaluation of semiquantitative analysis mode in ICP-MS. *Talanta*. 2008;74(5):1547-1555. doi:10.1016/j.talanta.2007.09.037

140. Livak KJ, Schmittgen TD. Analysis of Relative Gene Expression Data Using Real-Time Quantitative PCR and the 2−ΔΔCT Method. *Methods*. 2001;25(4):402-408. doi:10.1006/meth.2001.1262

141. Hirayama T, Nagasawa H. Chemical tools for detecting Fe ions. *J Clin Biochem Nutr*. 2017;60(1):39-48. doi:10.3164/jcbn.16-70

142. Brandt WW, Smith GF. Polysubstituted 1,10-Phenanthrolines and Bipyridines as Multiple Range Redox Indicators. *Anal Chem*. 1949;21(11):1313-1319. doi:10.1021/ac60035a003

143. Hennessy DJ, Reid GR, Smith FE, Thompson SL. Ferene — a new spectrophotometric reagent for iron. *Can J Chem*. 1984;62(4):721-724. doi:10.1139/v84-121

144. Stookey LL. Ferrozine---a new spectrophotometric reagent for iron. *Anal Chem*. 1970;42(7):779-781. doi:10.1021/ac60289a016

145. Ito S, Ikuta K, Kato D, et al. Non-transferrin-bound iron assay system utilizing a conventional automated analyzer. *Clin Chim Acta*. 2014;437:129-135. doi:10.1016/j.cca.2014.07.013

146. Breuer W, Epsztejn S, Cabantchik ZI. Iron acquired from transferrin by K562 cells is delivered into a cytoplasmic pool of chelatable iron(II). *J Biol Chem*. 1995;270(41):24209-24215. doi:10.1074/jbc.270.41.24209

147. Petrat F, Rauen U, de Groot H. Determination of the chelatable iron pool of isolated rat hepatocytes by digital fluorescence microscopy using the fluorescent probe, phen green SK. *Hepatology*. 1999;29(4):1171-1179. doi:10.1002/hep.510290435

148. Hua J, Wang YG. A highly selective and sensitive fluorescent chemosensor for Fe 3+ in physiological aqueous solution. *Chem Lett*. 2005;34(1):98-99. doi:10.1246/cl.2005.98

149. Bricks JL, Kovalchuk A, Trieflinger C, et al. On the Development of Sensor Molecules that Display Fe(III) -amplified Fluorescence. *J Am Chem Soc*. 2005;127(39):13522-13529.

doi:10.1021/ja050652t

150. Hirayama T, Okuda K, Nagasawa H. A highly selective turn-on fluorescent probe for iron(ii) to visualize labile iron in living cells. *Chem Sci*. 2013;4(3):1250-1256. doi:10.1039/c2sc21649c
151. Spangler B, Morgan CW, Fontaine SD, et al. A reactivity-based probe of the intracellular labile ferrous iron pool. *Nat Chem Biol*. 2016;12(9):680-685. doi:10.1038/nchembio.2116
152. Riemer J, Hoepken HH, Czerwinska H, Robinson SR, Dringen R. Colorimetric ferrozine-based assay for the quantitation of iron in cultured cells. *Anal Biochem*. 2004;331(2):370-375. doi:10.1016/j.ab.2004.03.049
153. Fish WW. Rapid colorimetric micromethod for the quantitation of complexed iron in biological samples. *Methods Enzymol*. 1988;158:357-364. doi:10.1016/0076-6879(88)58067-9
154. Prus E, Fibach E. Flow cytometry measurement of the labile iron pool in human hematopoietic cells. *Cytom Part A*. 2008;73(1):22-27. doi:10.1002/cyto.a.20491
155. Epsztejn S, Kakhlon O, Glickstein H, Breuer W, Cabantchik ZI. Fluorescence Analysis of the Labile Iron Pool of Mammalian Cells. *Anal Biochem*. 1997;248(1):31-40. doi:10.1006/abio.1997.2126
156. Smit S, Huijskes-Heins MIE, Leijnse B. Iron content of some tissue culture cells. *Cell Biol Int Rep*. 1982;6(8):741-744. doi:10.1016/0309-1651(82)90166-7
157. Potůčková E, Hrušková K, Bureš J, et al. Structure-activity relationships of novel salicylaldehyde isonicotinoyl hydrazone (SIH) analogs: iron chelation, anti-oxidant and cytotoxic properties. *PLoS One*. 2014;9(11):e112059. doi:10.1371/journal.pone.0112059
158. Chen Y-L, Kong X, Xie Y, Hider RC. The interaction of pyridoxal isonicotinoyl hydrazone (PIH) and salicylaldehyde isonicotinoyl hydrazone (SIH) with iron. *J Inorg Biochem*. 2018;180:194-203. doi:10.1016/j.jinorgbio.2017.12.007
159. Hider RC. Potential protection from toxicity by oral iron chelators. *Toxicol Lett*. 1995;82-83:961-967. doi:10.1016/0378-4274(95)03606-7
160. Işık M, Levorse D, Mobley DL, Rhodes T, Chodera JD. Octanol-water partition coefficient measurements for the SAMPL6 blind prediction challenge. *J Comput Aided Mol Des*. 2020;34(4):405-420. doi:10.1007/s10822-019-00271-3
161. Sangster J. *LOGKOW Databank*. Montreal, Quebec, Canada: Sangster Research Laboratories; 1994.
162. de Voogt P, Muir DCG, Webster GRB, Govers H. Quantitative structure-activity relationships for the bioconcentration in fish of seven polychlorinated dibenzodioxins. *Chemosphere*. 1990;21(12):1385-1396. doi:10.1016/0045-6535(90)90043-S
163. Pinnix ZK, Miller LD, Wang W, et al. Ferroportin and iron regulation in breast cancer progression and prognosis. *Sci Transl Med*. 2010;2(43):43ra56. doi:10.1126/scitranslmed.3001127
164. Wessling-Resnick M. Iron homeostasis and the inflammatory response. *Annu Rev Nutr*.

2010;30:105-122. doi:10.1146/annurev.nutr.012809.104804

165. Boult J, Roberts K, Brookes MJ, et al. Overexpression of cellular iron import proteins is associated with malignant progression of esophageal adenocarcinoma. *Clin Cancer Res*. 2008;14(2):379-387. doi:10.1158/1078-0432.CCR-07-1054

166. Chutvanichkul B, Vattanaviboon P, Mas-oodi S, U-pratya Y, Wanachiwanawin W. Labile iron pool as a parameter to monitor iron overload and oxidative stress status in β-thalassemic erythrocytes. *Cytom Part B Clin Cytom*. 2018;94(4):631-636. doi:10.1002/cyto.b.21633

167. Miyanishi K, Tanaka S, Sakamoto H, Kato J. The role of iron in hepatic inflammation and hepatocellular carcinoma. *Free Radic Biol Med*. 2019;133:200-205. doi:10.1016/j.freeradbiomed.2018.07.006

168. Kakhlon O, Gruenbaum Y, Cabantchik ZI. Ferritin expression modulates cell cycle dynamics and cell responsiveness to H-ras-induced growth via expansion of the labile iron pool. *Biochem J*. 2002;363(Pt 3):431-436. doi:10.1042/0264-6021:3630431

169. Torti S V, Torti FM. Iron and cancer: more ore to be mined. *Nat Rev Cancer*. 2013;13(5):342-355. doi:10.1038/nrc3495

170. Craven CM, Alexander J, Eldridge M, Kushner JP, Bernstein S, Kaplan J. Tissue distribution and clearance kinetics of non-transferrin-bound iron in the hypotransferrinemic mouse: a rodent model for hemochromatosis. *Proc Natl Acad Sci USA*. 1987;84(10):3457-3461. doi:10.1073/pnas.84.10.3457

171. Breuer W, Epsztejn S, Millgram P, Cabantchik IZ. Transport of iron and other transition metals into cells as revealed by a fluorescent probe. *Am J Physiol Physiol*. 1995;268(6 Pt 1):C1354-C1361. doi:10.1152/ajpcell.1995.268.6.C1354

172. Epsztejn S, Glickstein H, Picard V, et al. H-ferritin subunit overexpression in erythroid cells reduces the oxidative stress response and induces multidrug resistance properties. *Blood*. 1999;94(10):3593-3603. doi:10.1182/blood.v94.10.3593.422k26_3593_3603

173. Doulias P-T, Vlachou C, Boudouri C, Kanavaros P, Siamopoulos KC, Galaris D. Flow cytometric estimation of 'labile iron pool' in human white blood cells reveals a positive association with ageing. *Free Radic Res*. 2008;42(3):253-259. doi:10.1080/10715760801911649

174. Zhang A-S, Canonne-Hergaux F, Gruenheid S, Gros P, Ponka P. Use of Nramp2-transfected Chinese hamster ovary cells and reticulocytes from mk/mk mice to study iron transport mechanisms. *Exp Hematol*. 2008;36(10):1227-1235. doi:10.1016/j.exphem.2008.04.014

175. Ren Y, Walczyk T. Quantification of ferritin bound iron in human serum using species-specific isotope dilution mass spectrometry. *Metallomics*. 2014;6(9):1709-1717. doi:10.1039/C4MT00127C

176. Hoppler M, Zeder C, Walczyk T. Quantification of Ferritin-Bound Iron in Plant Samples by Isotope

Tagging and Species-Specific Isotope Dilution Mass Spectrometry. *Anal Chem*. 2009;81(17):7368-7372. doi:10.1021/ac900885j

177. Herbert V, Jayatilleke E, Shaw S, et al. Serum ferritin iron, a new test, measures human body iron stores unconfounded by inflammation. *Stem Cells*. 1997;15(4):291-296. doi:10.1002/stem.150291
178. Vaisman B, Santambrogio P, Arosio P, Fibach E, Konijn AM. An ELISA for the H-subunit of human ferritin which employs a combination of rabbit poly- and mice monoclonal antibodies and an enzyme labeled anti-mouse-IgG. *Clin Chem Lab Med*. 1999;37(2):121-125. doi:10.1515/CCLM.1999.022
179. Chahrour O, Cobice D, Malone J. Stable isotope labelling methods in mass spectrometry-based quantitative proteomics. *J Pharm Biomed Anal*. 2015;113:2-20. doi:10.1016/j.jpba.2015.04.013
180. Campion EM, Loughran ST, Walls D. Protein Quantitation and Analysis of Purity. In: *Methods in Molecular Biology*. New York, NY: Humana Press; 2017. doi:10.1007/978-1-4939-6412-3_12
181. Im K, Mareninov S, Diaz MFP, Yong WH. An introduction to performing immunofluorescence staining. In: *Methods in Molecular Biology*. New York, NY: Humana Press; 2019. doi:10.1007/978-1-4939-8935-5_26
182. Thyagarajan M. Impact of different iron sources on CHO metabolism and critical quality attributes. [Master thesis]. Hamburg, Germany: HAW Hamburg; 2020.
183. Graham RJ, Bhatia H, Yoon S. Consequences of trace metal variability and supplementation on Chinese hamster ovary (CHO) cell culture performance: A review of key mechanisms and considerations. *Biotechnol Bioeng*. 2019;116(12):3446-3456. doi:10.1002/bit.27140
184. Che M, Wang R, Li X, Wang H-Y, Zheng XFS. Expanding roles of superoxide dismutases in cell regulation and cancer. *Drug Discov Today*. 2016;21(1):143-149. doi:10.1016/j.drudis.2015.10.001
185. Holley AK, Bakthavatchalu V, Velez-Roman JM, St. Clair DK. Manganese Superoxide Dismutase: Guardian of the Powerhouse. *Int J Mol Sci*. 2011;12(10):7114-7162. doi:10.3390/ijms12107114
186. Dixon SJ, Stockwell BR. The role of iron and reactive oxygen species in cell death. *Nat Chem Biol*. 2014;10(1):9-17. doi:10.1038/nchembio.1416
187. Aguirre JD, Culotta VC. Battles with Iron: Manganese in Oxidative Stress Protection. *J Biol Chem*. 2012;287(17):13541-13548. doi:10.1074/jbc.R111.312181
188. Ganini D, Santos JH, Bonini MG, Mason RP. Switch of Mitochondrial Superoxide Dismutase into a Prooxidant Peroxidase in Manganese-Deficient Cells and Mice. *Cell Chem Biol*. 2018;25(4):413-425.e6. doi:10.1016/j.chembiol.2018.01.007
189. Ganini D, Petrovich RM, Edwards LL, Mason RP. Iron incorporation into MnSOD A (bacterial Mn-dependent superoxide dismutase) leads to the formation of a peroxidase/catalase implicated in

oxidative damage to bacteria. *Biochim Biophys Acta*. 2015;1850(9):1795-1805. doi:10.1016/j.bbagen.2015.05.006

190. Zhao B, Summers FA, Mason RP. Photooxidation of Amplex red to resorufin: Implications of exposing the Amplex red assay to light. *Free Radic Biol Med*. 2012;53(5):1080-1087. doi:10.1016/j.freeradbiomed.2012.06.034
191. Boeggeman E, Qasba PK. Studies on the metal binding sites in the catalytic domain of ß1,4-galactosyltransferase. *Glycobiology*. 2002;12(7):395-407. doi:10.1093/glycob/cwf045
192. Gu X, Harmon BJ, Wang DIC. Site- and branch-specific sialylation of recombinant human interferon-γ in Chinese hamster ovary cell culture. *Biotechnol Bioeng*. 1997;55(2):390-398. doi:10.1002/(SICI)1097-0290(19970720)55:2<390::AID-BIT16>3.0.CO;2-L
193. Ji JA, Zhang B, Cheng W, Wang YJ. Methionine, tryptophan, and histidine oxidation in a model protein, PTH: mechanisms and stabilization. *J Pharm Sci*. 2009;98(12):4485-4500. doi:10.1002/jps.21746
194. Zhou S, Zhang B, Sturm E, et al. Comparative Evaluation of Disodium Edetate and Diethylenetriaminepentaacetic Acid as Iron Chelators to Prevent Metal -Catalyzed Destabilization of a Therapeutic Monoclonal Antibody. *J Pharm Sci*. 2010;99(10):4239-4250. doi:10.1002/jps.22141
195. Sunda W, Huntsman S. Effect of pH, light, and temperature on Fe-EDTA chelation and Fe hydrolysis in seawater. *Mar Chem*. 2003;84(1-2):35-47. doi:10.1016/S0304-4203(03)00101-4
196. Ahile UJ, Wuana RA, Itodo AU, Sha'Ato R, Dantas RF. Stability of iron chelates during photo-Fenton process: The role of pH, hydroxyl radical attack and temperature. *J Water Process Eng*. 2020;36:101320. doi:10.1016/j.jwpe.2020.101320
197. Halliwell B. Oxidative stress in cell culture: An under-appreciated problem? *FEBS Lett*. 2003;540(1-3):3-6. doi:10.1016/S0014-5793(03)00235-7
198. Betteridge DJ. What is oxidative stress? *Metabolism*. 2000;49(2):3-8. doi:10.1016/S0026-0495(00)80077-3
199. Glahn RP, Lee OA, Yeung A, Goldman MI, Miller DD. Caco-2 cell ferritin formation predicts nonradiolabeled food iron availability in an in vitro digestion/Caco-2 cell culture model. *J Nutr*. 1998;128(9):1555-1561. doi:10.1093/jn/128.9.1555
200. Bianchi V, Toso RD, Debetto P, et al. Mechanisms of chromium toxicity in mammalian cell cultures. *Toxicology*. 1980;17(2):219-224. doi:10.1016/0300-483X(80)90097-9
201. Jomova K, Valko M. Advances in metal-induced oxidative stress and human disease. *Toxicology*. 2011;283(2-3):65-87. doi:10.1016/j.tox.2011.03.001
202. Sinicropi MS, Amantea D, Caruso A, Saturnino C. Chemical and biological properties of toxic metals and use of chelating agents for the pharmacological treatment of metal poisoning. *Arch*

Toxicol. 2010;84(7):501-520. doi:10.1007/s00204-010-0544-6

203. Camarasu C, Madichie C, Williams R. Recent progress in the determination of volatile impurities in pharmaceuticals. *TrAC - Trends Anal Chem*. 2006;25(8):768-777. doi:10.1016/j.trac.2006.05.013
204. Pandey S, Pandey P, Kumar R, Singh NP. Residual solvent determination by head space gas chromatography with flame ionization detector in omeprazole API. *Brazilian J Pharm Sci*. 2011;47(2):379-384. doi:10.1590/S1984-82502011000200019
205. Oriekhova O, Stoll S. Investigation of FeCl3 induced coagulation processes using electrophoretic measurement, nanoparticle tracking analysis and dynamic light scattering: Importance of pH and colloid surface charge. *Colloids Surfaces A Physicochem Eng Asp*. 2014;461:212-219. doi:10.1016/j.colsurfa.2014.07.049
206. Stefánsson A. Iron(III) Hydrolysis and Solubility at 25 °C. *Environ Sci Technol*. 2007;41(17):6117-6123. doi:10.1021/es070174h
207. Hove M, van Hille RP, Lewis AE. Iron solids formed from oxidation precipitation of ferrous sulfate solutions. *AIChE J*. 2007;53(10):2569-2577. doi:10.1002/aic.11264
208. Schnellbaecher A, Binder D, Bellmaine S, Zimmer A. Vitamins in cell culture media: Stability and stabilization strategies. *Biotechnol Bioeng*. 2019;116(6):1537-1555. doi:10.1002/bit.26942
209. Halliwell B, Clement MV, Ramalingam J, Long LH. Hydrogen Peroxide. Ubiquitous in Cell Culture and In vivo? *IUBMB Life*. 2000;50(4-5):251-257. doi:10.1080/713803727
210. Wang RJ, Nixon BT. Identification of hydrogen peroxide as a photoproduct toxic to human cells in tissue-culture medium irradiated with “daylight” fluorescent light. *In Vitro*. 1978;14(8):715-722. doi:10.1007/BF02616168
211. Cossarizza A, Chang HD, Radbruch A, et al. Guidelines for the use of flow cytometry and cell sorting in immunological studies. *Eur J Immunol*. 2017;47(10):1584-1797. doi:10.1002/eji.201646632
212. Eberle C, Kim IR, Lye M, Ke CY, Feld GK, Kim N. A Novel Sample Preparation Method for Improved Tumor-Infiltrating. *Curiox*. 2021.
213. Gross A, Schoendube J, Zimmermann S, Steeb M, Zengerle R, Koltay P. Technologies for Single-Cell Isolation. *Int J Mol Sci*. 2015;16(8):16897-16919. doi:10.3390/ijms160816897
214. Adam FI, Bounds PL, Kissner R, Koppenol WH. Redox properties and activity of iron-citrate complexes: Evidence for redox cycling. *Chem Res Toxicol*. 2015;28(4):604-614. doi:10.1021/tx500377b
215. Königsberger LC, Königsberger E, May PM, Hefter GT. Complexation of iron (III) and iron (II) by citrate. Implications for iron speciation in blood plasma. *J Inorg Biochem*. 2000;78(3):175-184. doi:10.1016/S0162-0134(99)00222-6

216. Shi F, Zhang P, Mao Y, Wang C, Zheng M, Zhao Z. The nitroxide Tempo inhibits hydroxyl radical production from the Fenton-like reaction of iron(II)-citrate with hydrogen peroxide. *Biochem Biophys Res Commun*. 2017;483(1):159-164. doi:10.1016/j.bbrc.2016.12.174
217. Xu S, Hoshan L, Chen H. Improving lactate metabolism in an intensified CHO culture process: productivity and product quality considerations. *Bioprocess Biosyst Eng*. 2016;39(11):1689-1702. doi:10.1007/s00449-016-1644-3
218. Luo J, Vijayasankaran N, Autsen J, et al. Comparative metabolite analysis to understand lactate metabolism shift in Chinese hamster ovary cell culture process. *Biotechnol Bioeng*. 2012;109(1):146-156. doi:10.1002/bit.23291
219. Nargund S, Qiu J, Goudar CT. Elucidating the role of copper in CHO cell energy metabolism using (13)C metabolic flux analysis. *Biotechnol Prog*. 2015;31(5):1179-1186. doi:10.1002/btpr.2131
220. Horn D, Barrientos A. Mitochondrial copper metabolism and delivery to cytochrome c oxidase. *IUBMB Life*. 2008;60(7):421-429. doi:10.1002/iub.50
221. Zeng H, Saari JT, Johnson WT. Copper Deficiency Decreases Complex IV but Not Complex I, II, III, or V in the Mitochondrial Respiratory Chain in Rat Heart. *J Nutr*. 2007;137(1):14-18. doi:10.1093/jn/137.1.14
222. Percival SS, Harris ED. Regulation of Cu,Zn superoxide dismutase with copper. Caeruloplasmin maintains levels of functional enzyme activity during differentiation of K562 cells. *Biochem J*. 1991;274(Pt 1):153-158. doi:10.1042/BJ2740153
223. Boyd SD, Ullrich MS, Skopp A, Winkler DD. Copper Sources for Sod1 Activation. *Antioxidants*. 2020;9(6):500. doi:10.3390/antiox9060500
224. M. Fetherolf M, Boyd SD, Winkler DD, Winge DR. Oxygen-dependent activation of Cu,Zn-superoxide dismutase-1. *Metallomics*. 2017;9(8):1047-1059. doi:10.1039/C6MT00298F
225. McGrew JT. Cell culture performance with vanadate. US Patent 6974681B1. 2005.
226. Zwolak I, Gołębiowska D. Protective activity of pyruvate against vanadium-dependent cytotoxicity in Chinese hamster ovary (CHO-K1) cells. *Toxicol Ind Health*. 2018;34(5):283-292. doi:10.1177/0748233718754979
227. Zwolak I. Increased Cytotoxicity of Vanadium to CHO-K1 Cells in the Presence of Inorganic Selenium. *Bull Environ Contam Toxicol*. 2015;95(5):593-598. doi:10.1007/s00128-015-1615-4
228. Capella Roca B, Alarcón Miguez A, Keenan J, et al. Zinc supplementation increases protein titer of recombinant CHO cells. *Cytotechnology*. 2019;71(5):915-924. doi:10.1007/s10616-019-00334-1
229. Graham RJ, Ketcham SA, Mohammad A, et al. Zinc supplementation modulates intracellular metal uptake and oxidative stress defense mechanisms in CHO cell cultures. *Biochem Eng J*. 2021;169:107928. doi:10.1016/j.bej.2021.107928

230. Graham RJ, Ketcham S, Mohammad A, et al. Zinc supplementation improves the harvest purity of β-glucuronidase from CHO cell culture by suppressing apoptosis. *Appl Microbiol Biotechnol*. 2020;104(3):1097-1108. doi:10.1007/s00253-019-10296-1

231. Grinnell C, Bareford L, Matthews TE, Brantley T, Moore B, Kolwyck D. Elemental metal variance in cell culture raw materials for process risk profiling. *Biotechnol Prog*. 2020;36(5):e3004. doi:10.1002/btpr.3004

232. Challener CA. Biopharma takes on raw material variability. *BioPharm Int*. 2016;29(3):20-24.

233. Dickens J, Khattak S, Matthews TE, Kolwyck D, Wiltberger K. Biopharmaceutical raw material variation and control. *Curr Opin Chem Eng*. 2018;22:236-243. doi:10.1016/j.coche.2018.10.007

7 Appendix

7.1 List of abbreviations

ACN	Acetonitrile
AM	Acetoxymethyl
APTS	8-aminopyrene-1,3,6-trisulfonic acid
Asn	Asparagine
BPY	2,2'-Bipyridyl
Caco-2	Colorectal adenocarcinoma cells 2
CCM	Cell culture medium
cDNA	Complementary DNA
CGE-LIF	Capillary gel electrophoresis with laser induced fluorescence
C_H	Constant domain of the heavy chain
CHO	Chinese hamster ovary
C_L	Constant domain of the light chain
Cp	Ceruloplasmin
CQA	Critical quality attribute
Ct	Cycle threshold
DCYTB	Duodenal cytochrome b
DEPC	Diethyl pyrocarbonate
DFP	Deferiprone
DHFR	Dihydrofolate reductase
DMSO	Dimethyl sulfoxide
DMT1	Divalent metal-ion transporter 1
DNA	Deoxyribonucleic acid
DO	Dissolved oxygen
DTT	Dithiothreitol
EDTA	Ethylenediaminetetraacetic acid
ELISA	Enzyme-linked immunosorbent assay
F(II)SC	Ferrous sodium citrate
F(III)SC	Ferric sodium citrate
Fab	Fragment antigen binding
FAC	Ferric ammonium citrate
FACS	Fluorescence activated cell sorting
FBS	Fetal bovine serum

FBXL5	F-box/leucine-rich repeat protein 5
Fc	Fragment crystalline
FC	Ferric citrate
$Fe(NO_3)_3$	Ferric nitrate
$Fe(OH)_3$	Ferric oxyhydroxide
Fe^{2+}	Ferrous ion
Fe^{3+}	Ferric ion
$FeCl_2$	Ferrous chloride
$FeCl_3$	Ferric chloride
Ferritin H	Ferritin heavy chain
Ferritin L	Ferritin light chain
Fe-S	Iron-sulfur cluster
$FeSO_4$	Ferrous sulfate
FPN	Ferroportin
Fuc	Fucose
Gal	Galactose
GalNAc	N-acetylgalactosamine
Gapdh	Glyceraldehyde 3-phosphate dehydrogenase
GlcNAc	N-acetylglucosamine
GOI	Gene of interest
GS	Glutamine synthetase
HEK	Human embryo kidney
HIF	Hypoxia-inducible factor
HMW	High molecular weight
HRE	Hypoxic response element
HR-ICP-MS	High resolution inductively coupled plasma mass spectrometry
HSAB	Hard and soft acids and bases
HT	Hypoxanthine and thymidine
ICP-MS	Inductively coupled plasma mass spectrometry
IFN-γ	Interferon gamma
Ig	Immunoglobulin
IRE	Iron responsive element
IRP1	Iron regulatory protein 1
IRP2	Iron regulatory protein 2
K_n	Complex stability constant for one individual complex formation step

K_{OW}	N-octanol-water partition coefficient
LIP	Labile iron pool
mAb	Monoclonal antibody
Man	Mannose
MEL	Murine erythroid leukemia
MFI	Mean fluorescence intensity
MFRN	Mitoferrin
mRNA	Messenger ribonucleic acid
MSX	Methionine sulfoximine
MTP1	Metal transporter protein 1
MTX	Methotrexate
NADPH	Nicotinamide adenine dinucleotide phosphate
nanoLC-MS/MS	Nanoscale liquid chromatography coupled to a tandem mass spectrometry
NTBI	Non-transferrin-bound iron
OD	Optical density
PAMPA	Parallel artificial membrane permeability assay
PBS	Phosphate-buffered saline
PCBP	Poly(rC)-binding protein
PES	Polyethersulfone
PHD	Prolyl hydroxylase
PIH	Parathyroid hormone
PL-PUFA	Phospholipid with polyunsaturated acyl tail
PTM	Post-translational modification
PVA	Polyvinyl alcohol
qPCR	Quantitative polymerase chain reaction
R^2	Coefficient of determination
RNA	Ribonucleic acid
ROS	Reactive oxygen species
RT	Room temperature
SA	Sialic acid
SD	Standard deviation
SEC-UV	Size-exclusion chromatography coupled to an UV detector
Ser	Serine
SHE	Standard hydrogen electrode
SIH	Salicylaldehyde isonicotinoylhydrazone

SOD1	Superoxide dismutase 1
SOD2	Superoxide dismutase 2
SS-IDMS	Species-specific isotope dilution mass spectrometry
STEAP3	Six-transmembrane epithelial antigen of the prostate 3
Tf	Transferrin
TFA	Trifluoracetic acid
TfR1	Transferrin receptor 1
Thr	Threonine
TRPC6	Transient receptor potential cation channel subfamily C member 6
TRPML1	Transient receptor potential mucolipin 1
UPLC	Ultra-performance liquid chromatography
UPLC-MS	Ultra-performance liquid chromatography coupled to a mass spectrometer
UTR	Untranslated region
UV	Ultraviolet
VCD	Viable cell density
V_H	Variable domain of the heavy chain
V_L	Variable domain of the light chain
ZIP14	Zrt- and Irt-like protein 14
ZIP8	Zrt- and Irt-like protein 8
β_n	Overall complex stability constant

7.2 List of figures

7.3 List of tables

7.4 List of equations

7.5 Acknowledgements

First of all, I would like to thank Prof. Dr. Harald Kolmar for the academic supervision of my doctoral thesis at TU Darmstadt. The successful cooperation with industrial research has supported the doctorate in many ways. Thank you for your interest in my work. Furthermore, I want to thank Prof. Dr. Karlheinz Preuß for taking over the part as a co-examiner and who already accompanied me during my studies at HS Mannheim. Additionally, I want to thank Prof. Dr. Katja Schmitz and PD Dr. Tobias Meckel for their willingness to serve as an expert examiner, as well as Prof. Dr. Markus Prechtl as the chairperson of my dissertation committee.

Moreover, I want to express my deepest gratitude to Dr. Aline Zimmer for giving me the opportunity to perform my doctoral thesis at Merck KGaA. Thank you for all your support, your trust in me, your valuable time and expertise, and your extraordinary supervision during the last years. Likewise, I would like to express my deepest gratitude to my supervisor Corinna Merkel. Thank you for the extraordinary supervision, your valuable time and guidance, and your assistance. It was a pleasure to work with you both (#GoTeamIron). I really enjoyed the scientific inputs, discussions, and creative ideas. You both helped me improving on a scientific and personal level and contributed significantly to the success of this work.

The warmest thank you goes to all current and former members of the LS-PBR-UA Advanced Cell Culture Technologies team at Merck KGaA. Thank you to Janine Caspari for being my #GoTeamIron partner and making lab work so enjoyable. Thanks to Dr. Alice Antonello, Dr. Stephanie Bellmaine, Susanne Bohl, Janike Ehret, Dr. Tim Hofmann, Carolina Kunkel, Dr. Maxime Le Mignon, Anja Licht, Melanie Nguyen, Brit Pardon, Dr. Almut Rapp, Corinna Schmidt, Alisa Schnellbächer, Petra Schott, Ronja Seibel, Anke Simon, Maria Wehsling, Dr. Dmitry Zabezhinsky and Dr. Martina Zimmermann. Please forgive me that I did not dedicate a separate and individual thank you to all of you herein. You guys are amazing. Thank you for the countless and great conversations about science and beyond. It was a pleasure to work in such a great and welcoming working atmosphere.

Finally, my deepest gratitude is dedicated to my parents, Ulla and Gerhard, my brother Markus, and my boyfriend Hendrik. Thank you for always believing in me, your encouragements along the way of my studies and your patience with me. Your unconditional support was and still is amazing. Thank you for everything.

8 Affirmations

Christine Hilde Weiß 14.12.2021

Erklärung

Ich versichere hiermit, dass die elektronische Version meiner Dissertation mit der schriftlichen Version übereinstimmt und für die Durchführung des Promotionsverfahrens vorliegt.

Christine Hilde Weiß

Christine Hilde Weiß 14.12.2021

Erklärung

Ich versichere hiermit, dass zu einem vorherigen Zeitpunkt noch keine Promotion versucht wurde und zu keinem früheren Zeitpunkt an einer in- oder ausländischen Hochschule eingereicht wurde. In diesem Fall sind nähere Angaben über Zeitpunkt, Hochschule, Dissertationsthema und Ergebnis des Versuchs mitzuteilen.

Christine Hilde Weiß

Christine Hilde Weiß 14.12.2021

Erklärung

Ich versichere hiermit, dass die vorliegende Dissertation selbstständig und nur unter Verwendung der angegebenen Quellen verfasst wurde.

_____

Christine Hilde Weiß

Christine Hilde Weiß 14.12.2021

Erklärung

Die Arbeit hat bisher noch nicht zu Prüfungszwecken gedient.

Christine Hilde Weiß